CalVal Envisat
CLS.DOS/NT/05.236
Version : 1rev2, February 6, 2006
Nomenclature : SALP-RP-MA-EA-21316-CLS

Ramonville, February 6, 2006

Envisat RA2/MWR ocean data validation and cross-calibration activities

Contract N° 03/CNES/1340/00-DSO310

	AUTHORS	COMPANY	DATE	INITIALS
WRITTEN BY	Y.Faugere	CLS		
APPROVED BY	J.Dorandeu	CLS		
QUALITY VISA	M.Destouesse	CLS		
APPLICATION AUTHORISED BY	N.Picot	CNES		

CLS - 8-10 Rue Hermès - Parc Technologique du Canal - 31520 Ramonville St-Agne - FRANCE
Telephone 33 5 61 39 47 00 / Fax 33 5 61 75 10 14

DISTRIBUTION LIST

COMPANY	NAMES	COPIES
CLS/DOS	Y.FAUGERE	1 electonic copy
	J.DORANDEU	1 electonic copy
	F.MERTZ	1 electonic copy
	V.ROSMORDUC	1 electonic copy
DOC/CLS	DOCUMENTATION	1 electonic copy
CNES	N.PICOT	1 copy + 1 electonic copy
CNES	D.SCHOLLER	1 copy + 1 electonic copy
CNES	J.LAMBIN	1 electonic copy
CNES	S.COUTIN-FAYE	1 electonic copy
CNES	P.SNINI	1 electonic copy
CNES	J.NOUBEL	1 electonic copy

CHRONOLOGY ISSUE

Control Initials	ISSUE	DATE	REASON FOR CHANGE
			Creation

LIST OF ACRONYMS

TBC	To Be Confirmed

List of Tables

List of Figures

Contents

APPLICABLE DOCUMENTS / REFERENCE DOCUMENTS

1 Introduction

This report is an overview of Envisat validation and cross calibration studies carried out at CLS during the year 2005. It is basically concerned with long-term monitoring of the Envisat altimeter system over ocean. Data from GDR cycles 10 through 40 spanning three years have been used for this analysis. All relevant altimeter parameters deduced from Ocean 1 retracking, radiometer parameters and geophysical corrections are evaluated and tested. This work is routinely performed at CLS, as part of the SSALTO and funded by ESA through F-PAC activities (SALP contract N° 03/CNES/1340/00-DSO310 Lot 2C). In this frame, besides continuous analyses in terms of altimeter data quality, Envisat GDR Quality Assessment Reports (e.g. Faugere et al. 2004) are routinely produced in conjunction with data dissemination. Some of the results described here were presented at the Quality Working Group (QWG) meeting (Toulouse, September 2005) and in a paper (Faugere et al, 2005 [18]).

The work performed in terms of data quality assessment also includes cross-calibration with Jason-1, ERS-2 and T/P. This kind of comparisons between coincident altimeter missions provides a large number of estimations and consequently efficient long-term monitoring of instrument measurements. This enables the detection of instrument drifts and inter-mission biases essential to obtain a consistent multi-satellite data set. Envisat Sea Level Anomalies (SLA) are also compared to an independent dataset, a tide gauge network.

After a preliminary section describing the data used, the report is split into 5 main sections: first, data coverage and measurement validity issues are presented. Second, monitoring of the main altimeter and radiometer parameters is performed, describing the major impact in terms of data accuracy. Then, performances are assessed and discussed with respect to the major sources of errors. Finally, Envisat Sea Surface height (SSH) bias and MSL issues are analyzed. Finally, the performance of the algorithms and corrections associated with the new generation of GDR are analysed.

2 Quality overview

Nearly three years of Envisat altimetric observations over ocean are available in Geophysical Data Record (GDR) products. Envisat data show good general quality over ocean. The unavailability of data is lower than 5% on most of the cycles from cycle 23 onwards. The MWR availability has also strongly improved. Moreover, some modifications have been performed by ESA to decrease the duration of the S-Band anomaly events. Statistics and performances of altimeter and radiometer parameters are consistent with expected values. A good orbit quality and a low level of noise allow Envisat to reach the high level of accuracy of other precise missions such as T/P and Jason-1. Some issues raised in this report, as the gravity induced orbit errors, will be solved in the next version of GDR products. Some others, as the Envisat Mean Sea Level in the first year, still need further investigation.

3 Data used and processing

3.1 Data used

Envisat Geophysical Data Records (GDRs) from cycle 10 to cycle 40 have been used to derive the results presented in this report. This corresponds to a nearly three-year time period spanning from September 30th 2002 to September 19th 2005. The routine production started on September 2003 with cycle 15. In parallel, a backward reprocessing of cycle 14 to 9 has been implemented. With only 7 days of available data, cycle 9 has not been used in this work.

12 GDR cycles have been produced this year: cycle 31 to 40 as part as the current processing and cycle 10 and 9 as part at the reprocessing activities.

As shown by table 1 several IPF processing chain and CMA Reference Software have been used to produce the 32 cycles of GDR. Tables 2 and 3 describe the main evolutions respectively associated with the version of IPF and CMA. During the processed period, only the change from IPF 4.54 to IPF 4.56 add an impact on the data. Consequently, from cycle 19 onwards and for the reprocessed cycles 10 to 14, the Automatic Gain Control (AGC) evaluation and the Intermediate Frequency (IF) mask correction (with slight impact on the data) have been modified. Note that GDR products of cycle 15 to 17 have been produced by the CMA software using Level 1B directly supplied by the two Payload Data Handling Station (PDHS) in Kiruna and Frascati. From cycle 18 there is a new step in the Level 1B generation loop: the Low Rate Reference Archive Center (LRAC) receives Level 1 B from PDHS and produces a consolidated Level 1B. The CMA uses now this consolidated Level 1B to produce GDRs.

Cycles	IPF version	CMA version
9 to 10	4.58	6.3
11 to 12	4.57	6.3
13 to 14	4.56	6.3
15 to 21	4.54	6.1
22 to 24	4.56	6.2
25 to 26	4.56	6.3
27 to 28	4.57	6.3
29 to 40	4.58	6.3

Table 1: *P*rocessing version

Version	Changes
IPF 4.56	-Extrapolation of AGC value to the Waveform center (49.5) for both Ku- and S-Band -Correction for an error found in the evaluation of S band AGC
IPF 4.57	No impact on data
IPF 4.58	-Addition of a Pass Number Field in FD Level
IPF 5.02	-MWR Side Lobe correction upgrade -USO clock period units correction -Rain Flag tunning to compensate for the increase of the S band Sigma0 -Monthly IF estimation -Level 1B S-Band anomaly flag -DORIS Navigator CFI upgrade (RA-2 and MWR)

Table 2: *I*PF versions

Version	Changes
CMA 6	-MSS CLS01 -Rain flag -Updated OCOG retracker thresholds Ice1/Sea Ice Conf file -Sea State Bias Table file -GOT00.2 Ocean Tide Sol 1 Map file -FES 2002 Ocean Tide Sol 2 Map file -FES 2002 Tidal Loading Coeff Map
CMA 7.1	-Improving the mispointing estimation -Addition of square of the SWH in Ku and S band -Addition of GOT2000.2 loading tide

.../...

Version	Changes
	-FES2004 tide and loading tide -New DEM AUX file (MACESS) merge of ACE land elevation data and Smith and Sandwell ocean bathymetry -New orbit -New SSB -new wind table -Mog2D -new S1S2 wave model in dry troposphere -GOT00.2 includes two extra waves, S1 and L2

Table 3: *C*MA versions

Note that Cycle 41 will be produce with the IPF 5.02/CMA 7.1 which includes a lot of changes. These evolutions are described in [12]

3.2 Processing

To perform this quality assessment work, conventional validation tools are used including editing procedures, crossover analysis, collinear differences, and a large number of statistical monitoring and visualization tools. All these tools are integrated and maintained as part of the CNES SSALTO (Segment Sol Altimétrie et Orbitographie) ground segment and F-PAC (French Processing and Archiving Centre) tools operated at CLS premises. Each cycle is carefully routinely analyzed before data release to end users. The main data quality features are reported in a cyclic quality assessment report available on http://www.aviso.oceanobs.com/html/donnees/calval/validation_report/en/welcome_uk.html. The purpose of this document is to report the major features of the data quality from the Envisat mission.

As for all other existing altimeters, the Envisat GDR data are ingested in the Calval 1-Hz altimeter database maintained by the CLS Spatial Oceanography Division. This allows us to cross-calibrate and cross-compare Envisat data to other missions. In this study data from Jason-1 (GDRs cycles 27 to 135), ERS-2 (OPRs Cycle 78 to 108), and TOPEX/Poseidon (T/P) (MGDRs cycle 370 to 478) are used. Jason-1 is the most suitable for Envisat cross calibration as it is available throughout the Envisat mission and has been extensively calibrated to T/P (Dorandeu et al., 2004b [9]). Comparisons between Jason-1 and Envisat altimeter and radiometer parameters have been carried out using 10-day dual crossovers for SSH comparison and 3-hour dual crossovers for altimeter and radiometer comparisons. The geographical distribution of the dual crossovers with short time lags strongly changes from one Envisat cycle to another. Indeed, contrary to Envisat which is sun-synchronous, Jason-1 observes the same place at the same local time every 12 cycles (120-day). Following the method detailed in Stum et al. (1998) [45], estimates of the differences are computed using a 120 day running window to keep a constant geographical coverage. ERS-2, flying on same ground track as Envisat only 30 minutes apart, has had a coverage limited to the North Atlantic since the failure of the on-board register in June 2003 (EOHelp message of 4 July 2003). To improve the significance of the Envisat/ERS-2 comparison, long term monitoring of altimeter parameters difference is performed on this restricted area all over the Envisat period using a repeat-track method. T/P is used for

global cross comparisons of the mean sea level trend as this mission provides a precise long term reference.

Most of this work has been carried out using parameters available in the GDR products. However, a few updates have been necessary to complete the analyses:

- a method has been developped to detect data corrupted by S-Band anomaly (see 4.3.1)
- a method has been developped to detect data corrupted by sea ice (see 4.3.2)
- filtered dual frequency ionosphere correction: A 300-km low pass filter is applied along track on the dual frequency ionosphere correction to reduce the noise of the correction.
- A correction to the range is also applied based on the Ultra-Stable Oscillator (USO) clock period variation correction. Indeed, the USO clock period, which performs the computation of the Ra-2 window time delay, is affected by a drift due to the ageing of the device. The method to correct the USO clock period is described in Celani (2002 [4]). The correction is regularly updated in the IPF ground processing via an Auxiliary data file. However, due to an anomaly in the ADF format, the correction is not taken into account (Martini, 2003 [31]) in the products. This anomaly will be corrected in the IPF 5.02. For the time being, ESA supplies auxiliary files to allow users correcting their own database (Martini, 2003 [31]), (http://earth.esa.int/pcs/envisat/ra2/auxdata/).
- pressure values used for computing the inverse barometer and the dry troposphere corrections have been derived from the ECMWF rectangular grids. Errors due to the bathymetry, up to several centimeters near the coasts, significantly impact the accuracy the so-called gaussian grids used as input of the Envisat (and Jason-1) ground processing (e.g. Dorandeu et al., 2004b [9]).
- as Jason-1 doesn't fly at the same altitude as Envisat, and ERS-2 has a mono-frequency altimeter on-board, it is not possible to use these satellites to assess the Envisat ionosphere path delay. Thus the JPL GPS-based global Ionospheric Maps (GIM) containing the vertical ionospheric total electron content are used here.

4 Missing and edited measurements

This section mainly intends to analyze the ability of the Envisat altimeter system to correctly sample ocean surfaces. This obviously includes the tracking capabilities, but also the frequency of unavailable data and the ratio of valid measurements likely to be used by applications after the editing process.

4.1 Missing measurements

From a theoretical ground track, a dedicated collocation tool allows determination of missing measurements relative to what is nominally expected. The cycle by cycle percentage of missing measurements over ocean has been plotted in figure 1. The measurement unavailability is more than 8% in average. Seven cycles have more than 10% of unavailability, notably from cycle 13 to cycle 17. Passes 1 to 452 of cycle 15 have not been delivered because of a wrong setting of RA-2. This explains the high ratio of missing measurements for this cycle. Several long RA-2 events occurred during cycles 13, 14, 16, 17, 22 and 34 which resulted in a significant number of missing passes. The list of instrument and platform event is available in Appendix 1. Apart from instrumental and platform events, up to 3% of measurements can be missing because of data generation problems at ground segment level. Notice however that the situation has been largely improved with a mean data availability of more than 95% from the beginning of 2004 (cycle 23 onwards). Figure 2 shows an example of missing measurements for cycle 40. Within this cycle, 20 passes are completely missing along with segments missing from several other passes. A part from the instrumental and platform event, 1 to 30 passes can be missing because of either to LRAC_PDHSs data generation to level1 problems or ingestion problems on F-PAC side.
The measurements which are missing over the Himalayan region are due first to the IF Calibration Mode. Moreover, daily instrument switch-offs (Heater 2 mode) are performed over this region to prevent the S-Band anomaly. Apart from that, the data retention rate is very good on every surface observed. This might be due to the tracker used by Envisat Ra-2, the Model Free Tracker (MFT).

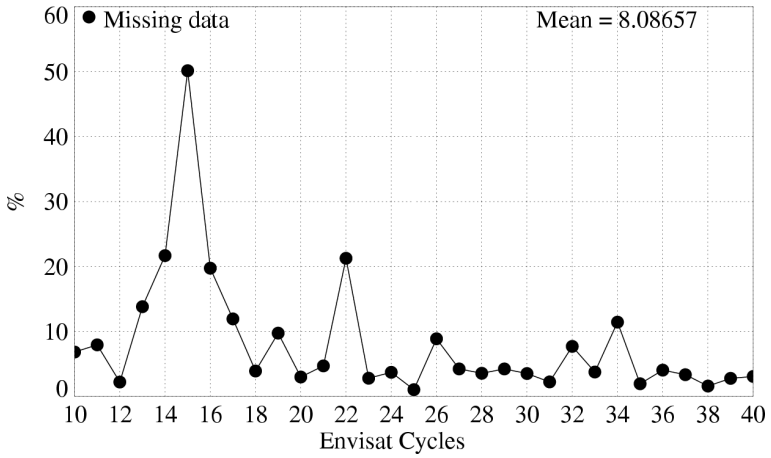

Figure 1: *Monitoring of the percentage of missing measurements relative to what is theoretically expected over ocean*

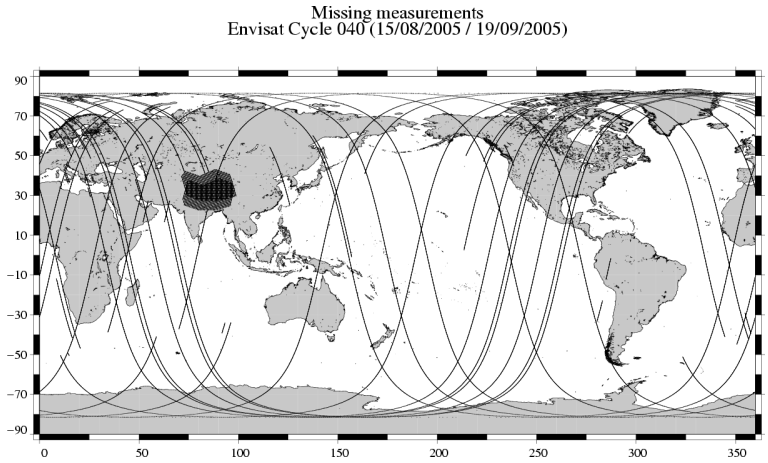

Figure 2: *Envisat missing measurements for cycle 40*

4.2 Missing mwr

The Envisat MWR exhibits nearly 100% (Dedieu et al., 2005) of availability since the beginning of the mission. However, MWR corrections can be missing in the GDRs due to data generation problems at ground segment level. When the Land/sea radiometer flag is set over ocean, it means that the radiometer data is missing. The percentage of missing MWR corrections over ocean has been plotted in figure 3. The mean value is around 2.6% but the radiometer unavailability is not constant. It is greater than 4% for cycles 14 to 19 but lower than 2% from cycle 21 onwards. From cycle 34 onwards the availability of the MWR correction is almost 100%, which is encouraging.

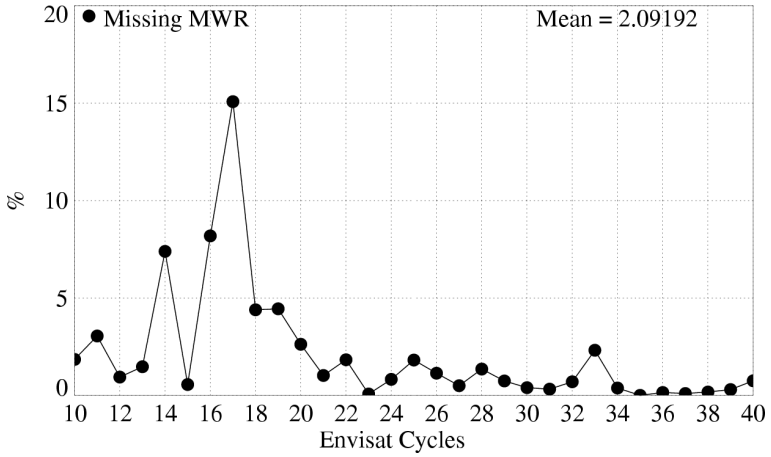

Figure 3: *Cycle per cycle percentages of missing MWR measurements*

4.3 Edited measurements

Data editing is necessary to remove altimeter measurements having lower accuracy. There are 4 steps in the editing procedure. The first step of the editing procedure consists in removing data impacted by the S-Band anomaly or corrupted by sea ice. Then, measurements are edited using thresholds on several parameters. The third step uses cubic splines adjustments to the ENVISAT Sea Surface Height (SSH) to detect remaining spurious measurements. The last step consists in removing entire pass where SSH-MSS mean and standard deviation have unexpected value.

4.3.1 Measurements impacted by S-Band anomaly

During the Commissioning Phase, it has been discovered that the RA-2 data are affected by the so-called S-Band anomaly. The anomaly results in the accumulation of the S-Band echo waveforms (Laxon and Roca, 2002 [24]). It happens randomly after an acquisition sequence and is only stopped by switching the Ra-2 in a Stand-By mode. When this anomaly occurs, the S-Band waveforms are not meaningful. Consequently, all the S-Band parameters and the Dual Frequency ionosphere correction are not reliable. Notably, the S-band Sigma0 is unrealistically high during these events. Thus applying a threshold of 5 dB on the (Ku-S) Sigma0 differences is very efficient for detecting the impacted data over ocean. The ratio of flagged measurements over ocean is plotted in figure 4. Between 0 and 8% of the data are impacted. From cycle 31 onwards, some modifications have been performed by ESA to decrease the duration of these events: instrument switch-offs (Heater 2 mode) are performed twice a day over the Himalayan region. This prevents the S-Band anomaly from lasting more than half a day when it occurs. Thanks to this procedure the ratio of impacted data decreased from 4.2% (cycles 11 to 30) to 2.2% (cycles 31 to 38). A method has been developed to flag the impacted data over all surfaces (Martini et al., 2005 [32]). It will be available in the next GDR version. The reconstruction of normal echoes from accumulated waveforms is also currently under study (Martini et al., 2005 [32]).

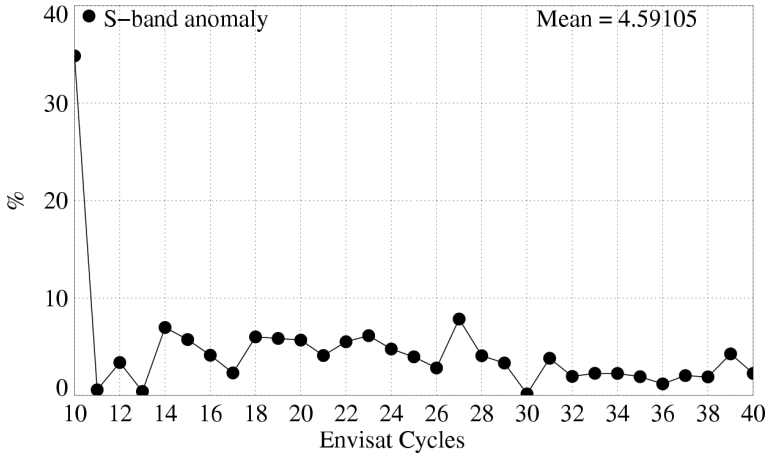

Figure 4: *Cycle per cycle percentages of data impacted by the S-Band anomaly*

4.3.2 Measurements impacted by Sea Ice

Since Envisat operates between 82N and 82S of latitude, sea ice is an important issue for oceanic applications. No ice flag is currently available in the Envisat products, therefore alternate sea ice detection techniques are employed in order to retain only open ocean data. A study performed during the validation phase showed that the combination of altimetric and radiometric criteria was particularly efficient to flag most of the data over ice. The method is described in detail in (Faugere et al, 2003 [16]). We employ the Peakiness parameter (Lillibridge et al, 2005 [28]) in conjunction with the MWR- ECMWF wet troposphere difference which appears to be a good means to complement the Peakiness parameter in all ice conditions. The ratio of flagged measurements over ocean is plotted on 5

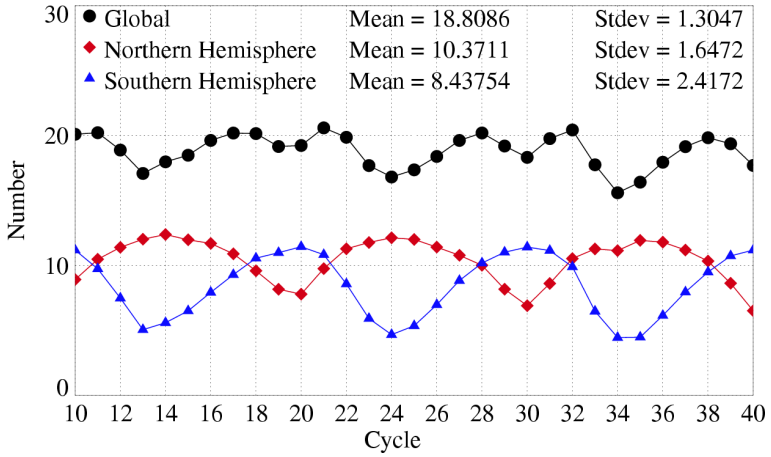

Figure 5: *% of edited points by sea ice flag over ocean, Northern Hemisphere (left), Southern Hemisphere (right)*

4.3.3 Editing by thresholds

The second step of the editing procedure consists in using thresholds on several parameters. The minimum and maximum thresholds used in the routine quality assessment are given in table 4.

Parameter	Min thresholds	Max thresholds
Sea surface height	−130	100
Variability relative to MSS (m)	−2	2
Number of 18Hz valid points	10	–
Std deviation of 18Hz range (m)	0	0.25
Off nadir angle from waveform (deg2)	−0.200	0.160
Dry troposphere correction	−2.500	−1.900
Inverted barometer correction	−2.000	2.000
		.../...

Parameter	Min thresholds	Max thresholds
MWR wet troposphere correction	-0.500	0.001
Dual Ionosphere correction	-0.200	-0.001
Significant waveheight	0.0	11.0
Sea State Bias	-0.5	0
Backscatter coefficient (dB)	7	30
Ocean tide height	-5	5
Long period tide height	-0.500	0.500
Earth tide	-1.000	1.000
Pole tide	-5.000	5.000
RA2 wind speed	0.000	30.000

Table 4: *E*diting criteria

The thresholds are expected to remain constant throughout the ENVISAT mission, so that monitoring the number of edited measurements allows a survey of data quality. The percentage of edited measurements over ocean for the main altimeter and radiometer parameters has been plotted in figure 6. These ratios are very stable and surprisingly low over the period if compared to other altimeters. The RMS of elementary measurements has the strongest ratio among the altimeter parameters, more than 1%. A slight seasonal signal is visible on the curve, mostly due to sea state seasonal variations. The number of elementary measurements has a surprisingly low ratio, except for cycles 14 and 20 when wrong configuration files were uploaded onboard after a RA-2 event. The square of the off-nadir angle derived from waveforms leads to very stable editing ratio. Variations of this parameter can reveal actual platform mispointing, if any, but can also reveal waveform contamination by rain or by sea-ice. It is indeed computed from the slope of trailing edge when fitting a typical ocean model to the waveforms. No seasonal signal is visible which may prove that the sea-ice detection method is efficient. The dual frequency ratio shows a slight increasing trend between cycles 15 and 28 which cannot be considered as significant, given the scatter of the curve. The Ku-band SWH, sigma0 and MWR ratios are very stable and low, less than 0.2% with no seasonal variations.

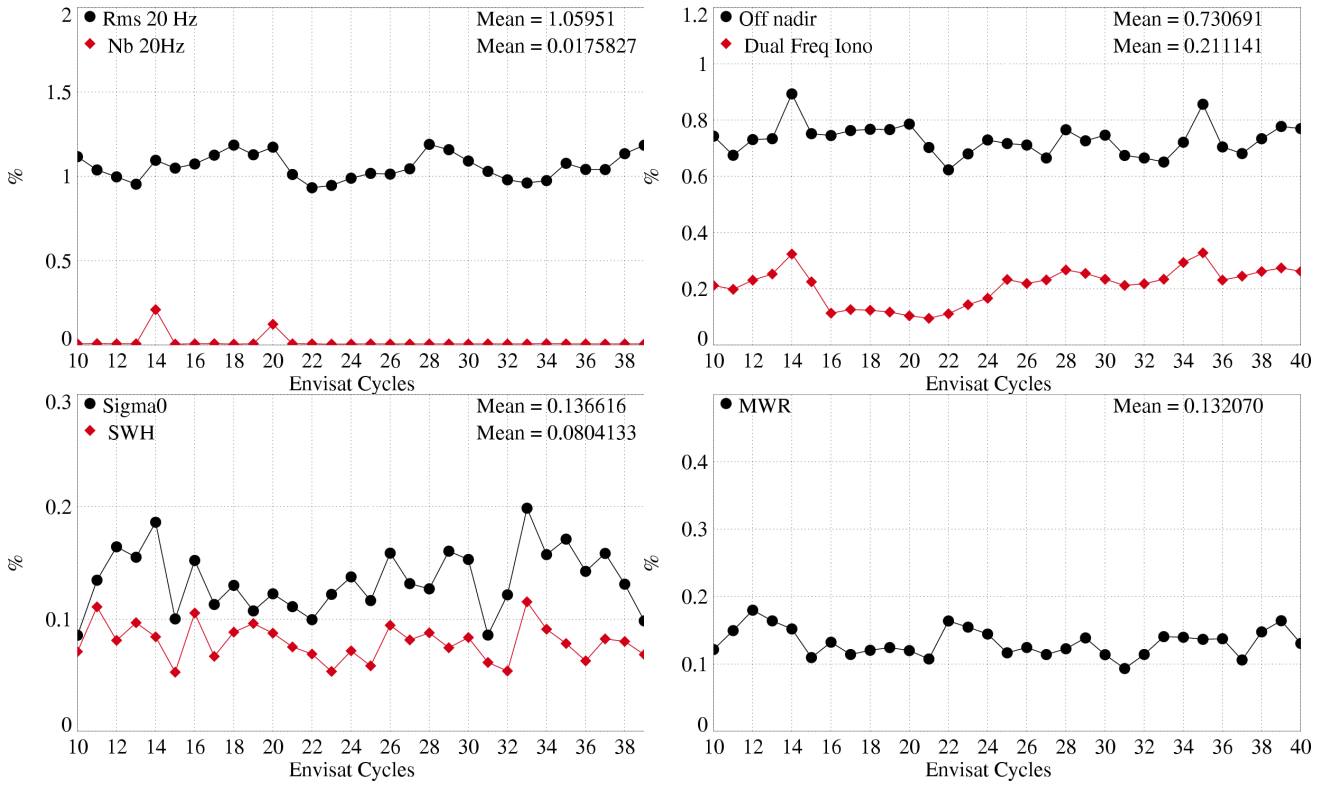

Figure 6: *Cycle per cycle percentages of edited measurements by the main Envisat altimeter and radiometer parameters: top-right) Standard deviation of 20 Hz range measurements ¿ 25 cm, Number of 20-Hz range measurements ¡ 10 top-left) Square of off-nadir angle (from waveforms) out of the [-0.2 deg2, 0.16 deg2] range, dual frequency ionosphere correction out of [-40 , 4 cm] bot-right) Ku-band Significant wave height outside ¿ 11 m, Ku band backscatter coefficient out of the [7 dB, 30 dB] range bot-left) MWR wet troposphere correction out of the [-50 cm, -0.1 cm] range.*

4.3.4 Editing on SLA

It has been necessary to apply additional editing criteria on SSH-MSS differences in order to remove remaining spurious data. The first criterion consists in removing measurements with SSH-MSS greater than 2m. The strong value on cycle 30 is due to abnormal behavior of the RA-2 sensor during nearly two days. Just after a RA-2 recovery, the range value jumped by several meters for a still unexplained reason. The second criterion was necessary to detect measurements impacted by maneuvers. Maneuvers are necessary to compensate the effect of gravitational forces but can have a strong impact on the orbit quality. Two types of maneuvers are operated to maintain the satellite ground track within the +/-1km deadband around the reference ground track: in-plane maneuvers, every 30-50 days, which only impact the altitude of the satellite and out-of-plane maneuvers, three times a year, to control the inclination of the satellite (Rudolph et al., 2005). The out-of-plane maneuvers are the most problematic for the orbit computation. The second criterion consists in testing the mean and standard deviation of the SSH-MSS over each entire pass. If one of the two values, computed on a selected dataset, is abnormally high, then the entire pass is edited.
A specific study has been performed to determine how to compute the statistics, and what threshold should be applied. The statistics have to be computed on very stable area. The criteria for selecting the area and the thresholds are detailed is:

- The latitude: the range value can be degraded near the ice, despite the use of the ice flag. Moreover, the MSS is less accurate over 66°, as it has been computed without Topex data.
- The oceanic variability: the standard deviation of SLA can be very high because of the mesoscale variability. Areas with high oceanic variability have to be removed to detect the abnormally high standard deviation.
- The bathymetry and distance from the coast: A lot of corrections (tides for example) are less accurate in low bathymetry areas and near the coast (Japan sea).
- The sample: The statistic have to be computed on a significant number of points

All those criteria have been tested and combined. The results are in Annex. The conclusion is that two criteria are needed:

1st criteria: for small portion of pass (less than 200 points) the sample is not big enough to compute reliable statistic. The selection must not be severe:

Selected areas: latitude>66°, variability<30cm, bathymetry>1000m, distance<100km

Threshold: 30 cm on mean and standard deviation

2nd criteria: for other passes

Selected areas: latitude>66°, variability<10cm, bathymetry>1000m, distance<100km

Threshold: 15 cm on mean and standard deviation

The percentage of edited measurements over ocean for the main altimeter and radiometer parameters has been plotted in figure 7. On cycles 11, 12, 21 and 26, several full passes have been edited because of bad orbit quality related to out-of-plane manoeuvre or lack of Doris data (cycle 11).

4.3.5 Conclusion

Figure 8 shows the cycle by cycle percentage of points edited.

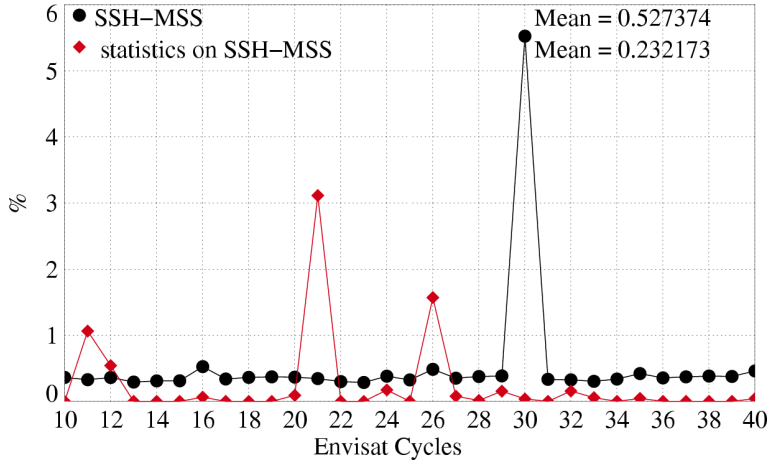

Figure 7: *SSH-MSS out of the [-2, 2m] and edited using thresholds on the mean and standard deviation of SSH-MSS on each pass*

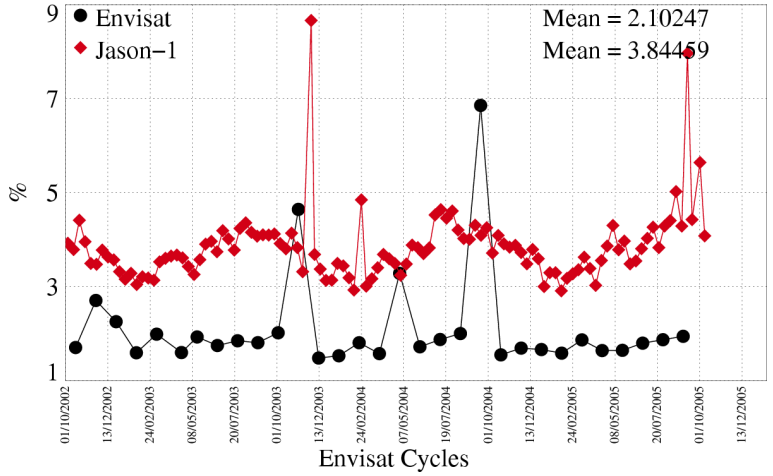

Figure 8: *Total percentage of edited points*

5 Long term monitoring of altimeter and radiometer parameters

All GDR fields are systematically checked and carefully monitored as part of the Envisat routine calibration and validation tasks. However, only the main Ku-band parameters are presented here, as they are the most significant in terms of data quality and instrumental stability. Furthermore, all statistics are computed on valid ocean datasets after the editing procedure.

5.1 Number and standard deviation of 20Hz elementary Ku-band measurements

As part of the ground segment processing, a regression is performed to derive the 1 Hz range from 20 Hz data. Through an iterative regression process, elementary ranges too far from the regression line are discarded until convergence is reached. The mean number and RMS of Ku 20Hz elementary data used to compute the 1Hz average are plotted in figure 9. These two parameters are nearly constant, which provides an indication of the RA-2 altimeter stability. The mean number of Ku 20Hz values over one cycle is about 19.97. This value is very high compared to other altimeters. It is almost not disturbed in wet areas or near the coast. The two drops on the Ku-band on cycles 14 and 20 are due to wrong setting of the RA-2 just after recovery. A slight seasonal signal is visible on the mean RMS of Ku 20Hz. Higher values correspond to higher waves occurring during the austral winter. The mean value is about 9.0 cm. This value represents a rough estimation of the 20 Hz altimeter noise (Zanifé et al. 2003, Vincent et al. 2003a).Assuming that the 20Hz measurements have uncorrelated noise, it corresponds to a noise of about 2 cm at 1Hz. It is consistent with the expected noise values.
Histograms of RMS of Ku and S-band Range are plotted in figure 10.

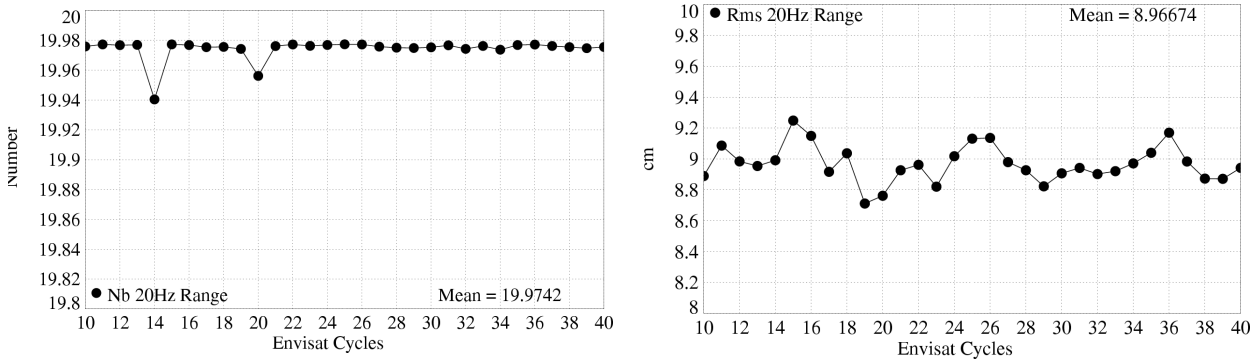

Figure 9: *top) Cycle mean of the number of 20 Hz elementary range measurements used to compute 1 Hz range. bot) Cycle mean of the standard deviation of 20 Hz measurements.*

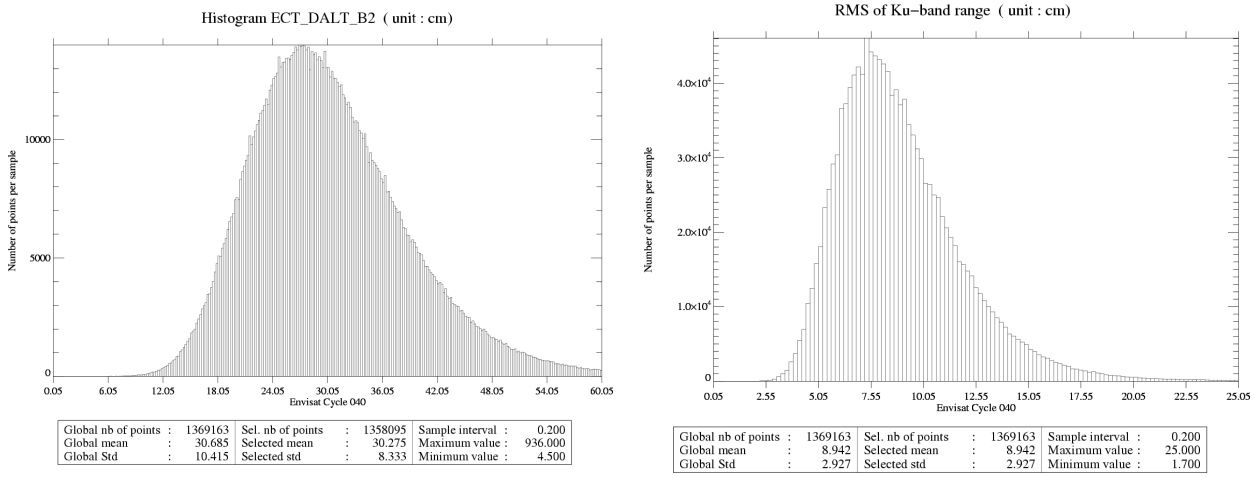

Figure 10: *Histogram of RMS of Ku and S range (cm)*

5.2 Off-nadir angle from waveforms

The off-nadir angle is estimated from the waveform shape during the altimeter processing. The square of the off-nadir angle is plotted in figure 11. The mean value is about 0.026 deg2. This mean value is not significant in terms of actual platform mispointing. This is due to the way the slope of the waveform trailing edge is computed and will be corrected in the next GDR version. The 0.005 deg2 jump between cycles 21 and 22 is due to the upgrade of the IF mask filter auxiliary data file. The slight rising trend observed on the curve might be due to the onboard filter which is not current (last update was November 2003).
The histogram of the squared mispointing is plotted in figure 12.

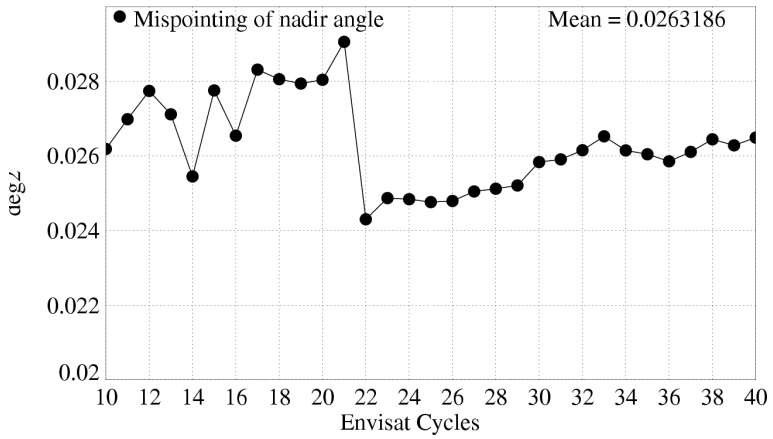

Figure 11: *Cycle mean of the square of the off-nadir angle deduced from waveforms (deg2).*

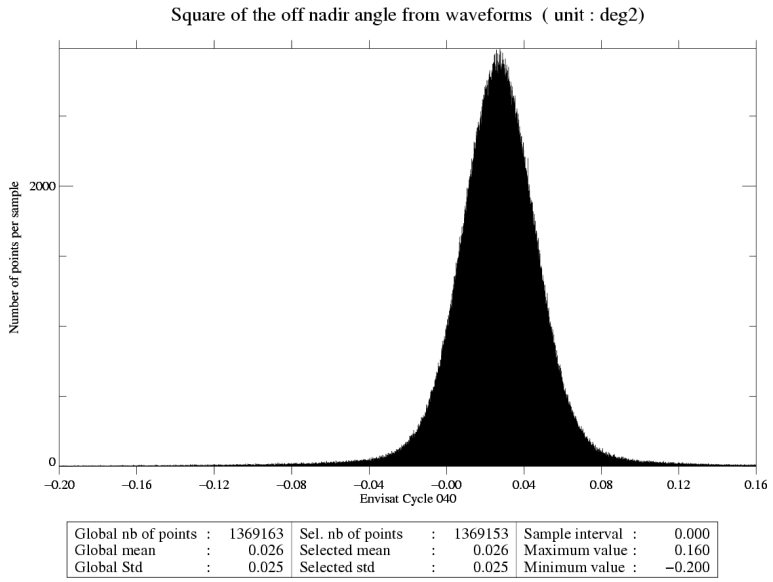

Figure 12: *Histogram of off-nadir angle from waveforms (deg2)*

5.3 Significant Wave Height

The cycle by cycle mean and standard deviation of Ku and S-band SWH are plotted in figure 13. The curve reflects sea state variations. The mean value of Ku SWH is 2.66 m. The S-band mean SWH is very close, less than 10 cm apart. The cycle by cycle mean of Envisat-Jason-1 differences and ERS-2-Envisat differences are plotted in figure 13. These differences are quite stable. Envisat SWH is respectively 15 cm and 22 cm higher than Jason-1 and ERS-2 SWH. Histograms of Ku and S-band SWH are plotted in figure

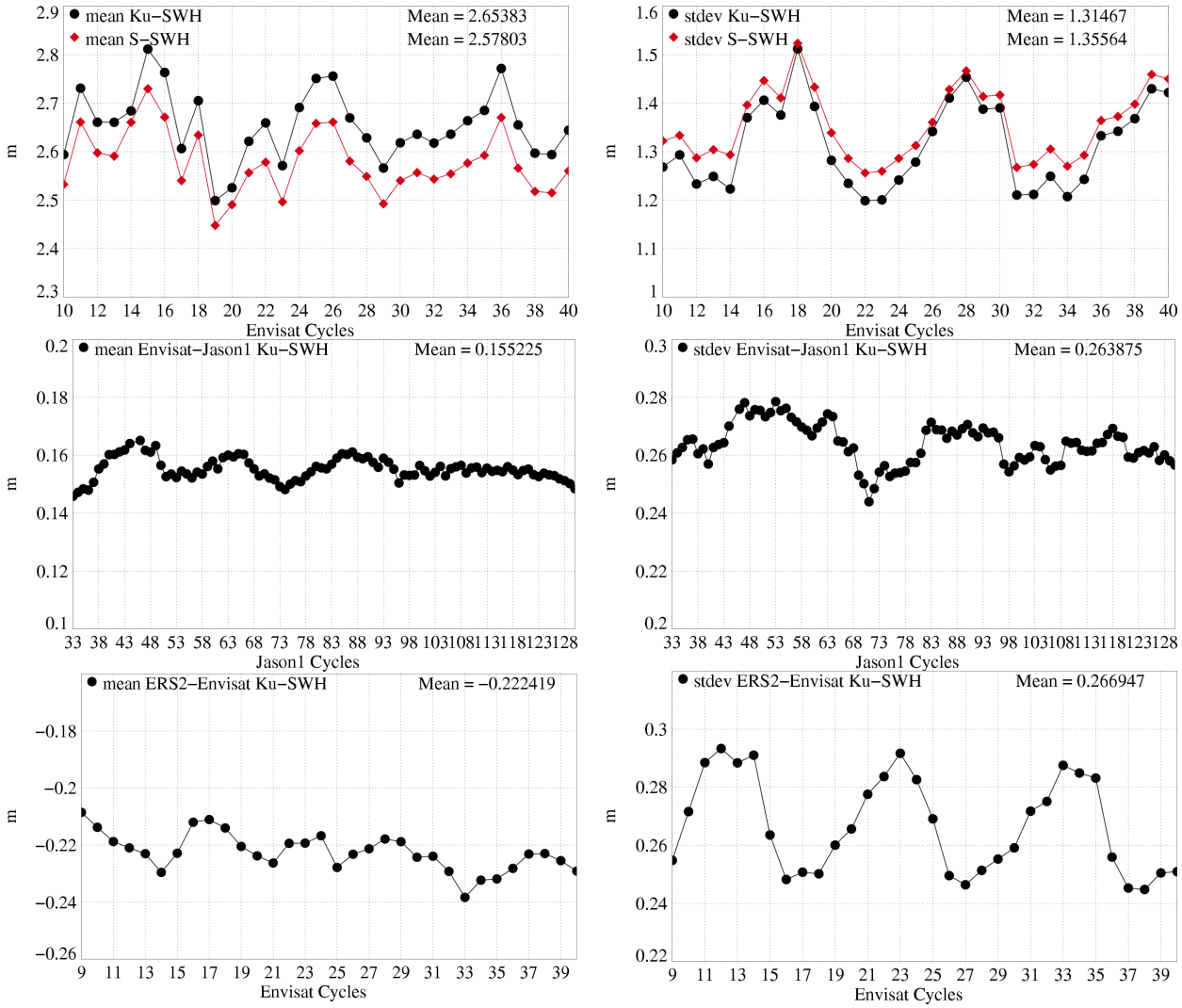

Figure 13: *Global statistics (m) of Envisat Ku and S SWH top-right) Mean and top-left) Standard deviation. bot-right) Mean Envisat-Jason-1 Ku SWH differences at 3h EN/J1 crossovers computed with 120 days running means. bot-left) Mean. ERS-2-Envisat Ku SWH collinear differences over the Atlantic Ocean.*

14. The Ku SWH histogram has a good shape.

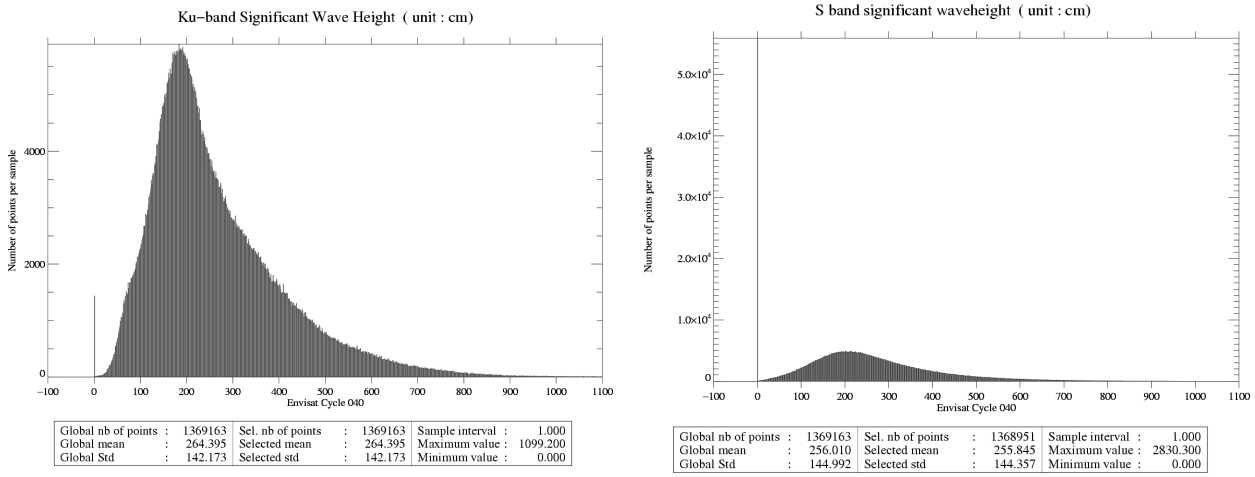

Figure 14: *Histogram of Ku and S SWH (m)*

5.4 Backscatter coefficient

The cycle by cycle mean and standard deviation Ku and S-band Sigma0 are plotted in figure 15. Note that a -3.5 dB bias has been applied (Roca et al., 2003 [39]) on the Ku-band Sigma0 in order to be compliant with the wind speed model (Witter and Chelton, 1991 [50]). The mean values in Ku band are stable, around 11.1 dB. Two 0.66 dB jumps are visible on the S-Band on cycles 14 and 22. They are due to a correction of the AGC evaluation. This modification has been included in IPF version 4.56, used from cycle 22 onwards for the current processing and for all the reprocessed cycles. The cycle by cycle mean of Envisat-Jason-1 differences and ERS-2-Envisat differences are plotted in figure 15. The mean difference between Envisat and Jason-1 Ku-band Sigma0 is -2.9 dB. This mean difference has increased by 0.07dB between cycles 48 and 118 which corresponds to 0.04 dB/year. This trend, though not really significant, has to be monitored in the next cycles. The mean ERS-2-Envisat Ku-band Sigma0 difference is 0.05 dB. However, this mean value accounts for the calibration correction applied in the ground processing to enter the wind speed algorithm (Witter and Chelton, 1991 [50]). The monitoring of (ERS-2 - Envisat) Sigma0 differences exhibits a 0.1 dB jump between cycles 38 and 39. This jump occurs at the end of cycle 38, on the 4th July 2005 11:29 UTC. Since no jump is observed on the Envisat/Jason-1 differences, it may be attributed to ERS-2. This jump is still under investigation.

Histograms of Ku and S-band Sigma0 are plotted in figure 16. The Ku Sigma0 histogram has a good shape.

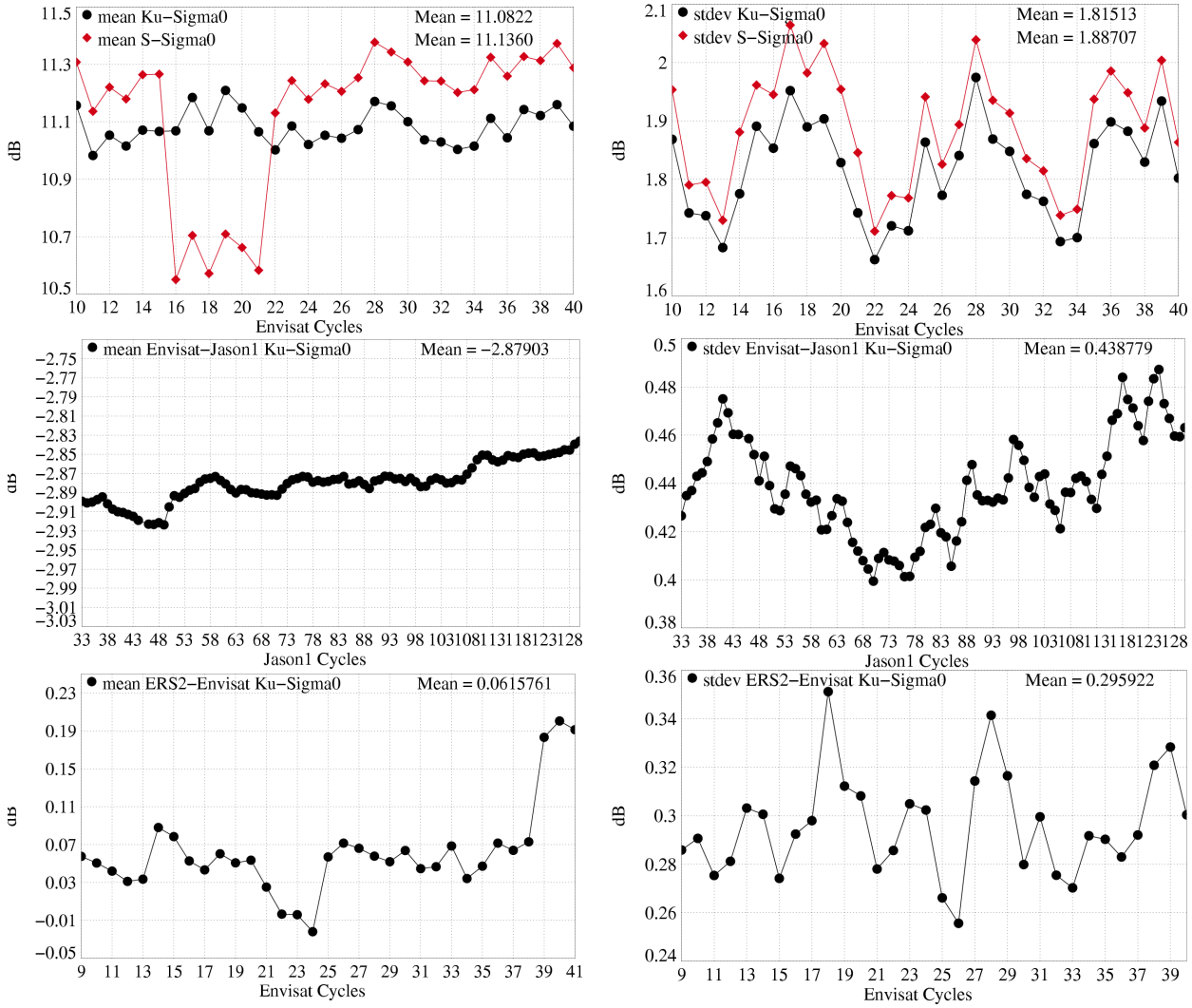

Figure 15: *Global statistics (dB) of Envisat Ku and S Sigma0 top-right) Mean and top-left) Standard deviation. bot-right) Mean Envisat-Jason-1 Ku Sigma0 differences at 3h EN/J1 crossovers computed with 120 days running means. bot-left) Mean ERS-2-Envisat Ku Sigma0 collinear differences over the Atlantic Ocean.*

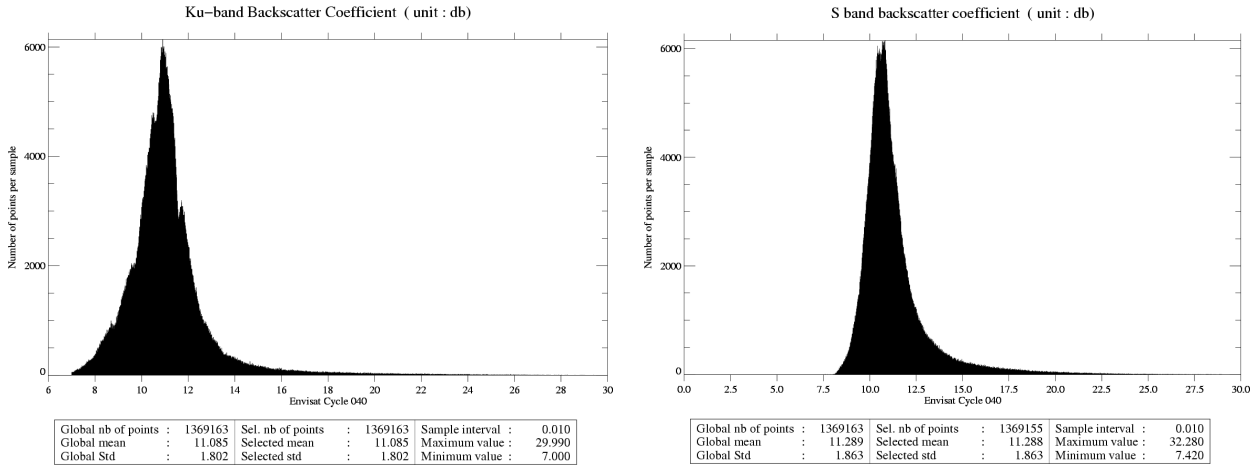

Figure 16: *Histogram of Ku and S Sigma0 (dB)*

5.5 Dual frequency ionosphere correction

As performed on TOPEX (Le Traon et al. 1994 [25]) and Jason-1 (Chambers et al. 2002 [5]) it is recommended to filter dual frequency ionosphere correction on each altimeter dataset to reduce noise. A 300-km low pass filter is thus applied along track on the dual frequency ionosphere correction. As previously mentioned, the JPL GIM ionosphere corrections are computed to assess the dual frequency altimeter based ionosphere correction. The cycle by cycle mean of dual frequency and JPL GIM ionosphere correction are plotted in figure 17. The mean value of the two corrections is clearly decreasing since the beginning of Envisat mission due to inter-annual reduction of the solar activity. The mean differences (GIM-Dual frequency), plotted in figure 17, is very stable around -0.7 cm. It is stronger in absolute value for high ionosphere corrections, for descending passes (in the daytime). The standard deviation of the difference is plotted in figure 17. Low values, less than 2 cm, indicate a very good correlation between Dual-frequency and GIM corrections. However, in this analysis, the same sea state bias (SSB) has been used to correct the Ku and S-Band Ranges, as it is done so far in the GDR processing. Indeed, SSB correction is needed on the two bands before computing the dual frequency ionosphere correction from Ku and S-band ranges. Labroue (2004 [23]) computed a new ionospheric correction based on a suitable S-band Sea State Bias. The differences with the GDR correction are very small with no impact on the global statistics and only small geographic variations between -1 mm and +1.5 mm (Labroue 2004 [23]).

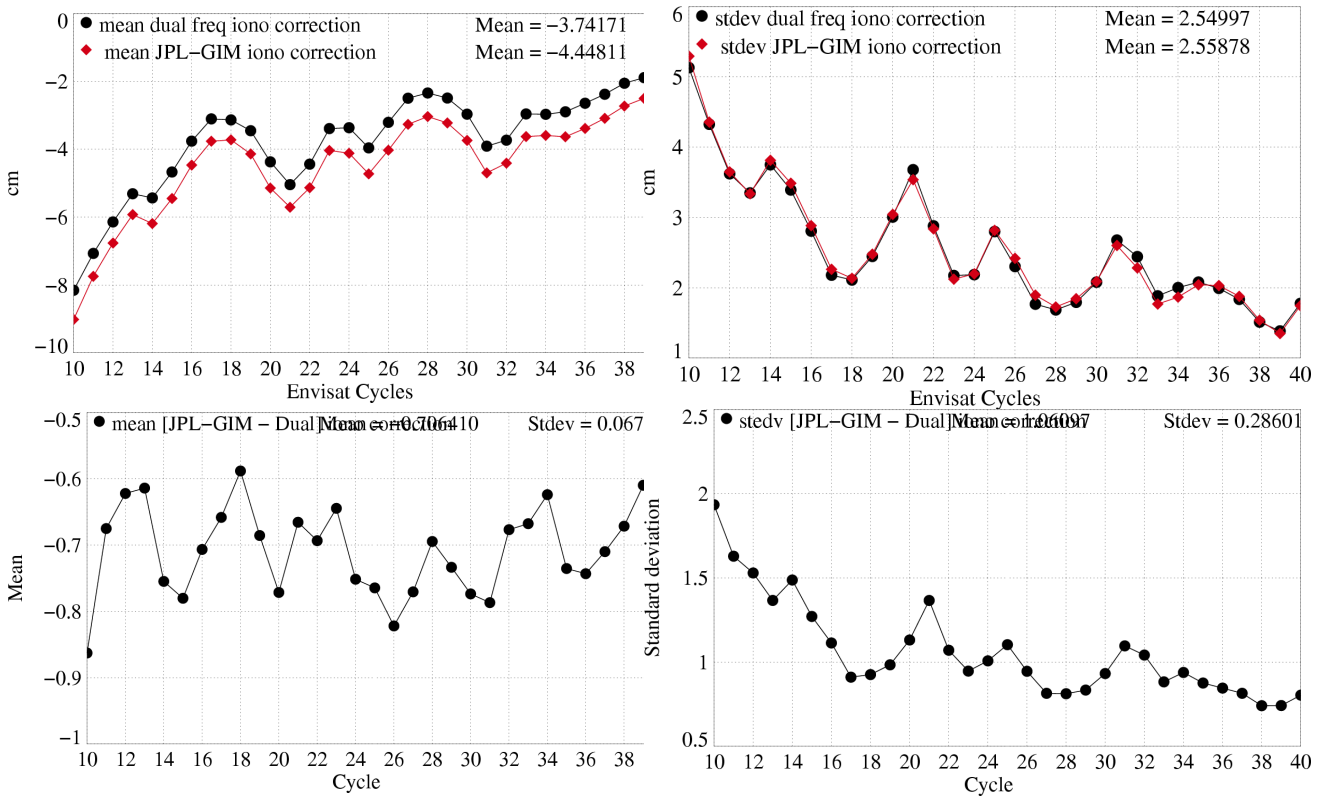

Figure 17: *Comparison of global statistics of Envisat dual-frequency and JPL-GIM ionosphere corrections (cm). top) Cycle mean and standard deviation of Dual Frequency and GIM correction. bot) Mean and standard deviation of the differences*

5.6 MWR wet troposphere correction

A neural network formulation has been used in the inversion algorithm retrieving the wet troposphere correction from the measured brightness temperatures (Obligis et al., 2005 [37]). As an example, the scatter plot of MWR correction according to ECMWF model for cycle 30 is given in figure 18. Since the beginning

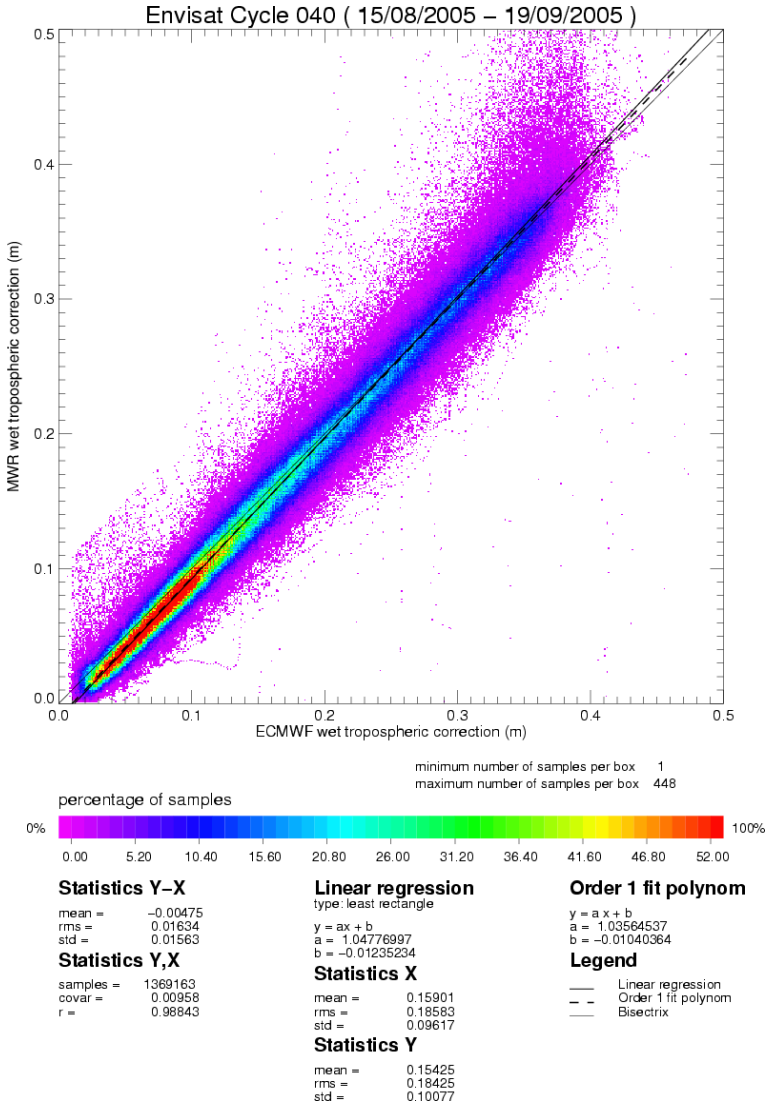

Figure 18: *Scatter plot of MWR correction according to ECMWF model (m)*

of the mission, the instrumental parameters at 36.5 GHz have been drifting and investigations are in progress to identify the source for these drifts. A correction of the TB36.8 GHz has been proposed in Tran et al., 2006 [48]. In particular, different behavior is observed depending on the brightness temperature values. Mean and standard deviation of (MWR-ECMWF model) differences are plotted in figure 19. The difference rises by 3mm between cycles 11 and 27, which corresponds to 1.8 mm/year. The difference seems to stabilize from cycle 27 onwards. The standard deviation drops down by 2 mm from cycle 13. This is due to a change in the ECMWF model on the 14th of January 2003 [11]. The impact of these changes has been found to be meteorologically positive, and it is confirmed by the improved consistency with the MWR. Note that this

change did not impact the MWR-ECMWF mean differences. A complete monitoring of all the radiometer parameters is available in the cyclic Envisat Microwave Radiometer Assessment (Dedieu et al., 2005 [6]).

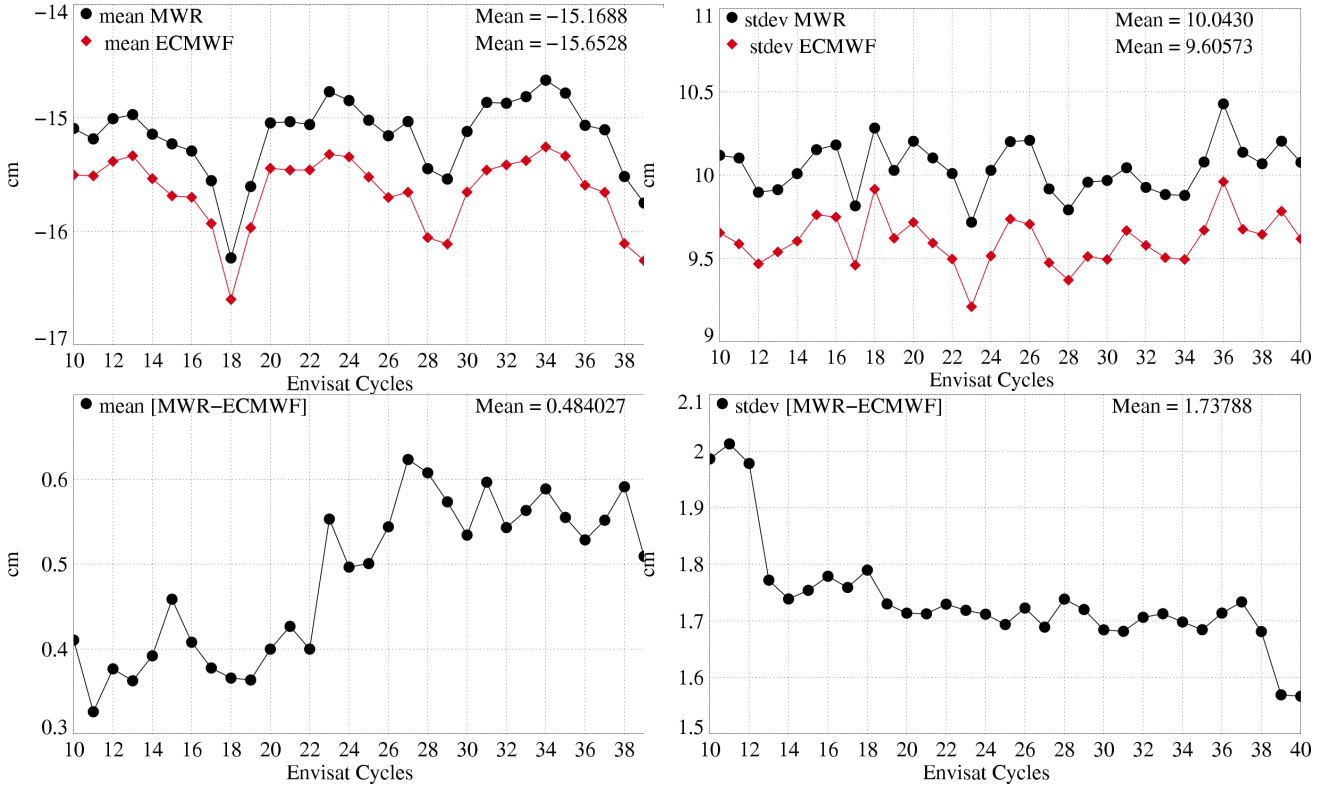

Figure 19: *Comparison of global statistics of Envisat MWR and ECMWF wet troposphere corrections (cm). top) Cycle mean and standard deviation of MWR and ECMWF corrections bot) Mean and standard deviation of the differences.*

The (ERS-2 -Envisat) cyclic 23.8 GHz brightess temperatures differences over the Atlantic area are plotted on figure 20. The ERS-2 drift proposed by Eymard et al., 2003 [14] is applied. The correction of the drift proposed by Scharroo et al., 2004 [44], should decrease the mean difference by 0.8K as described in Mertz et al., 2004 [34]. Nevertheless, the mean difference variations are more steady for the period after cycle 21.

The (ERS-2 -Envisat) TB36.5 GHz values are also reported in figure 20. The differences before and after cycle 18 have a different behaviour: one observes a great decrease from -2 to -4 K between cycles 13 and 17 whereas the curve seems to be steadier after cycle 18. This is not an impact of the coverage of the data since in the restricted area, the statistics reveals the same features. Tran et al., 2006 [48], propose a correction for the drift of the 36.5 GHz TB on Envisat. They also show an unusual behaviour of the TB values during that period. Note that this behaviour is not visible on hottest or coldest values but mainly on the mean values.

The impact of the drift of the TB36.5 on (ERS-2 -Envisat) wet troposphere correction differences is visible in figure 21. The correction proposed by Tran et al., 2006 [48] should reduce this trend.

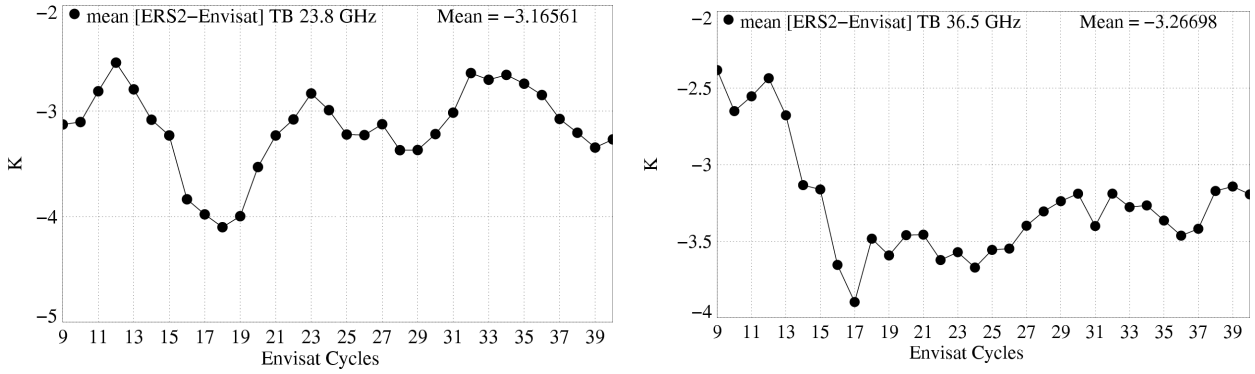

Figure 20: *Monitoring of the (ERS-2 - Envisat) brightness temperatures*

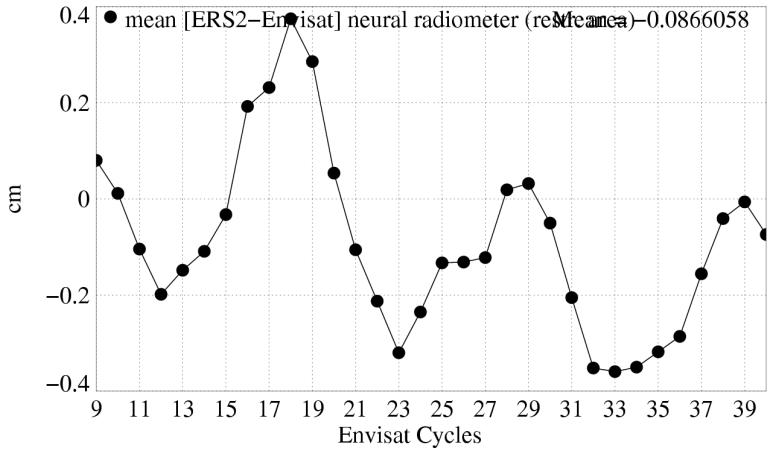

Figure 21: *Monitoring of the (ERS-2 - Envisat) wet troposphere correction*

6 Sea Surface Height performance assessment

One of the main objectives of the Calibration and Validation activities is to assess the performance of the whole altimeter system. This means that the quality of each parameter of the product is evaluated, in particular if it is likely to be used in the Sea Surface Height (SSH) computations. Conventional tools like crossover differences and repeat-track analyses are systematically used in order to monitor the quality of the system. The standard SSH calculation for Envisat is defined as: SSH= Orbit -Altimeter Range - SCorrections.

The orbit and corrections used for Envisat, Jason-1 and T/P are detailed in Table 1.

Correction	Description
Orbit	EN:CNES POE (grim5)
	J1:CNES POE (JGM3)
	TP:NASA POE (JGM3)
Additional Range correction	EN:USO correction
	J1:none
	TP:none
SSB	EN:Non parametric SSB (GDR)
	J1:Non parametric SSB (GDR)
	TP:Non parametric SSB (Labroue and gaspar, 2002 [20])
Inverse barometer	Based on ECMWF sea level pressure relative to global mean, rectangular grids
Wet troposphere	For performance assessment: MWR
	For MSL estimation: ECMWF model, Gaussian grids
Dry troposphere	Based on ECMWF sea level pressure, rectangular grids
Ionosphere J	Dual-frequency altimeter (filter 300km)
tides	Pole tide, solid earth tide, GOT00.2 ocean and load tides
Mean sea surface	CLS01V1

Table 5: *P*arameters used to compute SSH for ENVISAT and Jason

The Envisat SSB currently available in the GDR products has been designed during the validation phase from 3 cycles of data (10 to 12) (Labroue 2003 [22]). A new non parametric SSB has been estimated from crossover analyses from 1 year of data (17 to 26) and should be available in the next version. This new model leads to a SLA variance reduction of 0.35 cm2.

6.1 Crossover mean

SSH crossover differences are computed on a one-cycle basis, with a maximum time lag of 10 days, in order to reduce the impact of ocean variability which is a source of error in the performance estimation. The mean of crossover differences represents the average of SSH differences between ascending and descending passes. This difference can reflect orbit errors or errors in geophysical corrections. The fact that Envisat is Sun-synchronous can play a role since the ascending passes and descending passes respectively cross the equator at 10pm local time and 10am local time. Thus all the parameters with a daily cycle can induce errors resulting in ascending/descending differences. The error observed at crossovers can be split into two types: the time invariant errors and the time varying errors.

To analyze the time invariant errors, we have computed local averages of crossover differences over approximately one year (cycles 25 to 35). The map of the mean differences at crossovers is shown in figure 22. It shows systematic differences between ascending and descending passes in some areas. Mean ascending/descending differences are locally higher than 4 cm (Southern Pacific and Southern Atlantic). These patterns, called geographically correlated radial orbit errors, are induced by errors in the gravity models currently used in the orbit computation. It is worth recalling that the GRIM5 gravity model is presently used for Envisat precise orbit calculations. The DEOS Institute at Delft University computes a POE orbit with different standards (Doornbos et al., 2005 [10]). The main difference is the use of a Grace gravity model EIGEN-GRACE01S. The corresponding map of the mean differences at crossovers with the Delft POE is plotted in figure 22. The geographically correlated orbit errors are almost fully removed. Small signals remain in Indian and Pacific Oceans. A new POE orbit using a Grace gravity model is currently under development at CNES and will be included in the next version of GDR products. Notice that the signal visible around the equator on ERS-2 (Scharoo, 2002 [42]), related to poor quality of the ionosphere correction, is not present for Envisat thanks to a good correction of the dual frequency correction.

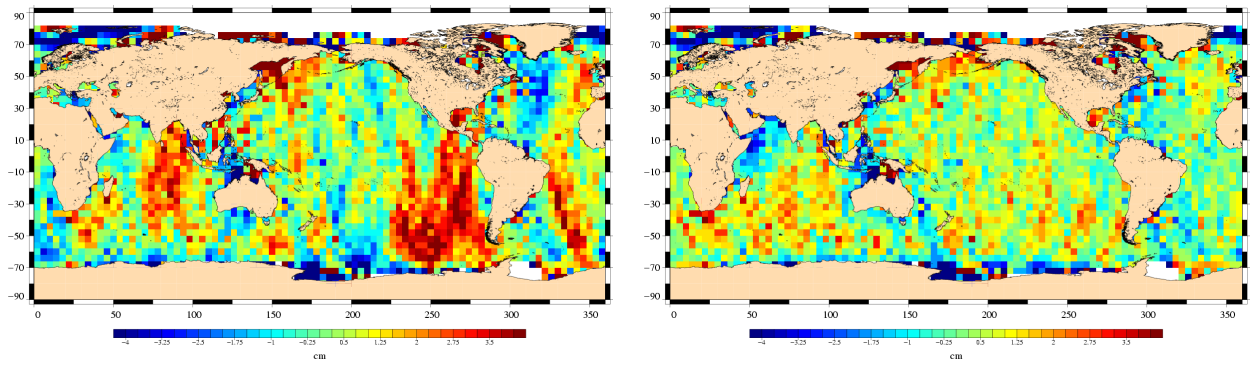

Figure 22: *Maps of the time invariant 35-day crossover mean differences (cm) for Envisat averaged in (4deg x 4 deg) geographical bins through a one year period (cycle 25-35) using GDRs POE orbit (left) and using a reprocessed POE orbit using a new gravity model (right).*

Besides the systematic ascending-descending errors, a time varying error can also be observed at crossovers. The cyclic mean ascending-descending SSH differences at crossovers shows this error in figure 23. The cyclic mean crossover differences have been plotted in three different configurations: full data set, deep ocean data, and deep ocean data with low variability, and excluding high latitudes. A strong annual signal is evidenced on the 3 curves. Its amplitude overtakes 1 cm in the second half of the Envisat period. That signal can either be due to non gravitational orbit errors, diurnal effects in the orbit or in some geophysical correction, or to an aliasing effect. Indeed, K1 oceanic tide component is aliased by Envisat into an annual signal. That means that an error in the estimation of such a tidal component induces an error with 1 year period. Furthermore, tide corrections are not only used in the SSH computation but are also used in the orbit

calculation, thus the two effects cannot be separated in such crossover analysis.

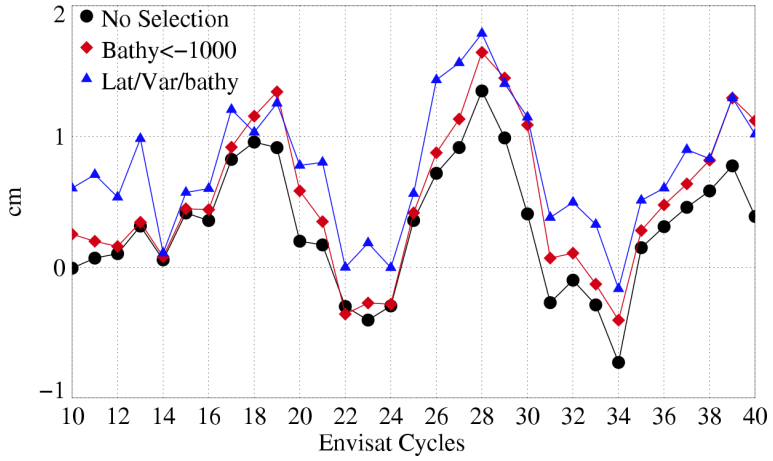

Figure 23: *Time varying 35-day crossover mean differences (cm). Cycle per cycle Envisat crossover mean differences. An annual cycle is clearly visible. Diamonds: shallow waters (1000 m) are excluded. Triangles: shallow waters excluded, latitude within [-50S, +50N], high ocean variability areas excluded*

In order to better analyze such annual signals, a temporal sinusoidal function with a 365 day period has been fitted to mean crossover differences averaged into 10x10 degree bins. For each bin, the following sinusoidal signal has been fitted:
S(t)=Acos(2pt/365 +f)
Where t is the time in days, A the amplitude and f the phase

Only open ocean data are used in this analysis. Latitudes higher than 70 degree are also removed because the seasonal data unavailability at high latitudes corrupts the estimation of the annual signal. Regions of high mesoscale variability are also removed to reduce noise. After smoothing, the amplitude A of the estimated sinusoidal signal has been plotted in figure 24. The amplitude of the annual signal is not homogeneous. High amplitudes, greater than 2 cm, are visible in two types of regions: some deep sea regions, in the Southern Pacific and Southern Atlantic, and some coastal regions: Asia an Oceania coasts, South and East African coasts, Gulf of Mexico. The use of FES02 or FES04 tide model instead of GOT00 strongly changes the map of amplitude. This indicates that this annual signal and these geographical patterns might be correlated with oceanic tides error, possibly the K1 diurnal component.

6.2 Variance at crossovers

The variance of crossover differences conventionally gives an estimate of the overall altimeter system performance. Indeed, it gathers error sources coming from orbit, geophysical corrections, instrumental noise, and part of the ocean variability. The standard deviation of the Envisat SSH crossover differences has been plotted in figure 25, depending on three data selection criteria. Without any selection, a seasonal signal is observed because variations in sea ice coverage induce changes in ocean sampling by altimeter measurements. When only retaining deep ocean areas, excluding high latitudes (higher than 50 deg.) and high ocean variability areas, the standard deviation then gives reliable estimate of the altimeter system performances. In that case most of the cycles have a standard deviation between 7.5 and 7.7 cm. But there are some exceptions

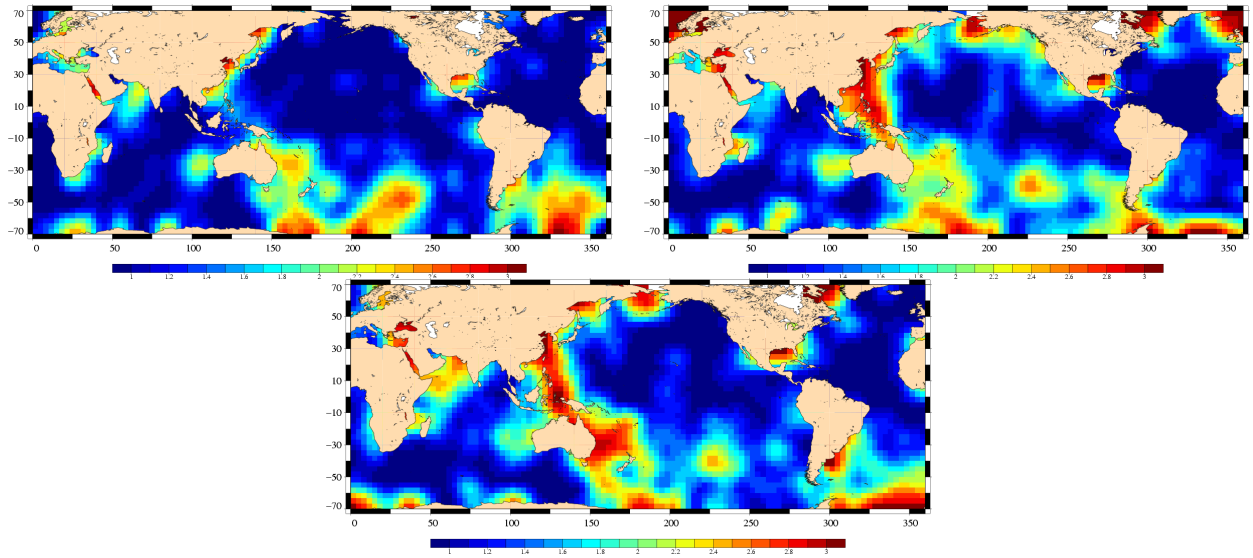

Figure 24: *Time varying 35-day crossover mean differences (cm). Map of the geographic distribution of the amplitude of the annual cycle of the crossover means shown in figure 23 averaged in 10deg x 10deg geographical bins (after smoothing) using (from top to bottom) GOT00, FES02, FES04*

that can be explained. Cycle 15 is strongly different because of the low number of crossover points. There are less than 10000 crossovers whereas other cycles lead to more than 20000. Cycles 12, 16, 21, 26 have higher values because of bad orbit quality over a few passes related to out-of-plane maneuvers. Cycle 21 has a strong value (8.5 cm) because of the combined effect of 2 maneuvers, intense solar activity between these 2 maneuvers, and lack of laser measurements between these two maneuvers. Cycle 11 has a relative high value because of missing Doris data.

In order to compare Envisat and Jason-1 performances at crossovers, Envisat and Jason-1 crossovers have been computed on the same area excluding latitude higher than 50 degree, shallow waters and using exactly the same interpolation scheme to compute SSH values at crossover locations. Performances at crossovers are compared, for the two satellites on figure 26. The standard deviation of Envisat/Envisat and Jason-1/Jason-1 SSH crossover differences are respectively 6.6 cm and 6.7 cm. Performances are slightly better for Envisat except for cycles 12, 16, 21 and 26. Note that the number of crossover points is considerably greater for Jason-1 between cycles 13 and 19 and for cycle 22 where a lot of passes are missing on Envisat.

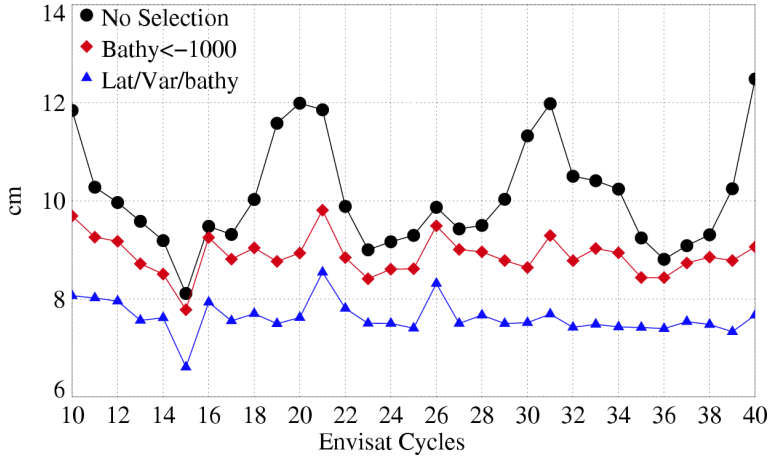

Figure 25: *Standard deviation (cm) of Envisat 35-day SSH crossover differences depending on data selection. Dots: without any selection. Diamonds: shallow waters (1000 m) are excluded. Triangles: shallow waters excluded, latitude within [-50S, +50N], high ocean variability areas excluded.*

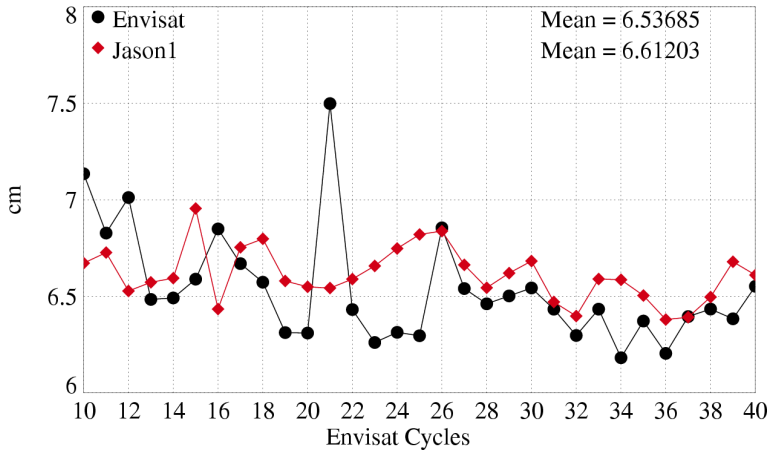

Figure 26: *Comparison of the Standard deviation (cm) of Envisat (dot) and Jason-1 (diamond) 10-day SSH crossover differences*

7 Mean Sea Level. Envisat SSH bias

To estimate accurately the Envisat mean sea level bias and trend, two factors have to be taken into account. First, as previously mentioned, the range has to be corrected to compensate for the Ultra Stable Oscillator drift. The distributed correction is smoothed over a 1-month period to filter peaks and short period variations. The cyclic mean of the USO correction is plotted in figure 27. The mean value is about 3 cm with a decreasing trend of about -4.5 mm/year between cycles 17 and 38. The supplied correction has to be subtracted from the original altimetric range (EOP-GOQ and PCF team, 2005) and consequently added to SSH. Secondly, as previously mentioned, a drift is suspected on the MWR correction. Consequently, the ECMWF wet troposphere correction is used, as no major change in the model has impacted the data since the beginning of the Envisat mission (ECMWF web page).

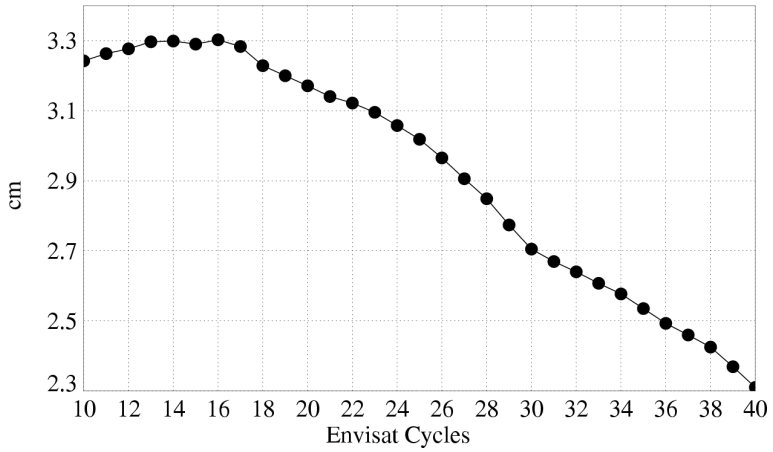

Figure 27: *USO correction computed from auxiliary files. The raw correction is averaged on 1 month*

Envisat Mean Sea Level (MSL) estimations are plotted in figure 28 for three different edit criteria in order to estimate the impact of shallow waters and high latitudes. The mean SSH bias relative to the CLS01 MSS is about 47.5 cm over this period. Seasonal signals are observed on the three curves, though the annual cycle is more pronounced on the full data-set.

In order to compare Envisat and Jason-1 SSH estimations, 10-day dual crossovers have been computed for each Envisat cycle. The same ECMWF correction has been used for both Jason-1 and Envisat to avoid potential radiometer errors. figure 29 shows the mean Envisat-Jason-1 differences at global and hemispheric scales. The global mean is about 29.9 cm over the period. There is a decreasing trend on the difference between cycles 10 and 20 then the differences seem to stabilize. This behavior remains unexplained. The hemispheric differences seem consistent from one cycle to another. From cycles 10 to 16, no hemispheric difference is observed, while after Cycle 16, high hemispheric biases are evidenced. The differences are periodically strongly reduced with a period of 6-8 Envisat cycles (200-300 days). The same kind of observation had been made on Jason-1 T/P differences (Dorandeu, 2004b). These differences might be attributed to residual orbit errors on at least one of the satellites.

Finally MSL estimations from Envisat, Jason-1 and T/P have been compared. The results are obtained

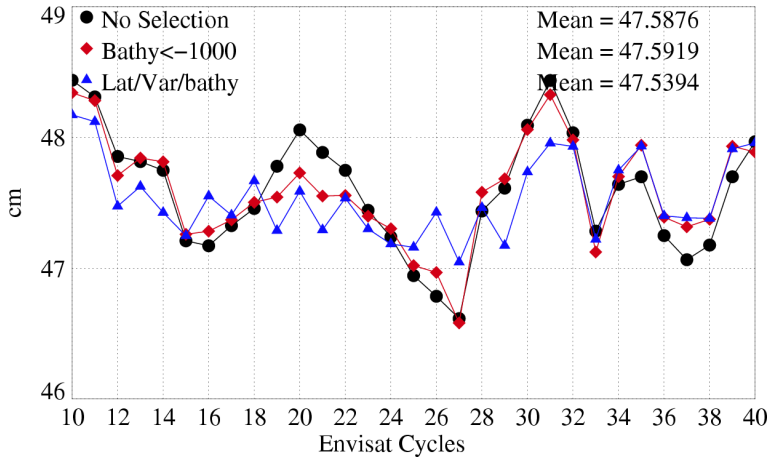

Figure 28: *Mean of Envisat Sea Level depending on data selection. Dots: without any selection. Diamonds: shallow waters (1000 m) are excluded. Triangles: shallow waters excluded, latitude within [-50S, +50N], high ocean variability areas excluded.*

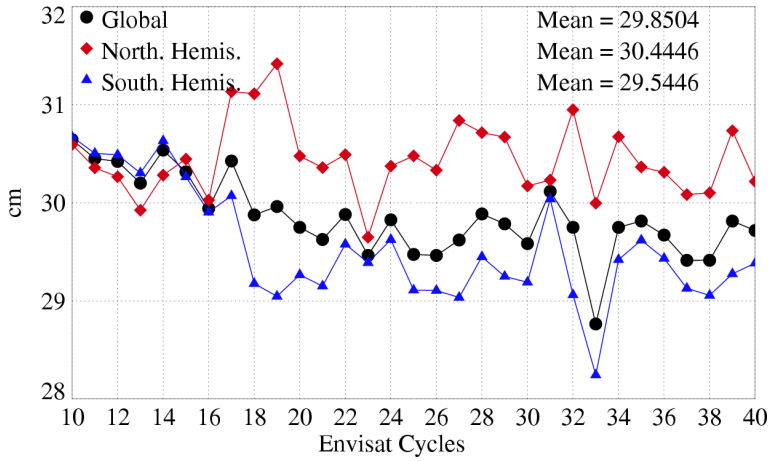

Figure 29: *Mean of Envisat -Jason-1 differences at 10-day dual crossovers. Dots: Global. Diamonds: Northern Hemisphere. Triangle: Southern Hemisphere.*

after area weighting (Dorandeu and Le Traon 1999). The same corrections are used for the 3 satellites. Annual and semi-annual signals have been removed. An additional 60-day period sinusoid has been fitted and removed on T/P and Jason to remove residual orbit errors (Luthcke et al. 2003). Biases relative to MSS have been removed for each mission to ease the comparison. Figure 30 shows the global MSL trend for the three satellites and for three different periods of time. First, the whole Envisat period is analyzed. The Envisat curve shows a quasi null trend whilst Jason-1 and T/P lead to an increasing trend of 2-3 mm/year. This difference is mostly due to the unexplained behavior of Envisat MSL estimations on the first cycles. Indeed the MSL has a decreasing trend until the last months of 2003, around cycle 20. This is consistent with the Envisat-Jason-1 trend observed at dual crossovers. To further check these changes in MSL trend, two different periods have been considered: the first two years (cycles 10 to 29) and the last two years (cycles 19 to 38). A -3 cm/year trend is obtained on the first two years. This is completely the opposite of Jason-1 and T/P trends. On the last two years, Envisat is fully consistent with Jason-1 and T/P. The unexplained behavior of the first year of Envisat data is still currently under investigation.

A complete study on the MSL seen by all the operational altimeter missions and its comparison to the Reynolds SST is available in Appendix 2.

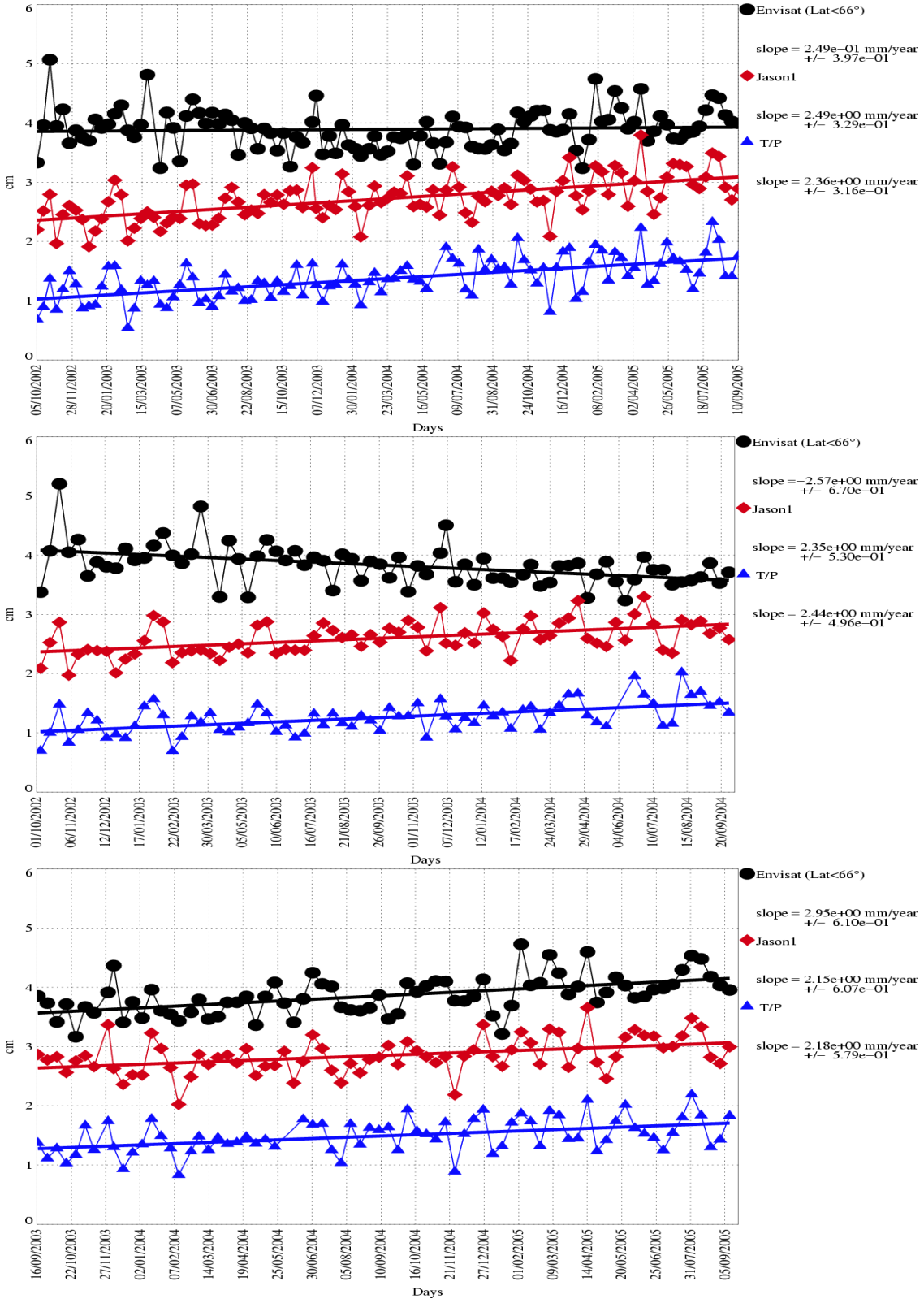

Figure 30: *Envisat, Jason-1 and T/P global MSL trends (top) over the whole Envisat mission, (mid) over the two first years of Envisat mission (cycle 10 to 29), (bot) over the two last years of Envisat mission (cycle 19 to 38)*

8 New Standards

From cycle 41 onwards, a new operational production chain (IPF 5.02/CMA 7.1) has been implemented. These evolutions, fully described in [12], have been analyzed and validated. In this chapter the performance assessment of the new geophysical corrections (FES2004 tide model, the Mog2D correction and the S1-S2 tides) and of the new orbit are described.

8.1 Statistical evaluation of Fes2004 tide model

8.1.1 Introduction

First, the FES04 model is compared to GOT00 model. Then, it is compared to older models, GOT99 and Fes99. Finally the impact of the new dynamic long period tide component is analyzed.
The performance criteria are the variance of SSH differences at crossovers and the variance of along track Sea Level anomalies. The analysis has been done on Jason-1, Envisat and GFO. The results for Jason-1 satellite are similar to those which would have been obtained for TOPEX/Poseidon satellite, as both satellites are on the same ground track.

8.1.2 Comparison Between FES2004 and GOT00V2

In this part, the FES04 model is compared to GOT00 model on a two-year period on Jason-1 (31-104), Envisat (11-31) and GFO (98-140).

8.1.2.1 SSH formulae

The parameters used to compute the sea surface height (SSH) for Jason-1 and Envisat are:

- radiometer wet troposphere correction
- ECMWF dry troposphere correction (rectangular grids)
- dual frequency ionospheric correction
- non parametric SSB
- MOG2D
- pole tide correction
- earth tide correction
- oceanic tide correction

The FES04 tide correction contains:

- the S1 and S2 atmospheric tide
- the dynamic long period tide

The original GOT00 tide correction contains:

- the S2 atmospheric tide
- the static long period tide

to be consistent, GOT00 has been computed as following:

$$\begin{aligned} GOT00_{used} &= original\ GOT00\ tide \\ &+ the\ S1\ atmospheric\ tide \\ &- static\ long\ period\ tide \\ &+ dynamic\ long\ period\ tide \end{aligned}$$

8.1.2.2 Along track differences

Figure 31 shows the mean differences between FES04 and GOT00 on the 3 satellites. The differences are around 0 for Jason-1. On Envisat, the differences can locally overtake 1 cm. The strongest differences are in Indonesia and at high latitude. On GFO, the differences are weak at mid and low latitude, but have strong values above 60°. This behavior is not explained so far.

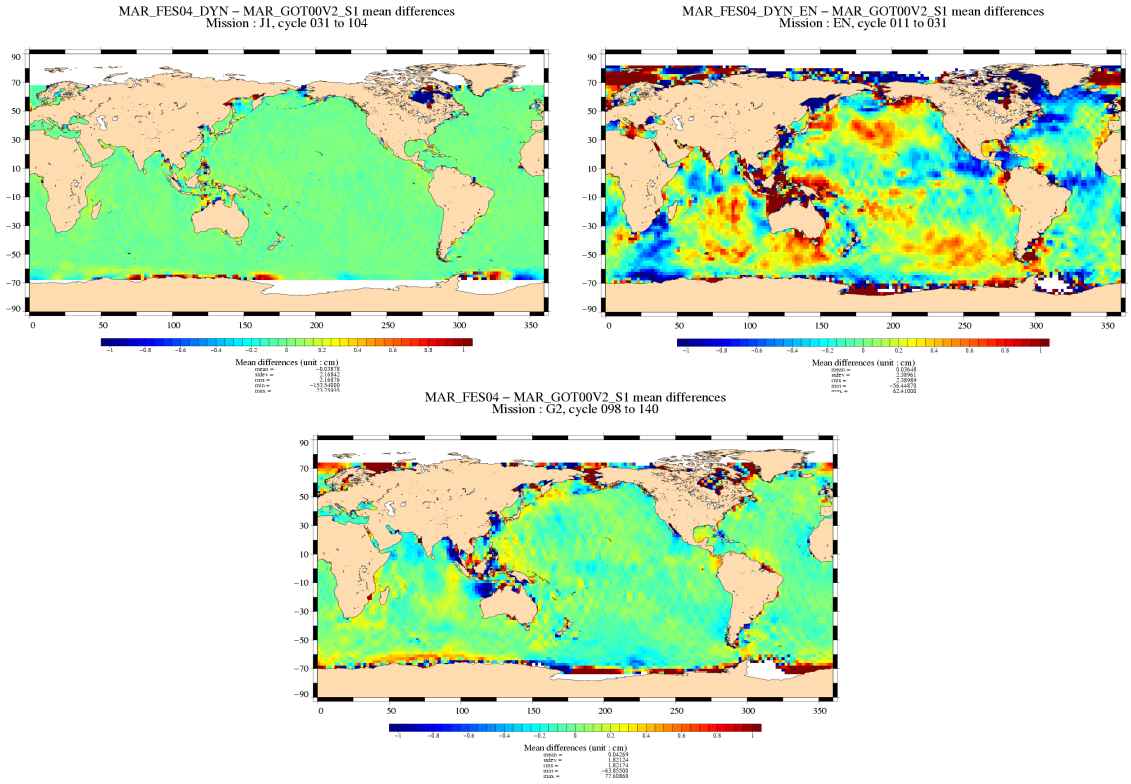

Figure 31: *Mean differences*

Figure 32 shows the variance of the difference between FES04 and GOT00 on the 3 satellites. The 3 maps are similar. High differences are found on low bathymetry areas and at high latitudes.

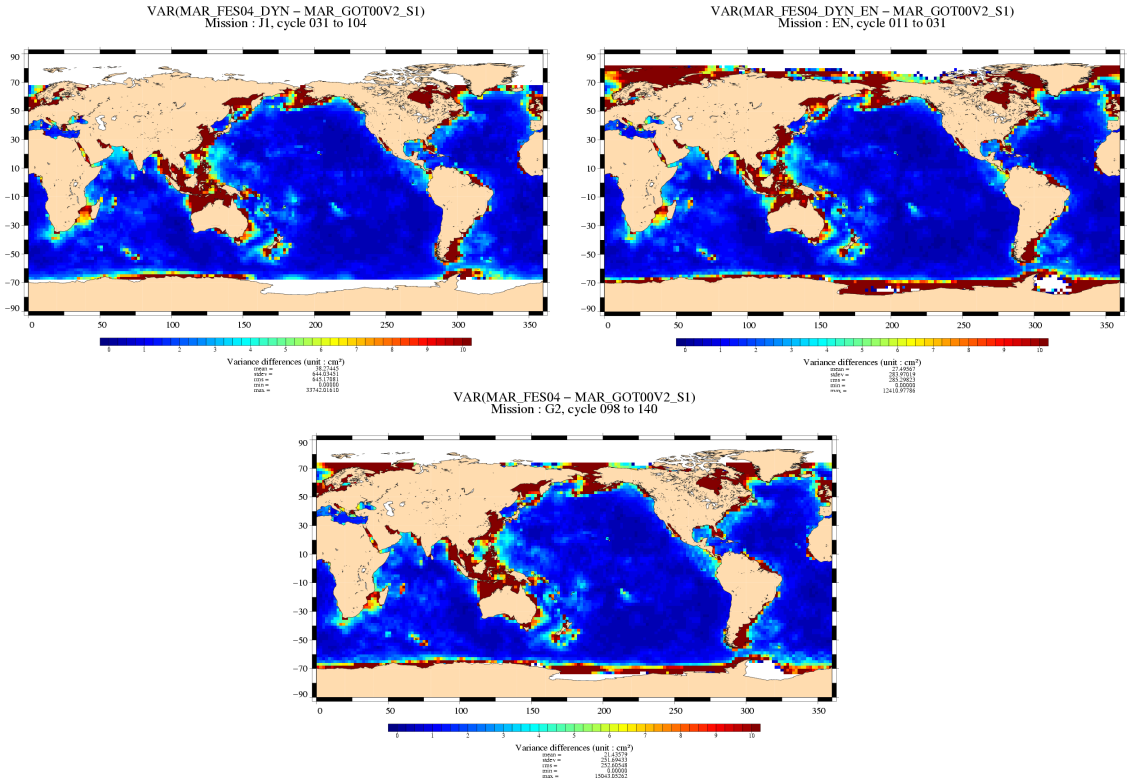

Figure 32: *Variance differences*

8.1.2.3 Performance at crossovers

Figures 33 and 34 show respectively the gain and the normalized gain at crossovers between FES04 and GOT00 on the 3 satellites. The blue color means that FES04 has a lower variance of SSH differences at crossover than GOT00. The red color means that FES04 has a larger variance of SSH differences at crossover than GOT00. For the 3 satellites, in open ocean at mid and low latitude, FES04 and GOT00 have approximately the same performances. In coastal regions and semi enclosed seas, at mid and low latitude, GOT00 better performs than FES04. It is especially true for Indonesia, China sea, Okhotsk Sea, Bering Sea or Hudson bay. This is due to the use of regional models in GOT00. At high latitude FES04 better performs than GOT00. This is particularly visible on Envisat because of its inclination.
The average variance differences over the period are summarized on tables 6, 7 and 8. These values confirm the pattern observed on the figures.

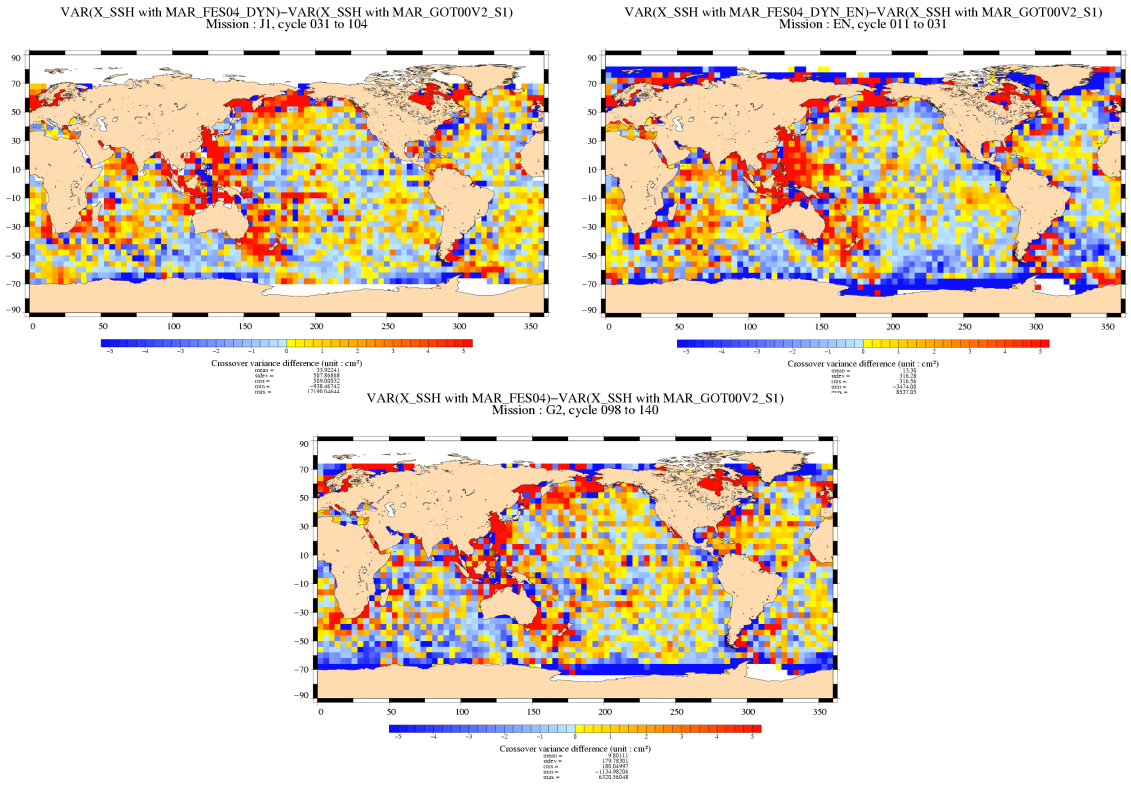

Figure 33: *Gain at crossovers*

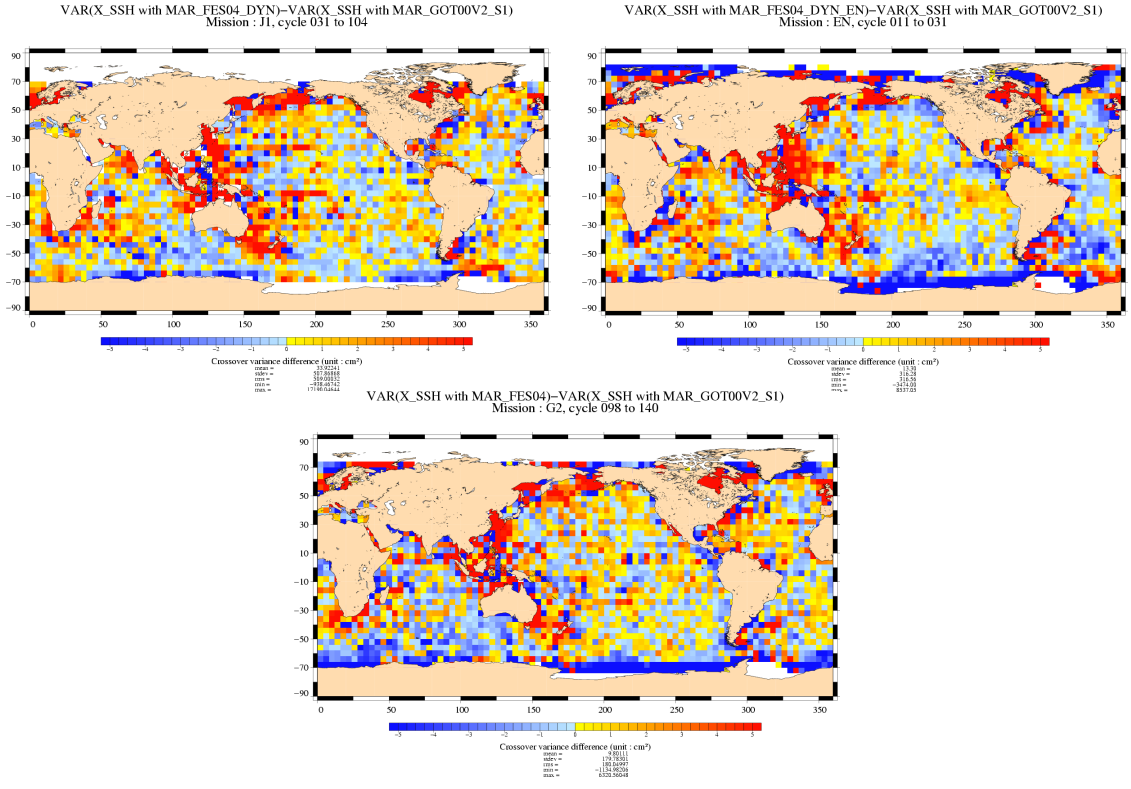

Figure 34: *Normalized gain at crossovers*

Bathy \ Lat	No selection	$\|Lat\| < 50$	$\|Lat\| > 50$
No selection	13.25	–	–
Bathy < -1000 (m)	0.15	0.41	-0.05
Bathy > -1000 (m)	110.4	167.6	83.22

Table 6: *J*ASON var(X_SSH_FES04)-var(X_SSH_GOT00V2)

Bathy \ Lat	No selection	$\|Lat\| < 50$	$\|Lat\| > 50$
No selection	-1.64	–	–
Bathy < -1000 (m)	-1.80	0.008	-4.50
Bathy > -1000 (m)	4.83	55.50	-12.15

Table 7: *E*NVISAT var(X_SSH_FES04)-var(X_SSH_GOT00V2)

Bathy \ Lat	No selection	$\|Lat\| < 50$	$\|Lat\| > 50$
No selection	1.09	–	–
Bathy < -1000 (m)	-0.01	0.31	-2.34
Bathy > -1000 (m)	13.79	36	5.82

Table 8: *G*FO var(X_SSH_FES04)-var(X_SSH_GOT00V2)

8.1.2.4 Along track performances

Figures 35 and 36 show respectively the gain and the normalized gain along track between FES04 and GOT00 on the 3 satellites. The blue color means that FES04 has a lower variance of SLA than GOT00. The red color means that FES04 has a larger variance.
The results obtained along track are similar to those obtained at crossovers. Some oceanic signals are however observed on Envisat and GFO notably around the equator.

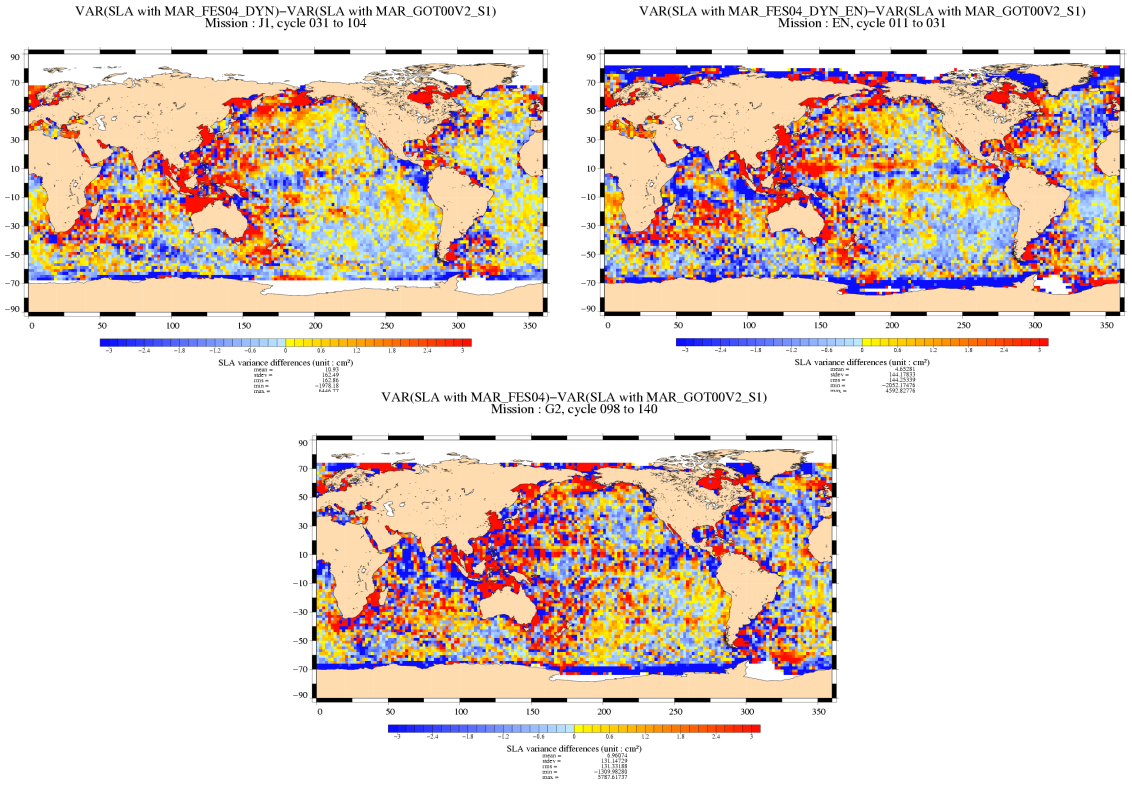

Figure 35: *Along track gain*

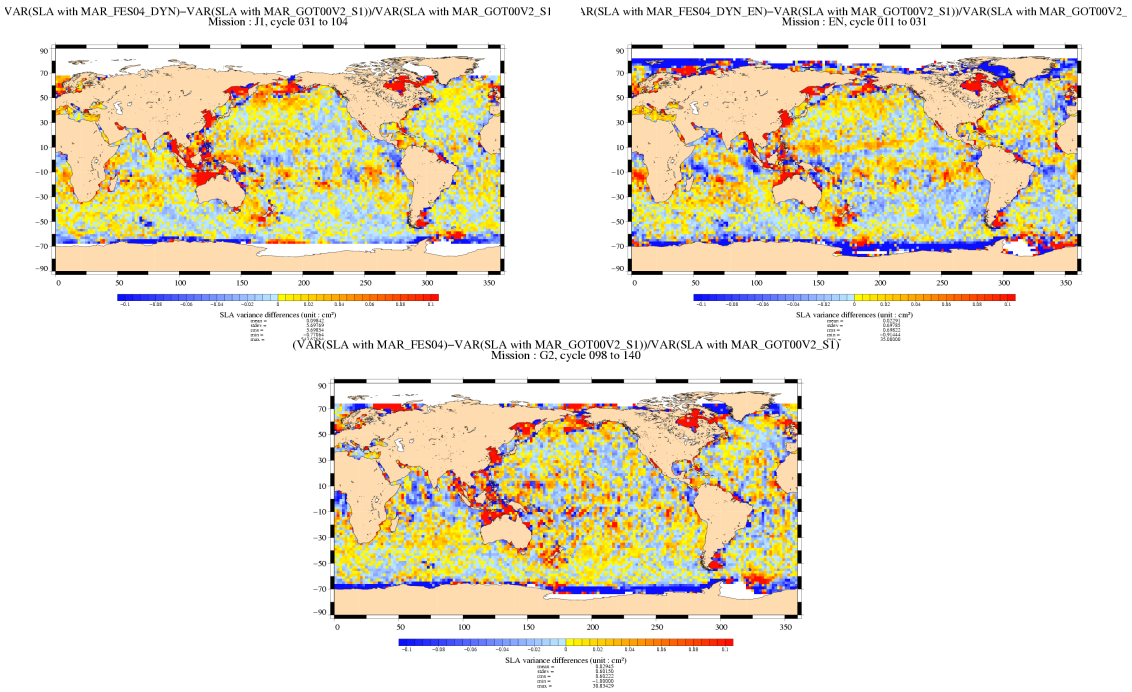

Figure 36: *Normalized gain at crossovers*

8.1.3 Comparison between FES2004, GOT99 and FES99

In this part, the FES04 model is compared to older models, GOT99 and FES99.
Note that FES04 and GOT00 include S1 and S2 atmospheric tide and dynamic long period tide.
FES04 is compared to GOT00 on Envisat (11-30) (a two-year period of data)

8.1.3.1 SSH formulae

The parameters used to compute the sea surface height (SSH) for Envisat are:

- radiometer wet troposphere correction
- ECMWF dry troposphere correction (rectangular grids)
- dual frequency ionospheric correction
- non parametric SSB
- MOG2D
- pole tide correction
- earth tide correction
- oceanic tide correction

The FES04 tide correction contains:

- the S1 and S2 atmospheric tide
- the dynamic long period tide

The original FES02 tide correction contains:

- neither contains S1 nor S2 atmospheric tide
- contains the static long period tide

The original GOT99 tide correction contains:

- the S2 atmospheric tide
- the static long period tide

For this analysis, FES04 has been computed as following:

$$\begin{aligned} FES04 &= original\ FES04\ tide \\ &+ static\ long\ period\ tide \\ &- dynamic\ long\ period\ tide \end{aligned}$$

So FES04 is not fully consistent with FES02 and GOT99.

8.1.3.2 Along track differences

Figure 37 shows the mean differences FES04-FES02 and FES04-GOT99 on Envisat. The S2 signal is clearly visible on the first map. The FES04-GOT99 differences are very similar to the FES04-GOT00 differences.

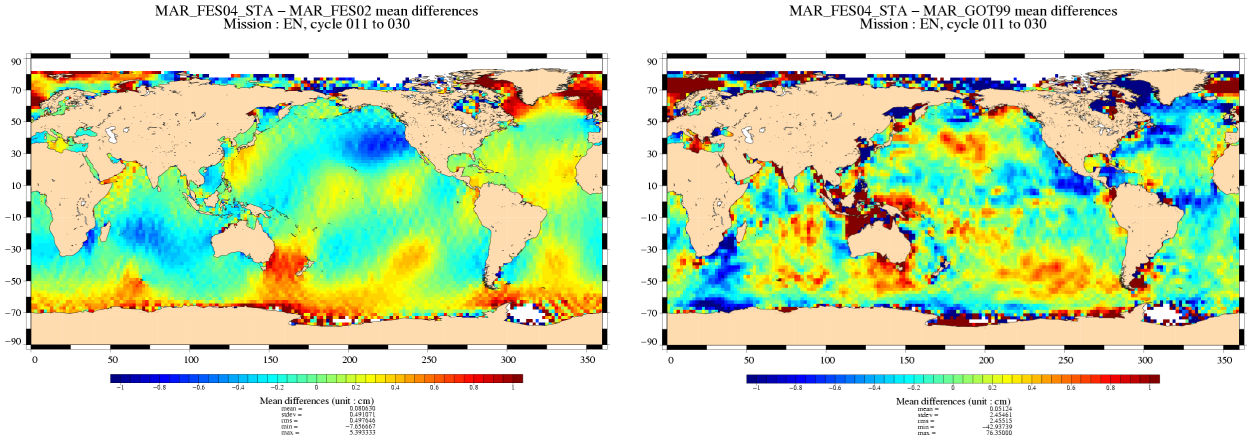

Figure 37: *Mean differences*

Figure 38 shows the variance of the differences FES04-FES02 and FES04-GOT99 on Envisat. As expected, the differences FES04 and FES02 are consistent. High differences are found on FES04-GOT99 in low bathymetry areas and at high latitudes.

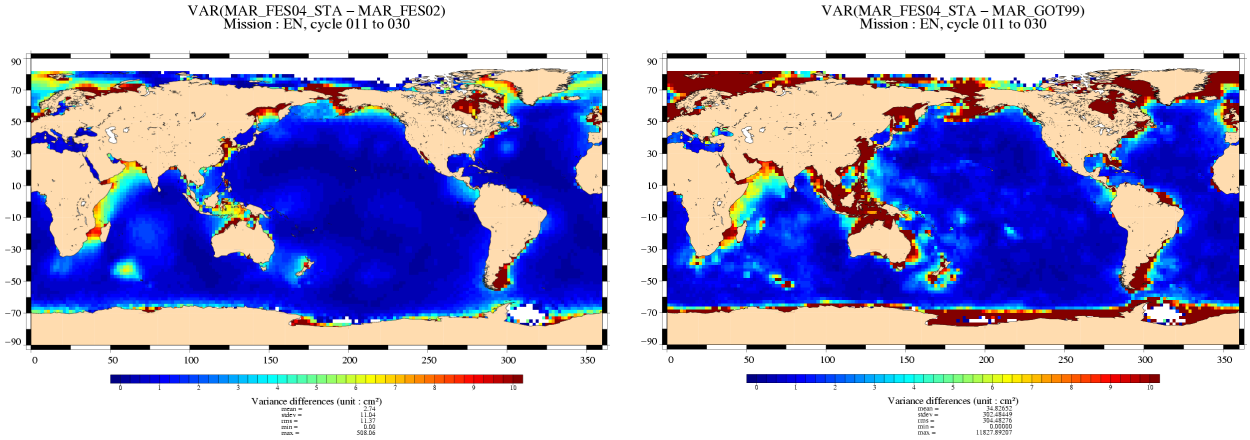

Figure 38: *Variance differences*

8.1.3.3 Performance at crossovers

Figure 39 shows the gain at crossovers between FES04/FES99 FES04/GOT99 on Envisat. The blue color means that FES04 has a lower variance of SSH differences at crossover than FES99 or GOT99. FES04 has, in average, lower variance than FES99 and GOT99, especially in high latitude and low bathymetry areas. However, GOT99 has, locally, a lower variance: over Indonesia and in the Indian ocean for example.

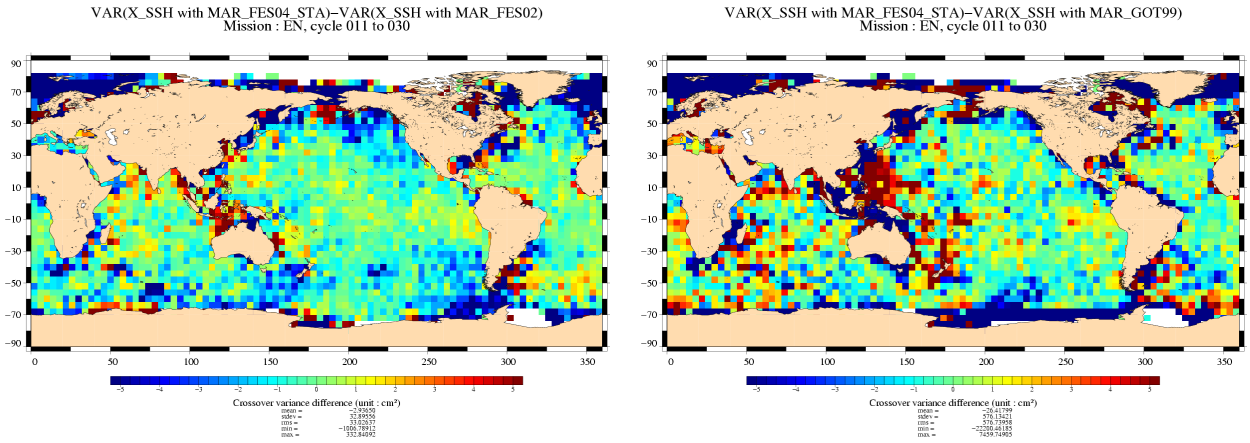

Figure 39: *Gain at crossovers*

8.1.3.4 Along track performances

Figure 40 shows the gain along track between FES04 and GOT00 on the 3 satellites. The results obtained along track are similar to those obtained at crossovers. Some oceanic signals are however observed.

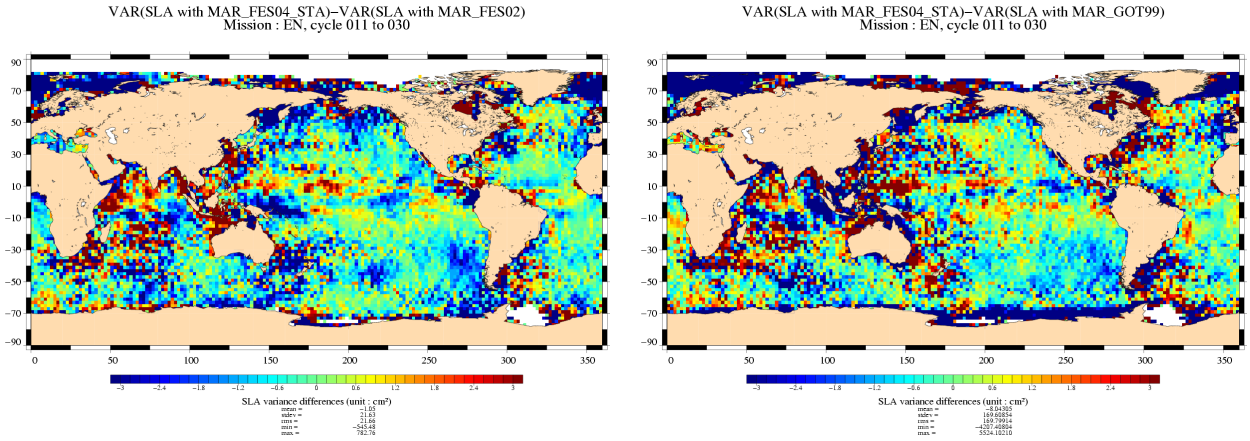

Figure 40: *Along track gain*

8.1.4 Impact of the dynamic long period tides

In this part, the impact of the new dynamic long period tide is analyzed on Envisat.
FES04 (dynamic) is compared to FES04 (static) on Jason-1 (1-101) (a three-year period of data)

8.1.4.1 SSH formulae

The parameters used to compute the sea surface height (SSH) for Jason-1 are:

- radiometer wet troposphere correction
- ECMWF dry troposphere correction (rectangular grids)
- dual frequency ionospheric correction
- non parametric SSB
- MOG2D
- pole tide correction
- earth tide correction
- oceanic tide correction

8.1.4.2 Along track differences

Figure 41 shows the mean difference Dynamic-Static long period tide. The differences are not very important, lower than 1cm.

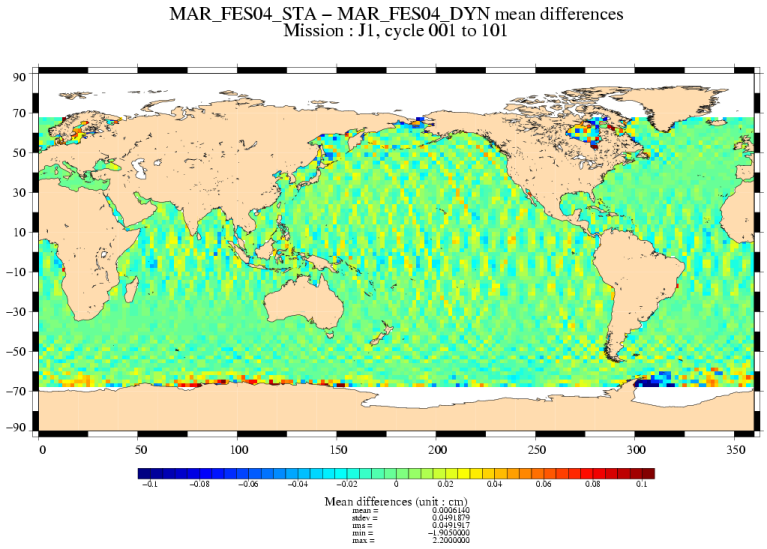

Figure 41: *Mean differences*

Figure 42 shows the variance of the difference Dynamic-Static long period tide.

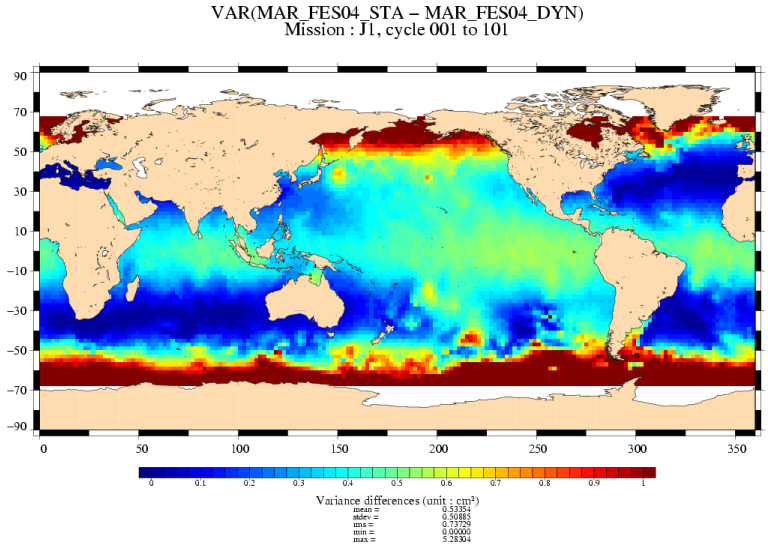

Figure 42: *Variance differences*

8.1.4.3 Performance at crossovers

Figure 43 shows the gain at crossovers between Static and dynamic. The red color means that the dynamic long period tide correction has a lower variance of SSH differences at crossover than the static long period tide correction. The differences are around 0 (-0.066 cm2). However, in the Pacific Ocean at mid latitude the dynamic long period tide has lower variance, and at latitude lower than 50˚S the static long period tide has lower variance.

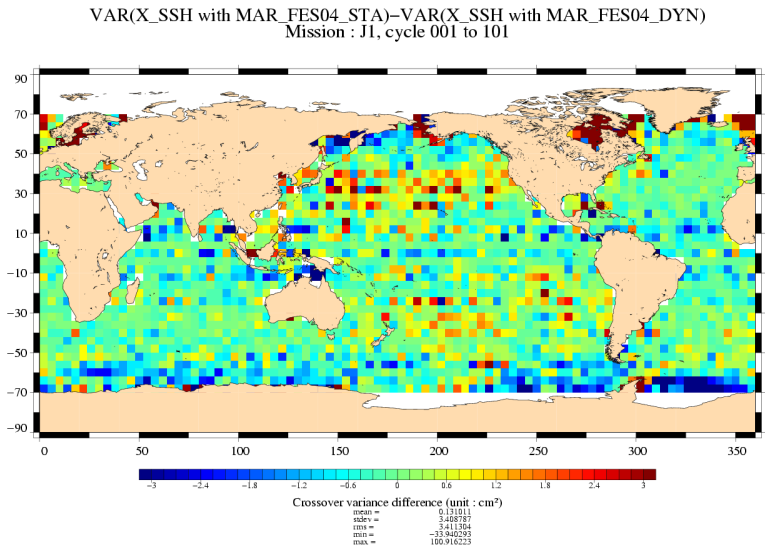

Figure 43: *Gain at crossovers*

8.1.4.4 Along track performances

Figure 44 shows the gain along track between Static and dynamics. The results obtained along track are similar to those obtained at crossovers.

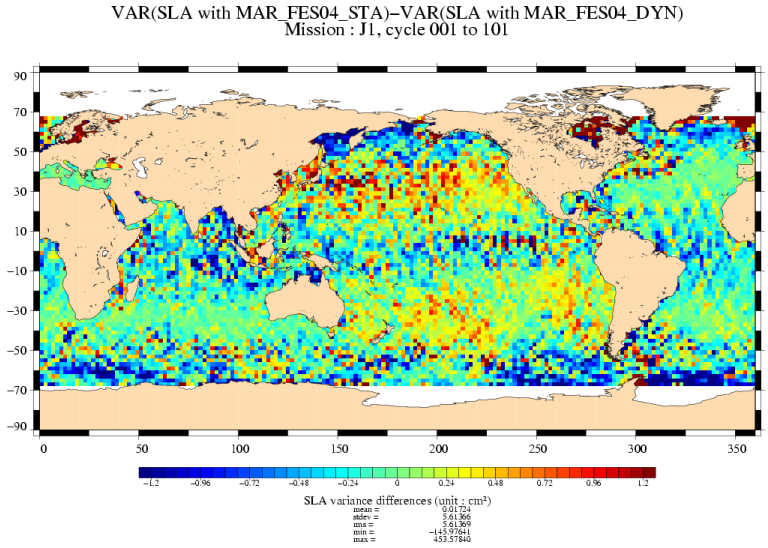

Figure 44: *Along track gain*

8.1.5 Conclusion

These 3 analyzes allow us to choose a tide model for our products between FES04 and GOT00. In open ocean at mid and low latitudes the performances of the 2 models are very close. FES04 better performed at high latitudes which is strongly visible on Envisat and GFO, but less obvious on Jason-1. GOT00 is better in coastal areas thanks to the use of regional model.

FES04 assimilation technique is more physical than GOT00. GOT00 is strongly adjusted on altimetric data. So with equivalent performance, the best choice would be FES04. Moreover the dynamic long periods have been computed for FES04. However the fact that FES04 has, locally, lower performances than GOT00 is an argument leading to the choice of GOT00.

8.2 Impact of the MOG2D correction

As a first approximation, the so-called Inverse Barometer correction is conventionally used to correct altimeter data. This simple correction assumes a static ocean response to atmospheric pressure forcing. Neither dynamical effects at high frequency nor wind effects are taken into account in this correction.

In order to take account of dynamical effects and wind forcing, a new correction is computed from the MOG2D (Carrere and Lyard, 2003 [2]) barotropic model forced by pressure (without S1 and S2 constituents) and wind. Only the high frequency part of these model outputs are retained and combined to the low frequency inverse barometer.

A comparison between the 2 types of corrections was made for the Envisat period. The Figure 45 displays comparisons between the two types of correction. It shows that in comparison to the inverse barometer correction, the MOG2D correction reduces greatly the crossover variance and SLA variance in regions of high frequency variability (high latitudes and shallow water).

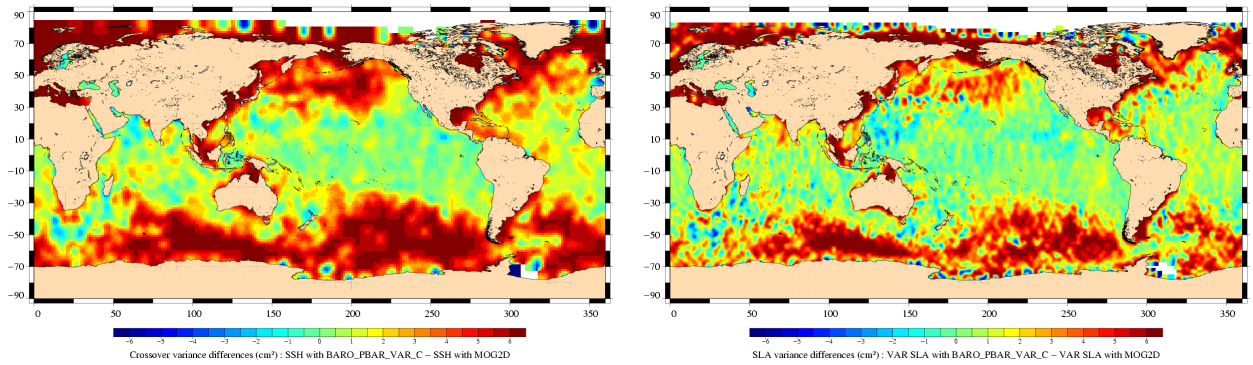

Figure 45: *Crossover variance difference (left) and SLA variance difference (right) when using correction MOG2D rather than inverse barometer correction*

8.3 Impact of new S1S2 wave model in dry troposphere

The S1 and S2 radiational tides are not well retrieved by ECMWF atmospheric fields (in particular because of poor temporal sampling). Following the QWG recommendation, the original S1 and S2 components are now filtered out from atmospheric and re-estimated using an S1/S2 model (Ponte and Ray, 2003 [38]) before computing the dry troposphere correction.

The figure 46 displays comparisons between the two dry tropospheric corrections for Envisat period. The two corrections are very close.

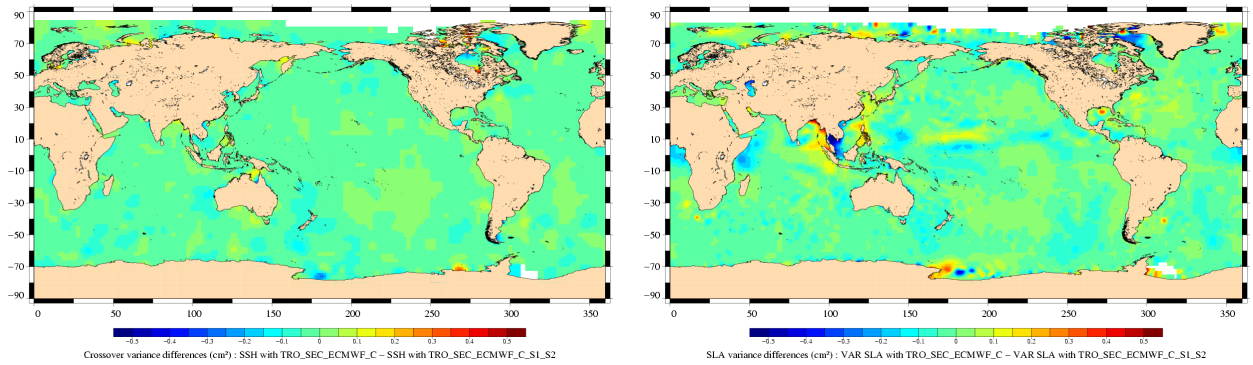

Figure 46: *Crossover variance difference (left) and SLA variance difference (right) when using dynamic S1S2 or only static S1S2 contributions for dry troposphere correction*

8.4 Assessment of new POE orbits

8.4.1 Introduction

Two new configurations have been developed at CNES for the computation of the POE orbit in July and October 2005. A new processing software and preliminary standards have been used. Cycle 25 to 35 have been reprocessed in the "July" and "October" configurations. The objective of this study is to assess and compare the reprocessed POE orbits to the GDR POE orbit. In addition, a comparison with the orbit computed routinely at Delft university is performed.

8.4.2 Data

8.4.2.1 Processing

Cycle 25 to 35 (arcs 91-145) have been computed and delivered on only nominal 7 day arcs, i.e. excluding out-of-plane manoeuvres or large DORIS data gaps. This leads to the following missing arcs :
-Arc 96 : MCO
-Arc 103 : DORIS1 incident
-Arc 104 : DORIS1 incident
-Arc 105 : DORIS2 chain startup
-Arcs 110-111: Master beacon pb
-Arc 119: MCO
-Arcs 121-122: DORIS incident
-Arc134 : MCO
-Arc 144 : MCO

The reprocessed POE and Delft orbit have been updated in our database for cycles 25-35 allowing us to compare them to the GDR orbit.

After a first analysis, poor performances have been noticed on the reprocessed orbit for the 3 following days:
-2004-04-13 (Cycle 26): Orbit Inclination manoeuvre
-2004-11-07 and 2004-11-08 (Cycle 31,32): Strong solar activity
These additional 3 days have therefore been removed.

Poor performances have been noticed on the delft orbit on the following day:
2004-09-21 (Cycle 30): Orbit Maintenance manoeuvre this day has been removed for the Delft/POE July 2005 comparison.

Note that, in each comparison study (POE July 2005/GDR POE and Delft/POE July 2005), the maps and statistics have been computed on common valid points.

8.4.2.2 Orbit configurations

The main details of the processing of the July POE are:
- Software: ZOOM
- Doris: new preprocessing
- Coordinate DORIS ITRF2000, LASER ITRF2000, special processing on bad Doris devices
- Gravity: GGM02C
- Tides: new model FES2004
- Thermospheric density: MSIS-86
- earth and pole tides: Obélix
- atmospheric tides: Haurwitz/Cawley

The additional changes in the October POE are:
- Gravity: EIGEN3

- Doris: 6.5 micros time tag bias on Doris data
- eccentricity correction on Laser data
- Ponderation Laser according to the quality of the site
- Oceanic load correction on laser station

The main details of processing of the Delft orbit are:
· Software: GEODYN-II (GSFC)
· Gravity: EIGEN-GRACE01S (GFZ-Potsdam)
· Tides: PGS7751E (GSFC)
· Non-gravitational forces: ANGARA (TU Delft, ESOC, HTG)
· Thermospheric density: MSIS-86
· Earth-orientation parameters: from IERS EOP-C04
· DORIS data sigma: 0.50 mm/s
· SLR data sigma: 4 cm + 1-20 cm depending on station
· Arc length: 5.5 days, new arc every 3.5 days, 2 days overlap
· Drag estimation sub-arc length: 1/4 orbit (25.1496 minutes)
· cpr along/cross-track sub-arc length: 12 hours

8.4.3 Comparison July POE/GDR POE

8.4.3.1 Orbit differences

Figure 47 shows the mean differences over the period 25-35. On the two figures on the top, the ascending and descending passes have been plotted separately. On the bottom figure all the passes have been taken into account. There are strong local biases that can reach +2 and -2 cm in some areas. In South-West Pacific for example, between longitude 225 and 250, the reprocessed orbit has sensitively higher values than the GDR orbit. These local differences are mostly due to the use of the gravity model GGM02C instead of GRIM5. The mean difference is very different on ascending and descending passes. In North Atlantic for example, the difference is negative on ascending passes, positive on descending passes and consequently around zero using both.

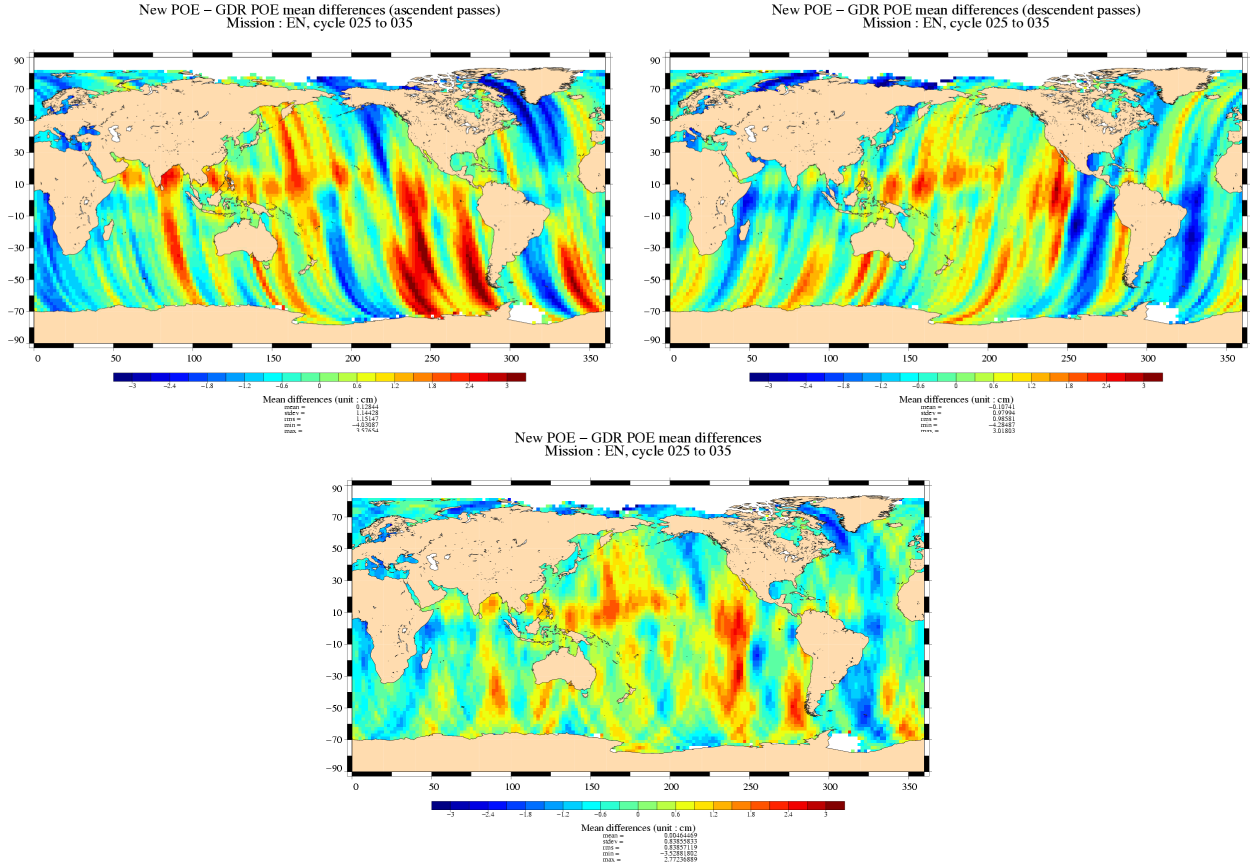

Figure 47: *POE July 2005 - GDR POE mean differences. Ascending passes (left), descending passes (right) and total (bot).*

Figure 48 shows the variance of the differences. The variance is quite low on ascending and descending passes, less than 1cm2 almost everywhere. It means that the features detected previously haven't strong variations in time. On the total data set most of the differences have a low variability as well. However, there are several areas of strong difference variability. The area of strongest variability is around South America where the variance of the difference can reach 5cm2. It means that the ascending and descending passes of

the two orbits are not consistent in this area. That fact is confirmed by the crossover analysis.

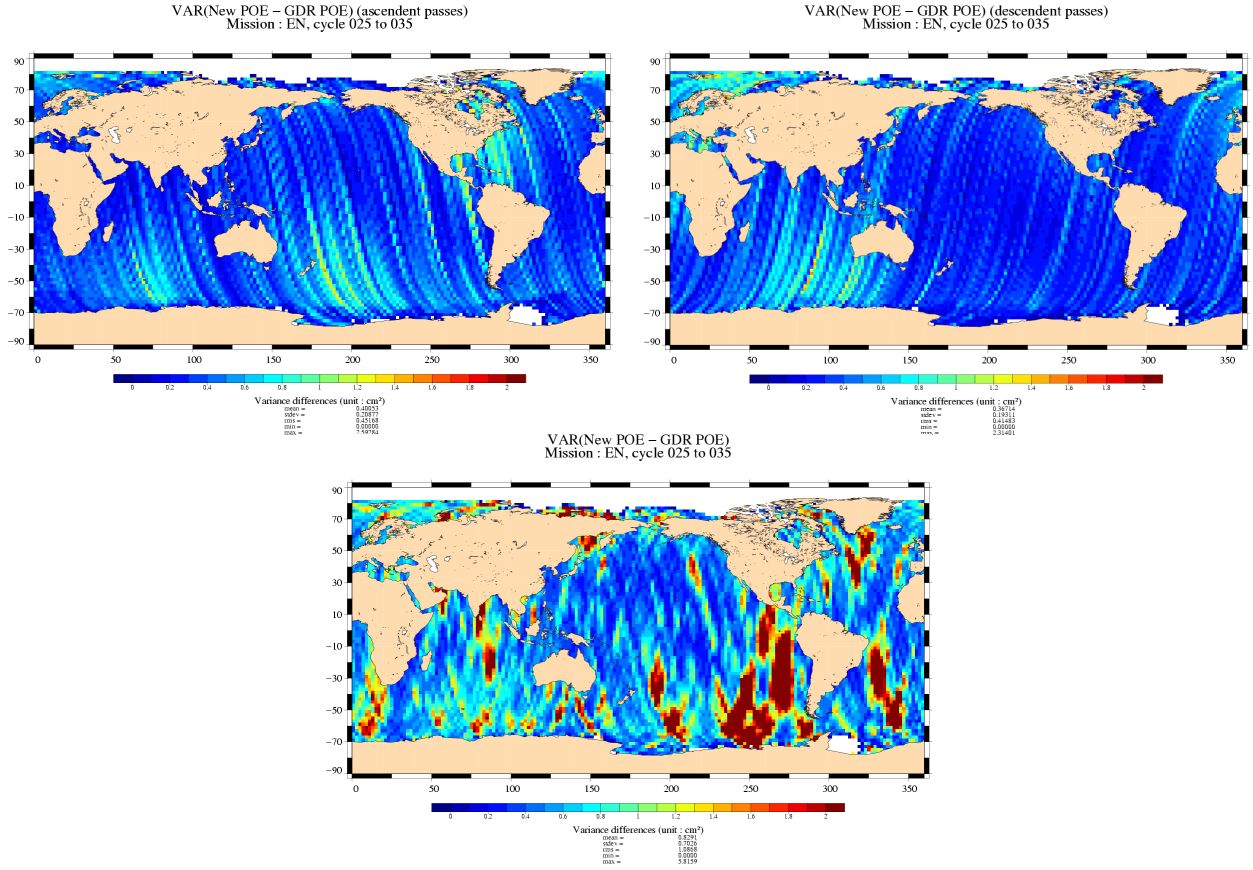

Figure 48: *Var(POE July 2005 - GDR POE). Ascending passes (left), descending passes (right) and total (bot).*

Figure 49 shows the cycle by cycle mean and variance of differences. The global bias between the two orbits is less than 1 mm. It is quite stable over the period. The variance is about 1.5 cm2.

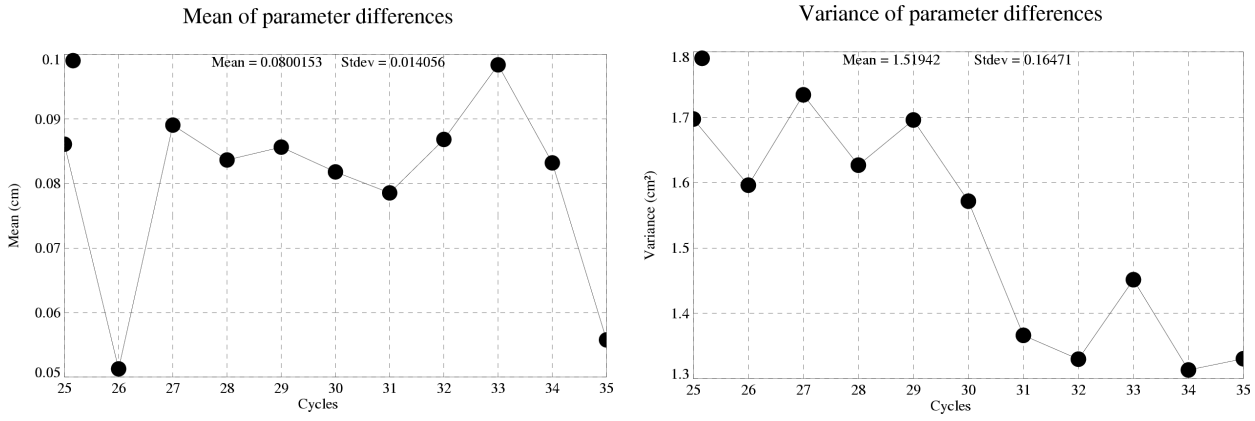

Figure 49: *Statistics per cycle of differences: mean (left) and variance (right).*

8.4.3.2 Performance at crossovers

Figure 50 shows the mean SSH differences at crossovers using the GDR orbit and the POE July. With the GDR orbit, there are strong geographically correlated signals. On these areas (in red) the difference is positive which means that SSH on descending tracks > SSH on ascending tracks.

The geographically correlated signals are largely reduced with the new orbit. That is due to the use of the GGM02C gravity model in the new configuration.

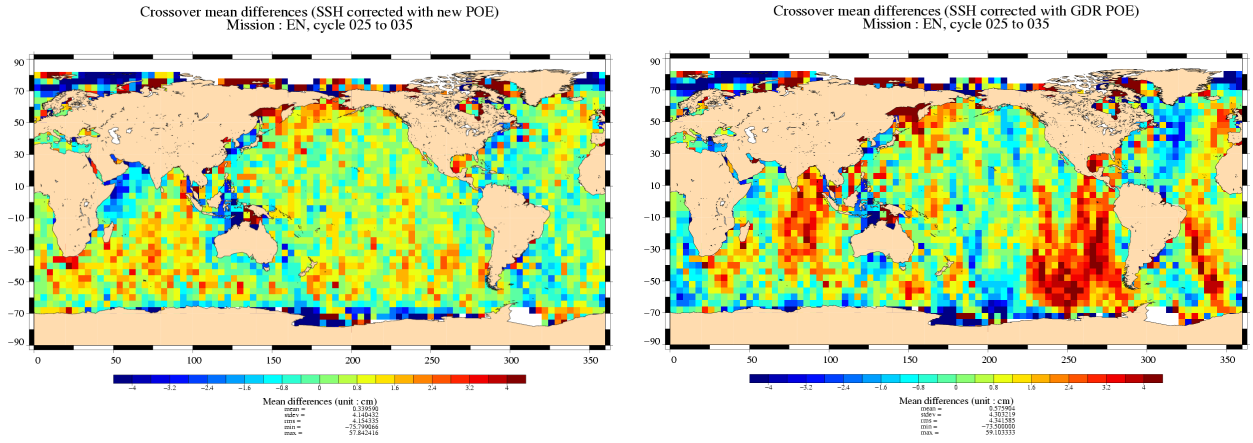

Figure 50: *Crossover mean differences. SSH corrected with POE July 2005 (left) and GDR POE (right).*

Figure 51 shows the gain in variance of SSH differences at crossovers using the July/GDR orbit. The blue color means that the July orbit has a lower variance of SSH differences at crossover than the GDR. The gain is very weak. The July orbit slightly improves the performances in south Pacific.

Figure 52 shows the cycle by cycle mean and standard deviation of differences. There is a strong annual signal on the 2 curves. This signal is not centered on zero and has an amplitude of 1-2 cm. The mean differences at crossovers using the July orbit is slightly different on cycles 25-27. On Cycle 28 onwards, the 2 curves are very close. The fact that the satellite is heliosynchroneous is probably the cause of this annual signal. This signal has to be investigated. It can either be due to the orbit or to a range correction. The standard deviation of the SSH difference at crossovers using the July orbit is lower by about 1mm in average (9.86cm to 9.76cm). The gain in variance is plotted on Figure 53. Using the July orbit allows us to improve the performance by 1 to 3 cm2, depending on the cycle.

8.4.3.3 Along track Performance

Figure 54 shows the gain in variance of SSH differences at crossovers using the July/GDR orbit. The blue color means that the July orbit has a lower variance of SSH differences at crossover than the GDR. The gain is more significant than at crossovers. The July orbit strongly improves the performances in areas where the geographically correlated ascending-descending differences have been reduced. The improvement

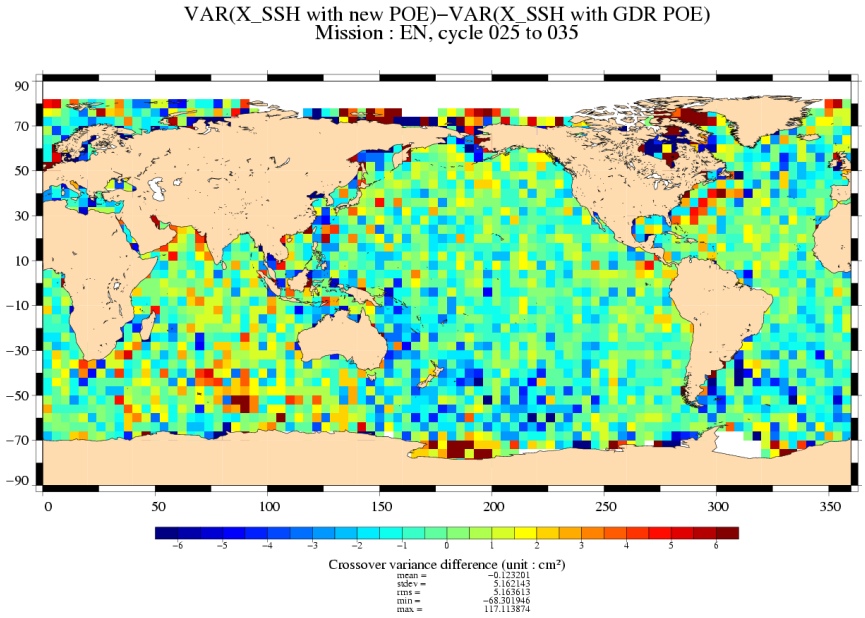

Figure 51: *VAR(X_SSH with POE July 2005) - VAR(X_SSH with GDR POE).*

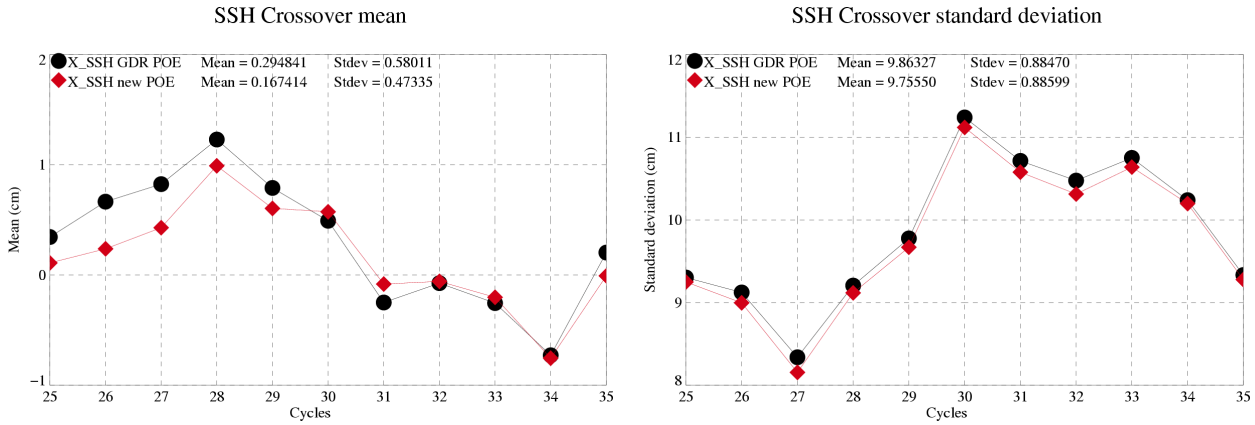

Figure 52: *Statistics per cycle of SSH: crossover mean (left) and crossover standard deviation (right).*

in South West Pacific, South Atlantic or Okhotsk is really significant: more than 5cm2 which correspond to 10% of the signal in this area. However a signal in North-West Indian appears (in blue) in the July configuration.

Figure 55 shows the cycle by cycle mean and standard deviation of SLA with the two orbits. As previously seen, there is almost no impact on the Mean Sea level. The SLA standard deviation are very close as well. The gain in variance is plotted on Figure 56. Using the July orbit allows us to improve the performance by 0 to 2 cm2, depending on the cycle.

Figure 57 shows the cycle by cycle mean SLA with the two orbits decomposing ascending and descending passes. As already seen on figure 52 the sea level has not the same mean value on ascending and descending passes.

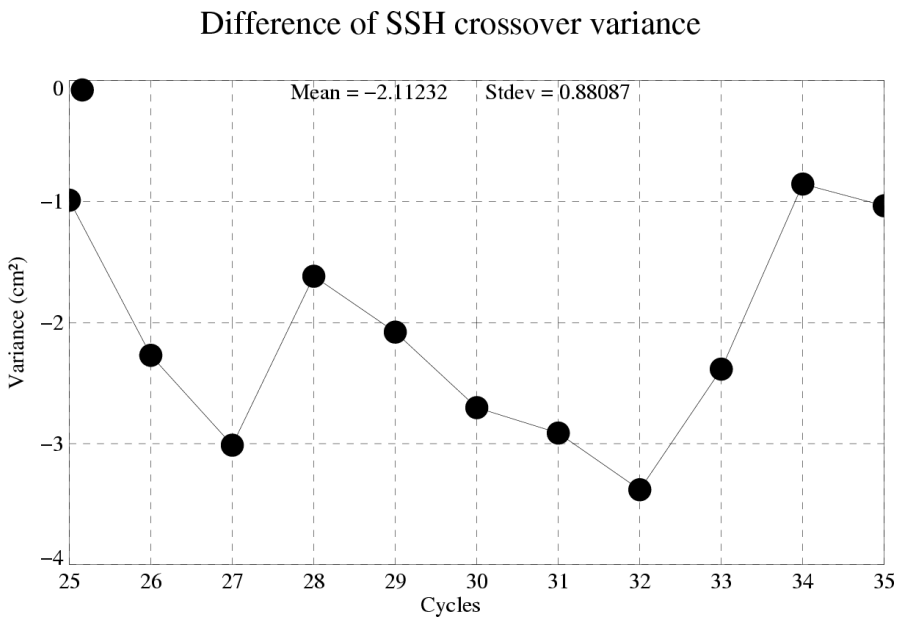

Figure 53: *Var(SSH differences at Xovers with POE July 2005) - Var(SSH differences at Xovers with GDR POE).*

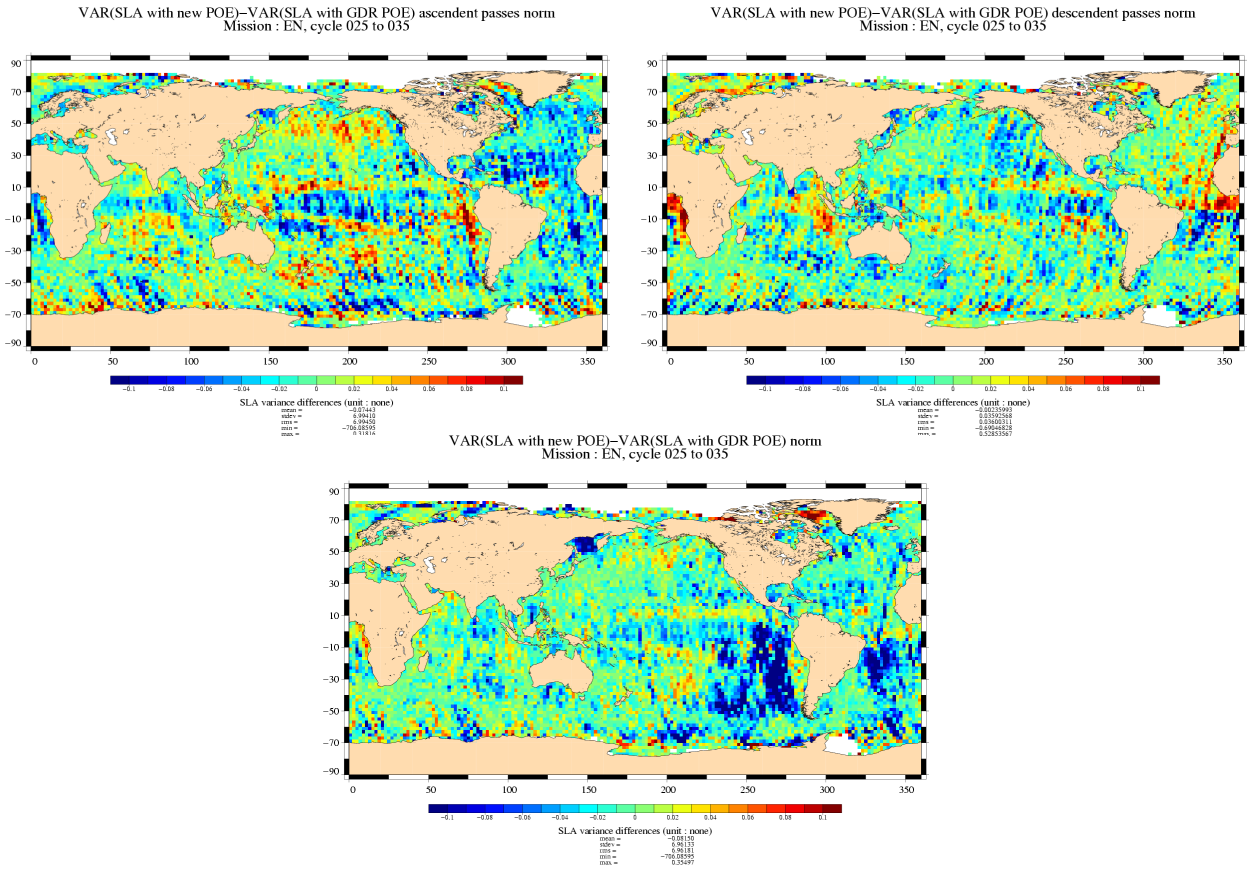

Figure 54: *[Var(SLA with POE July 2005) - Var(SLA with GDR POE)]/Var(SLA with POE July 2005) . Ascending passes (left), descending passes (right) and total (bot).*

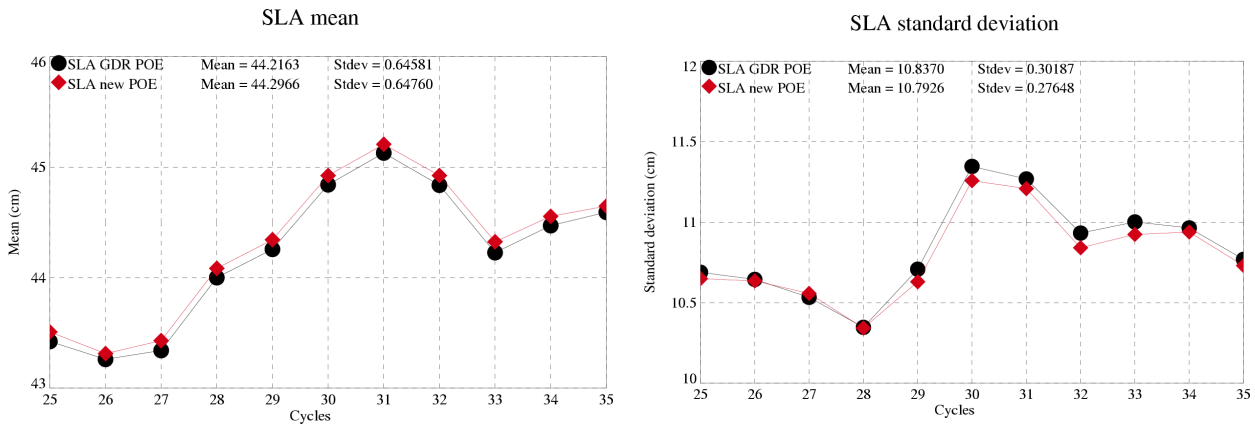

Figure 55: *SLA mean (left) and standard deviation (right) per cycle.*

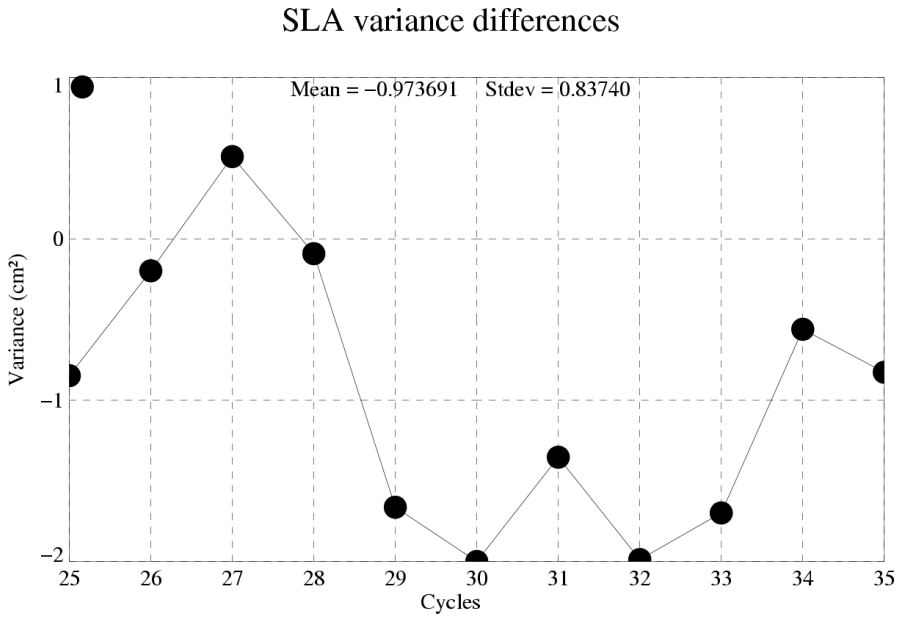

Figure 56: *Var(SLA with POE July 2005) - Var(SLA with GDR POE).*

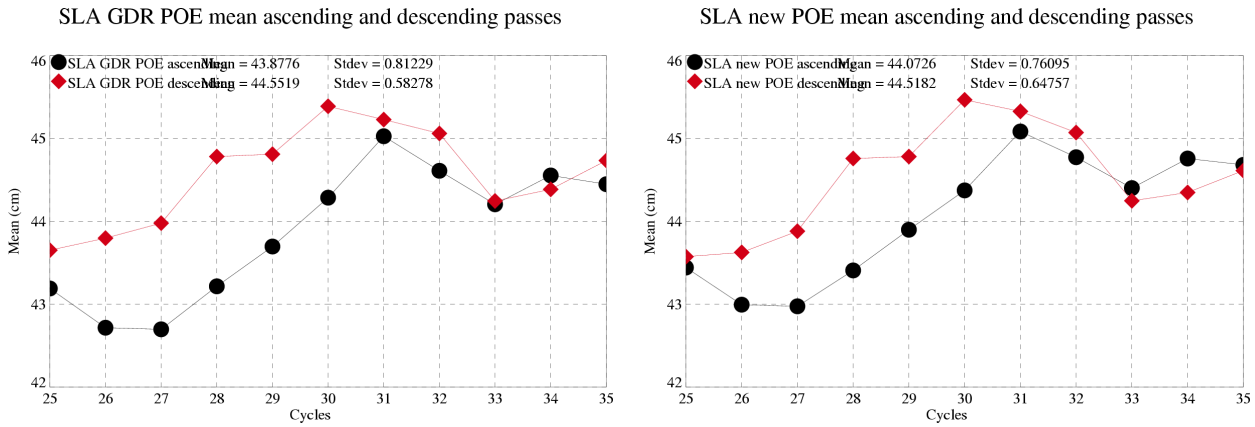

Figure 57: *SLA mean with GDR POE (left) and POE July 2005 (right) per cycle.*

8.4.4 Comparison July POE/October POE

8.4.4.1 Orbit differences

Figure 58 shows the mean differences over the period 25-35. On the two figures on the top, the ascending and descending passes have been plotted separately. On the bottom figure all the passes have been taken into account. The differences, lower than 1cm, are correlated along track. The sign of the difference is alternatively positive and negative on small packets of passes (around 30 ascending passes or 30 descending passes).

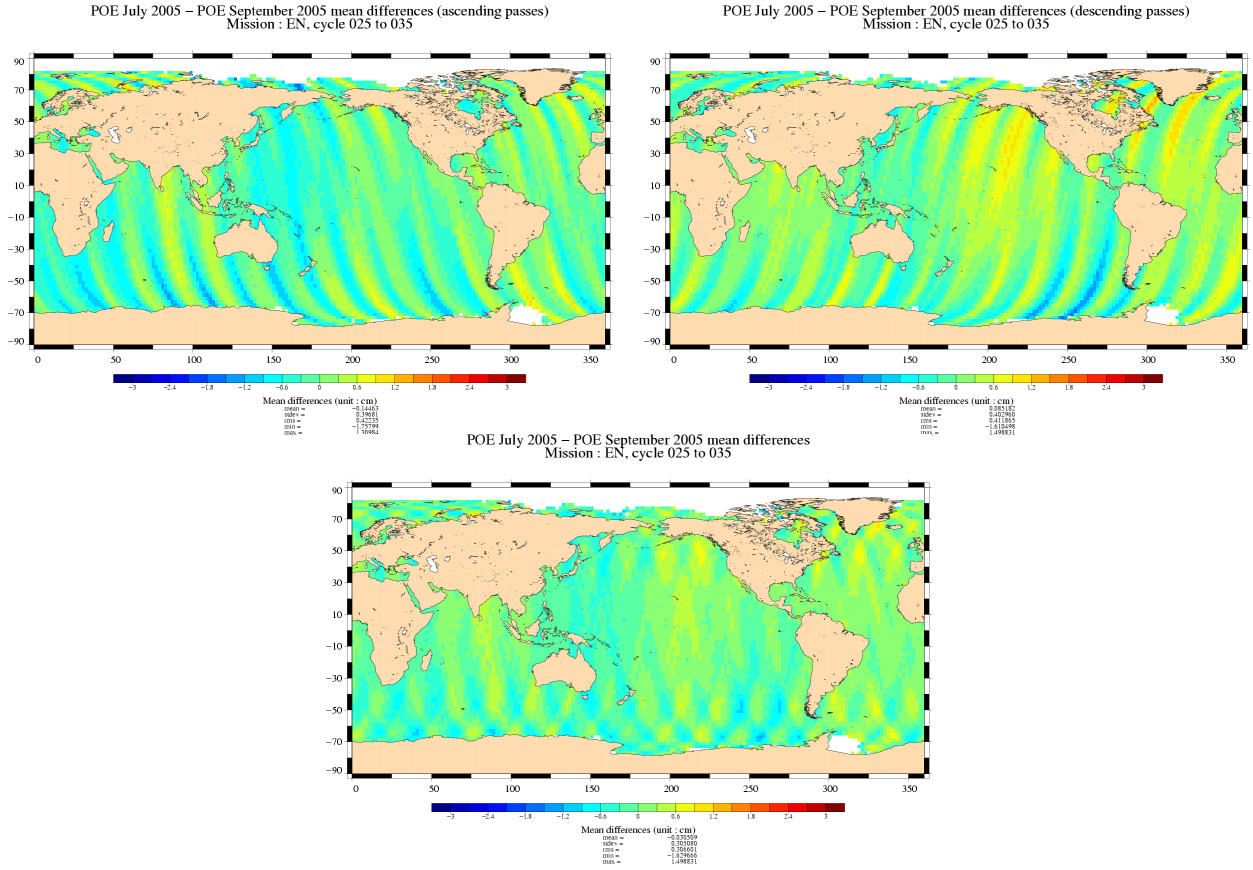

Figure 58: *POE July 2005 - POE October 2005 mean differences. Ascending passes (left), descending passes (right) and total (bot).*

Figure 59 shows the variance of the differences. The variance is low and quite homogeneous. The maximum values, about 1cm2, are observed at high latitudes.

Figure 60 shows the cycle by cycle mean and variance of differences. The global bias between the two orbits is about 0. It is quite stable over the period. The variance is about 0.3 cm2.

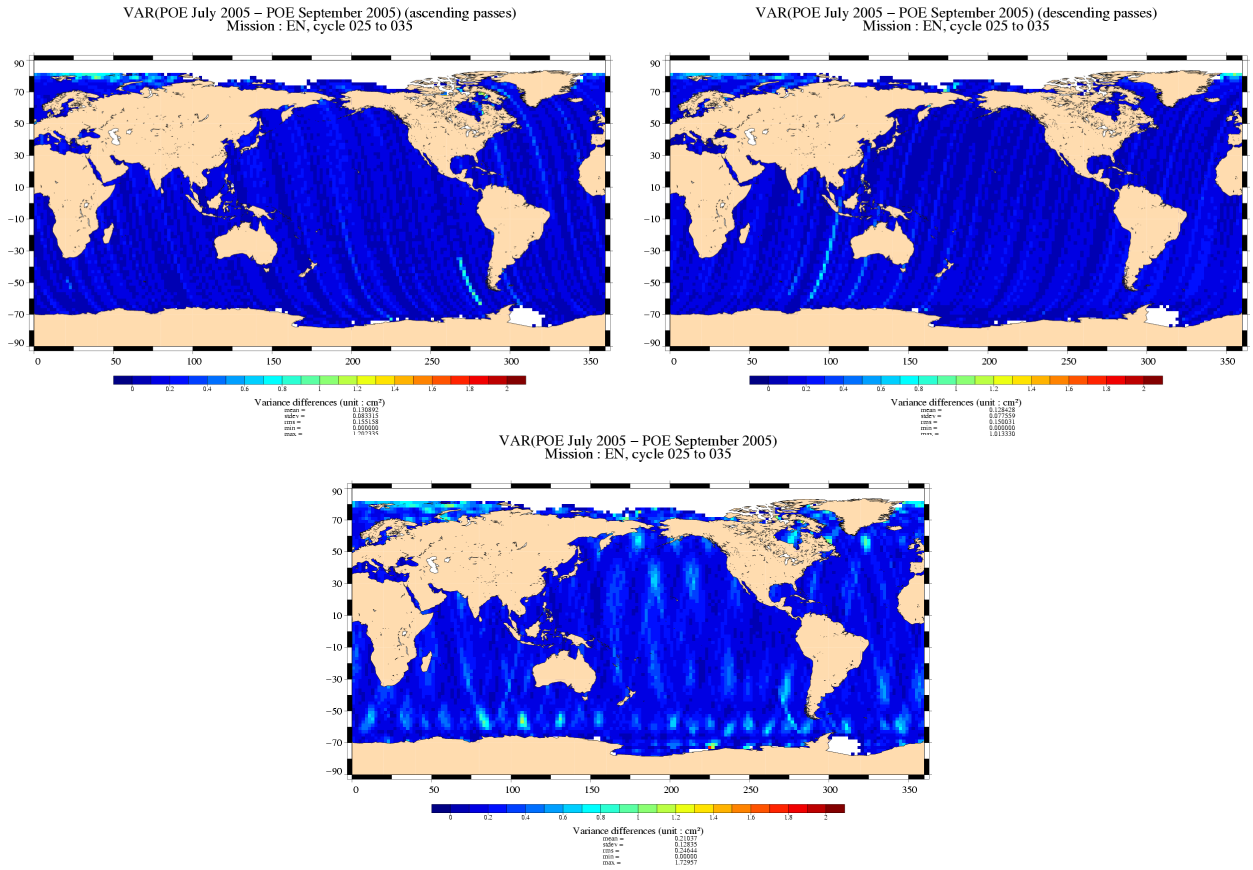

Figure 59: *Var(POE July 2005 - POE October 2005). Ascending passes (left), descending passes (right) and total (bot).*

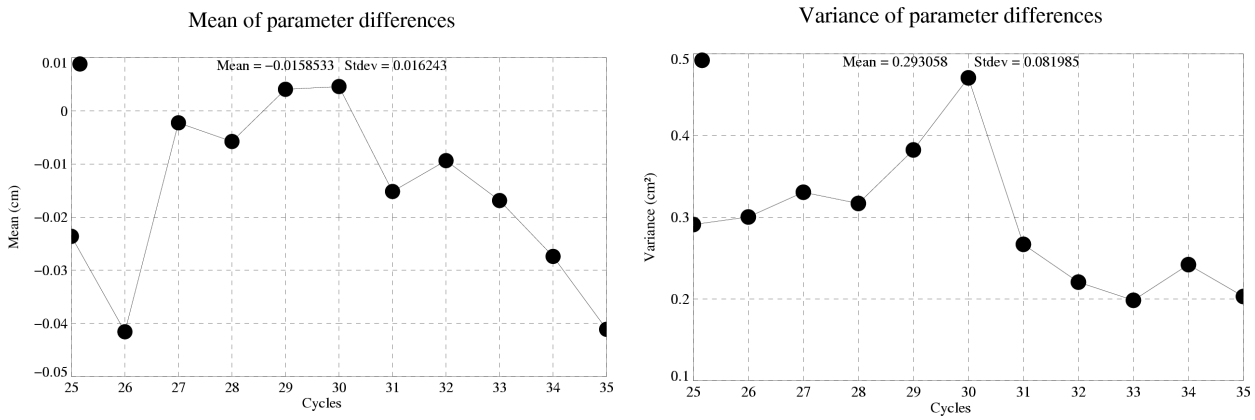

Figure 60: *Statistics per cycle of differences: mean (left) and variance (right).*

8.4.4.2 Performance at crossovers

Figure 61 shows the mean SSH differences at crossovers using the July orbit and the October orbit. The geographically correlated errors are lower in the October configuration reduced. The signal in North-West Indian is still visible (in blue).

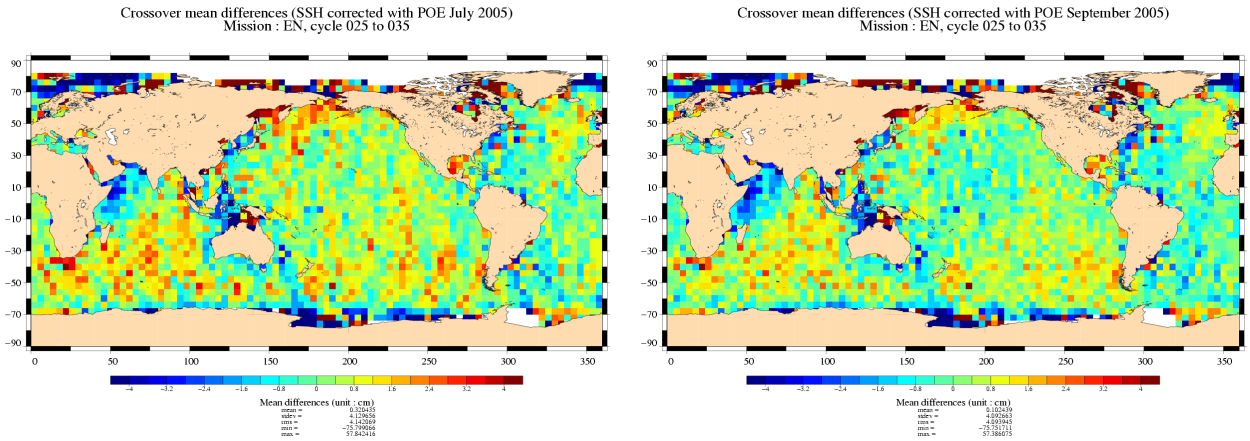

Figure 61: *Crossover mean differences. SSH corrected with POE July 2005 (left) and POE October 2005 (right).*

Figure 62 shows the gain in variance of SSH differences at crossovers using the July/October orbit.

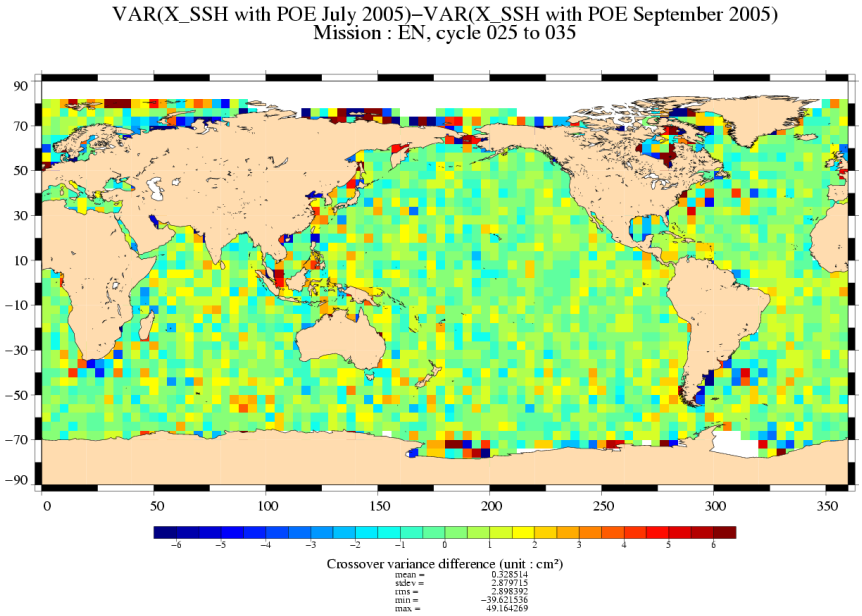

Figure 62: *VAR(X_SSH with POE July 2005) - VAR(X_SSH with POE October 2005).*

Figure 63 shows the cycle by cycle mean and standard deviation of differences. The amplitude of the annual signal is lower in the October configuration by 0.5 cm. The standard deviation of the SSH difference at crossovers are about the same in the two cases. The gain in variance is plotted on Figure 64. Using the October orbit allows us to improve the performance by 0 to 2 cm2, depending on the cycle.

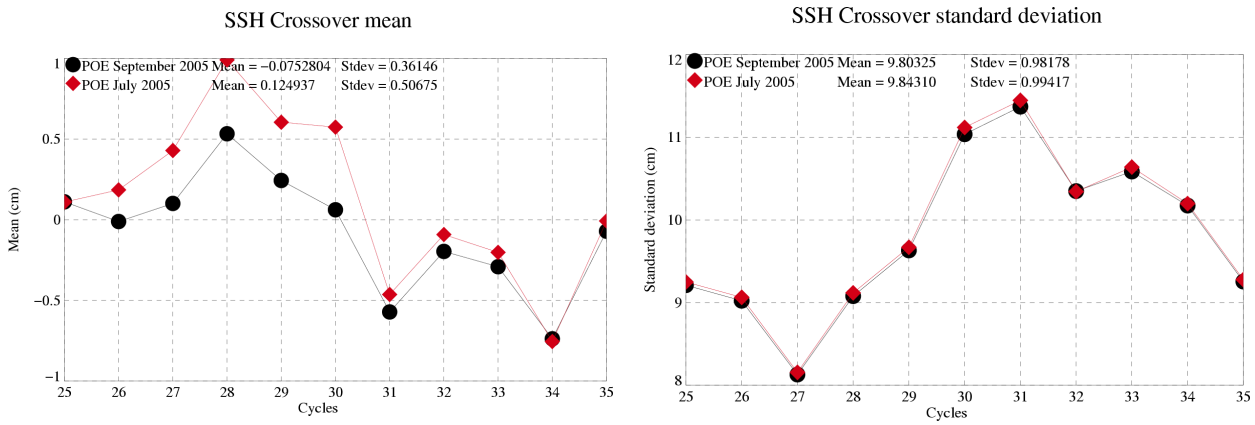

Figure 63: *Statistics per cycle of SSH: crossover mean (left) and crossover standard deviation (right).*

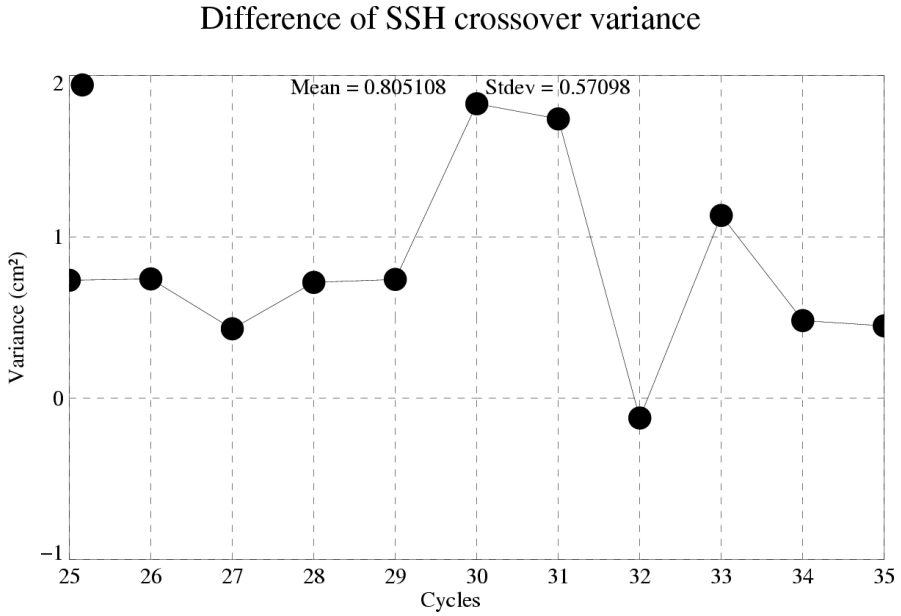

Figure 64: *Var(SSH differences at Xovers with POE July 2005) - Var(SSH differences at Xovers with POE October 2005).*

8.4.4.3 Along track Performance

Figure 65 shows the gain in variance of SSH differences at crossovers using the new/GDR orbit. The differencea are not significant.

Figure 66 shows the cycle by cycle mean and standard deviation of SLA with the two orbits.

Figure 68 shows the cycle by cycle mean SLA with the two orbits decomposing ascending and descending passes.

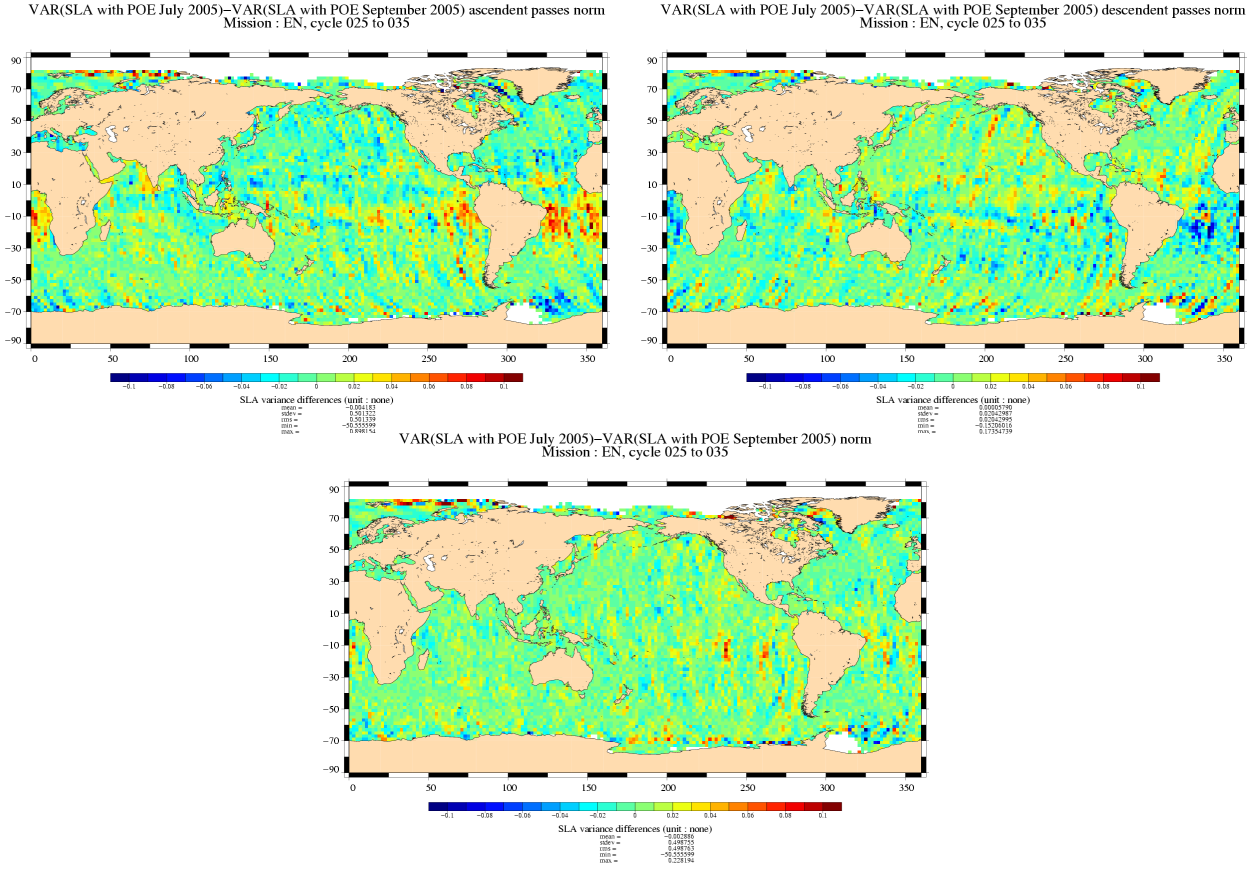

Figure 65: *[Var(SLA with POE July 2005) - Var(SLA with POE October 2005)]/Var(SLA with POE July 2005) . Ascending passes (left), descending passes (right) and total (bot).*

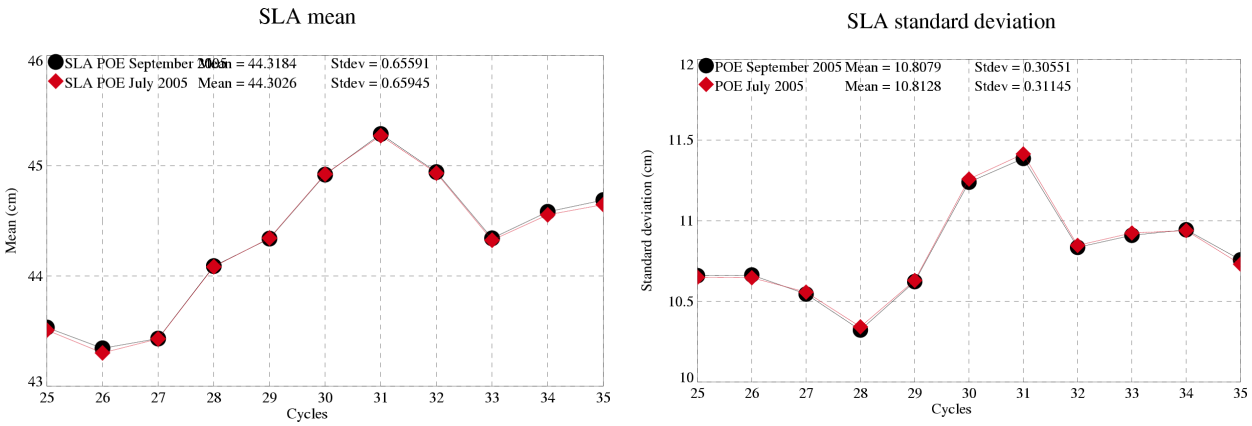

Figure 66: *SLA mean (left) and standard deviation (right) per cycle.*

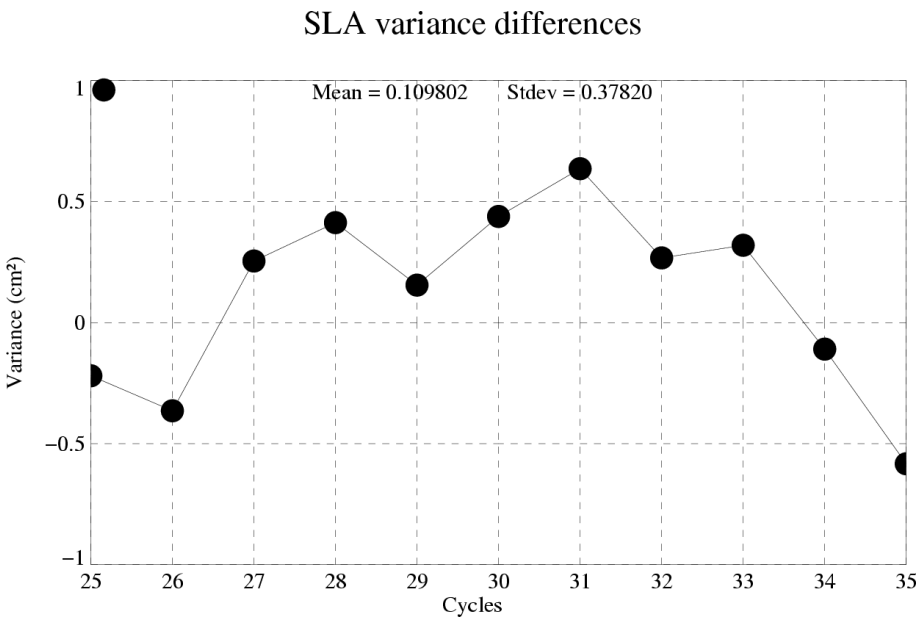

Figure 67: *Var(SLA with POE July 2005) - Var(SLA with POE October 2005).*

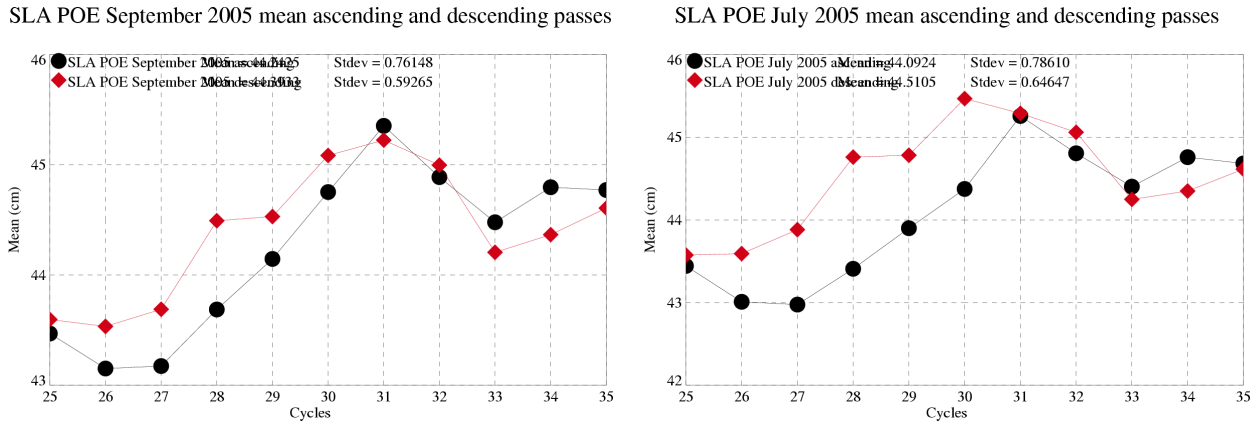

Figure 68: *SLA mean with POE October 2005 (left) and POE July 2005 (right) per cycle.*

8.4.5 Comparison Delft/July POE

8.4.5.1 Orbit differences

Figure 69 shows the mean differences over the period 25-35. On the two figures on the top, the ascending and descending passes have been plotted separately. On the bottom figure all the passes have been taken into account. The differences are quite small, lower than 1 cm. Delft is slightly higher than the POE July 2005 in the Pacific Ocean and slightly lower in the Atlantic and Indian Ocean.

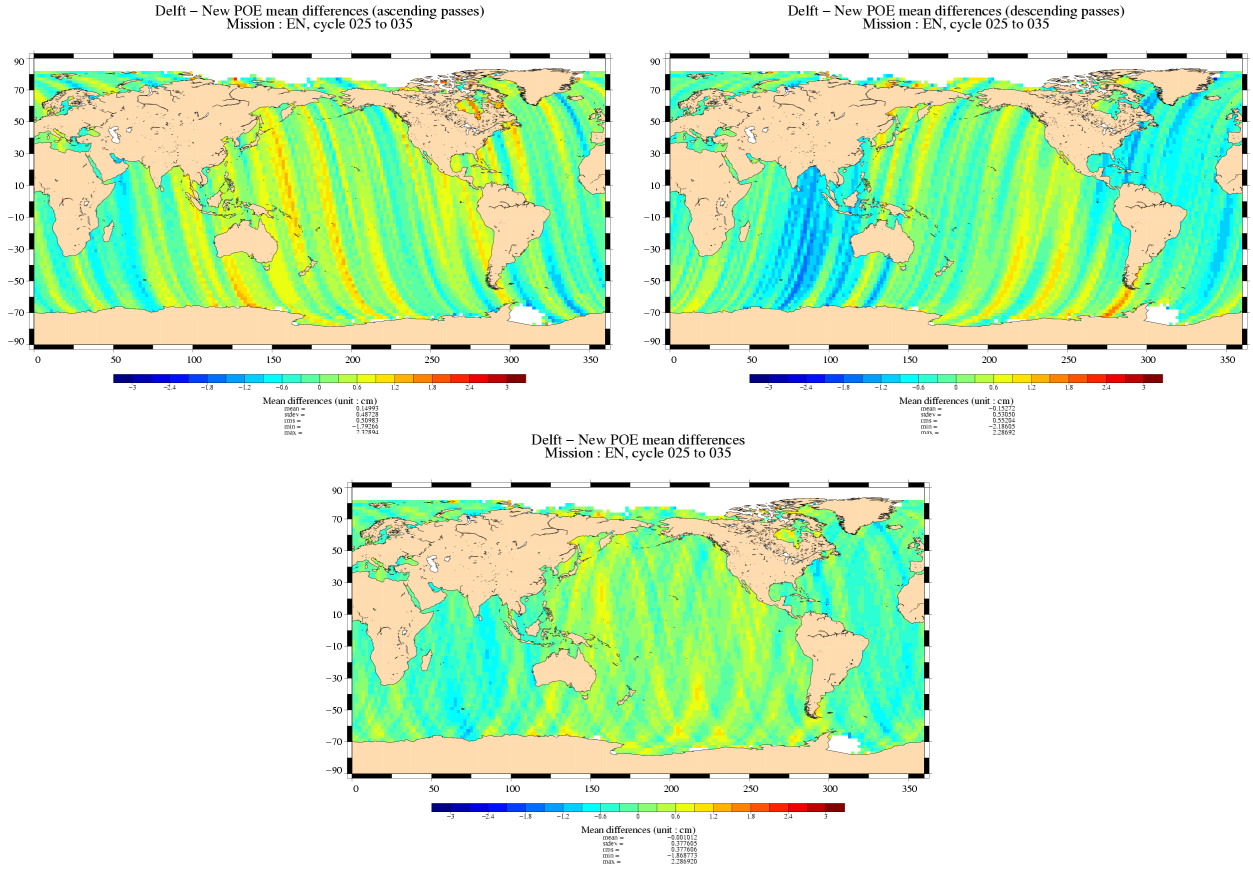

Figure 69: *Delft - POE July 2005 mean differences. Ascending passes (left), descending passes (right) and total (bot).*

Figure 70 shows the variance of the differences. The variance of the difference Delft/New orbit is lower than the difference New/GDR. However it has values greater than 1 cm2 on passes crossing Australia and in Atlantic Ocean (>2cm2).

Figure 71 shows the cycle by cycle mean and variance of differences. The global bias between the two orbits is about 0. It is quite stable over the period. The variance is about 0.9 cm2.

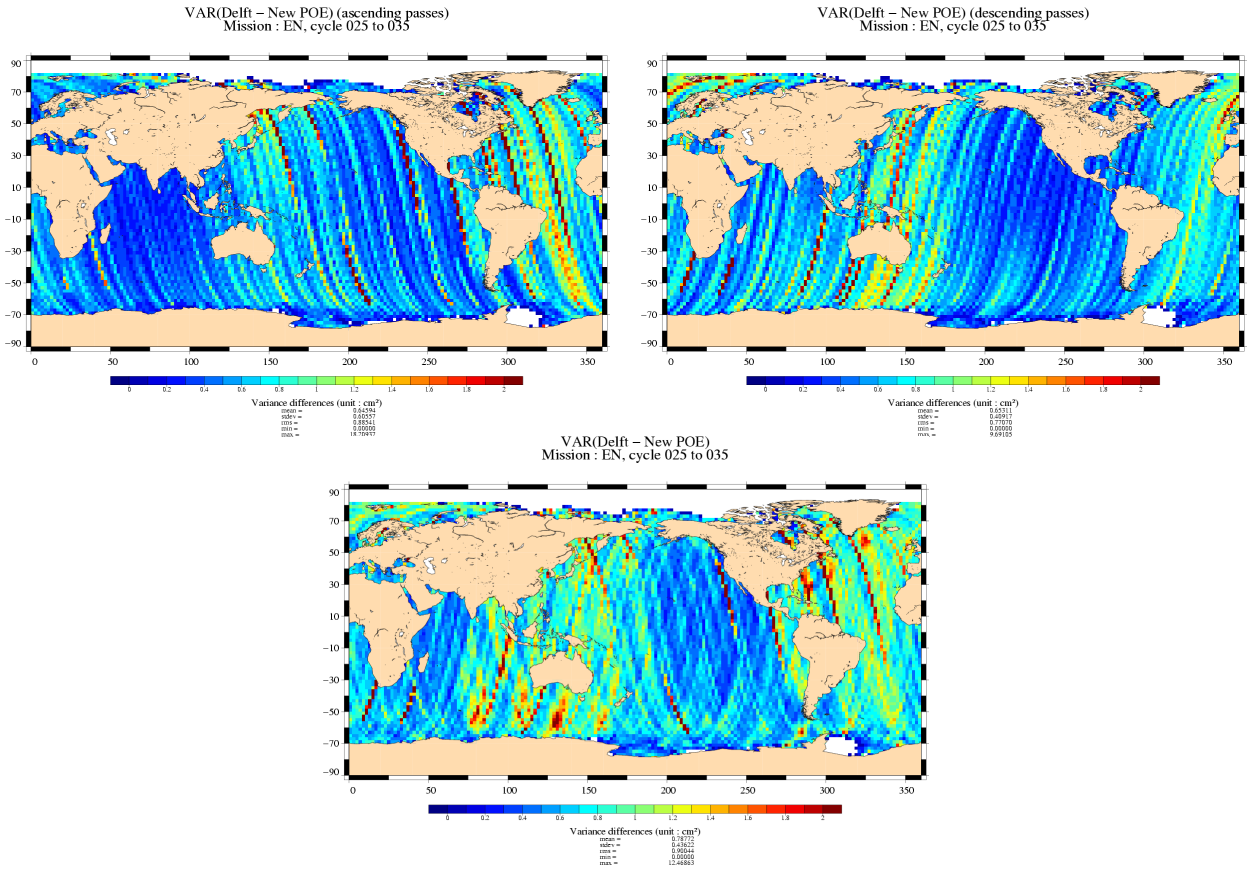

Figure 70: *Var(Delft - POE July 2005). Ascending passes (left), descending passes (right) and total (bot).*

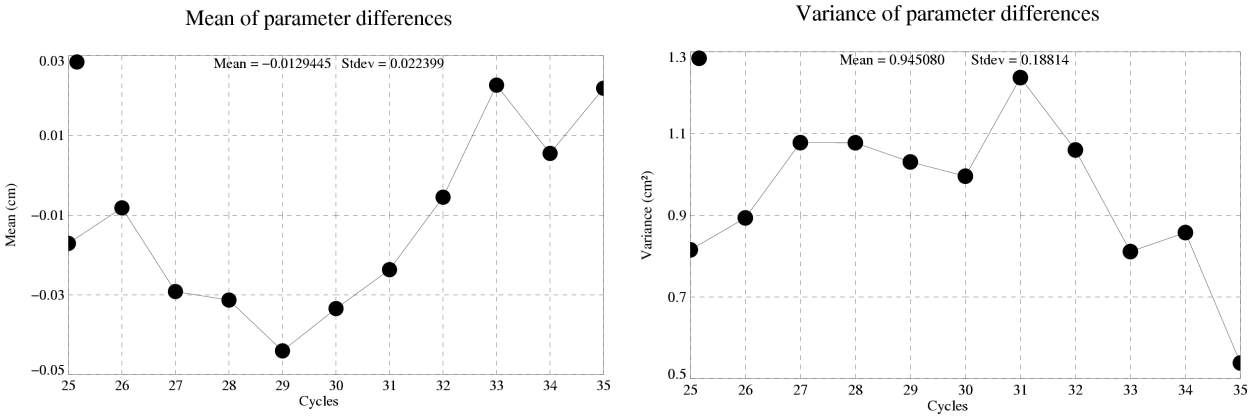

Figure 71: *Statistics per cycle of differences: mean (left) and variance (right).*

8.4.5.2 Performance at crossovers

Figure 72 shows the mean SSH differences at crossovers using the Delft orbit and the new orbit. The 2 maps are very similar. However some slight geographically correlated errors seem to be visible in Pacific and Indian Ocean.

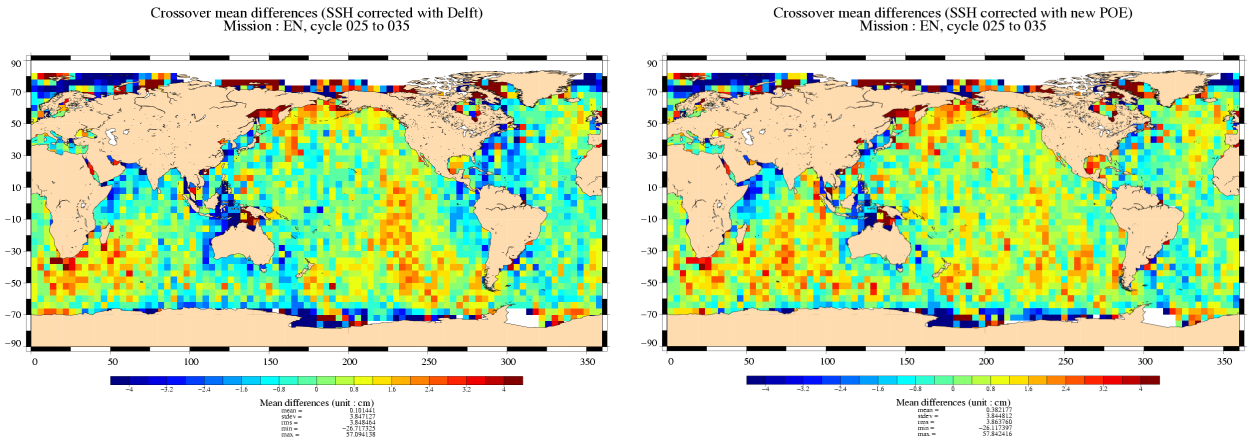

Figure 72: *Crossover mean differences. SSH corrected with Delft (left) and POE July 2005 (right).*

Figure 73 shows the gain in variance of SSH differences at crossovers using the Delft/New orbit. The two orbits seem to have similar performances.

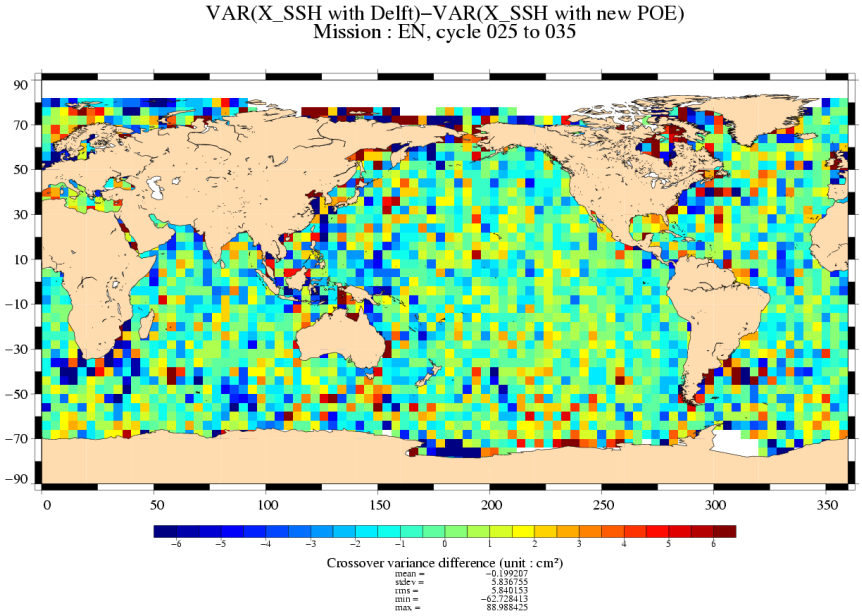

Figure 73: *VAR(X_SSH with Delft) - VAR(X_SSH with POE July 2005).*

Figure 74 shows the cycle by cycle mean and standard deviation of differences. There is a strong annual signal on the 2 curves. The amplitude of the annual signal is a bit lower on the Delft orbit but is still present. The standard deviation of SSH difference at crossovers is strictly the same for the two orbits. The gain in variance is plotted on Figure 75. The gain is between -1 and 1 cm2 that is not significant.

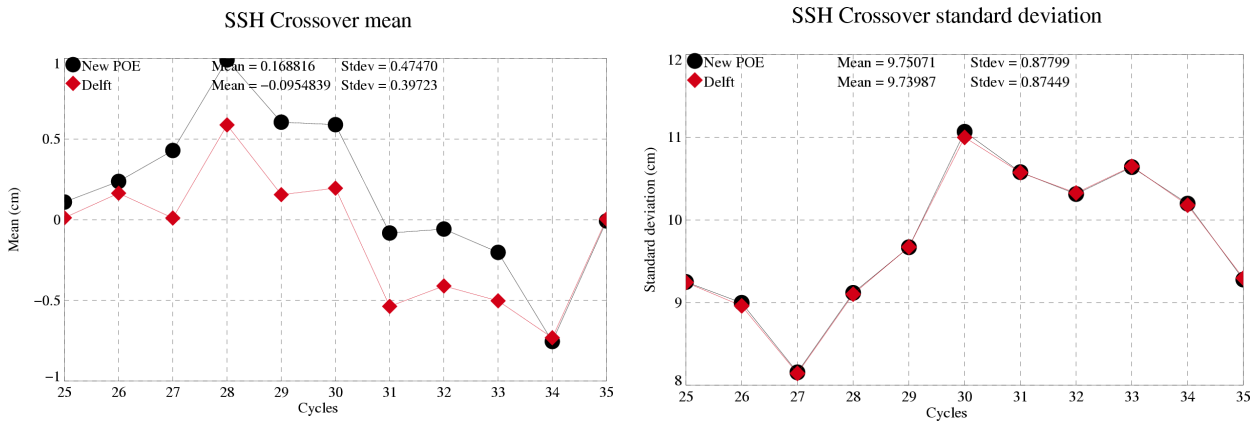

Figure 74: *Statistics per cycle of SSH: crossover mean (left) and crossover standard deviation (right).*

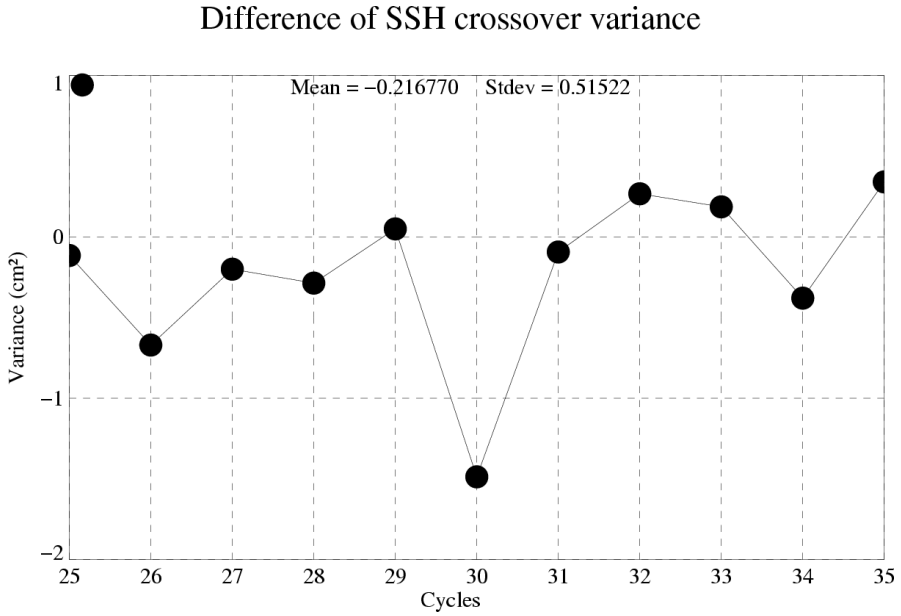

Figure 75: *Var(SSH differences at Xovers with Delft) - Var(SSH differences at Xovers with POE July 2005).*

8.4.5.3 Along track Performance

Figure 76 shows the gain in variance of along track SLA using the Delft/new orbit. The along track performances are, in average, similar. However, some differences are visible in Equatorial Pacific and Atlantic.

Figure 77 shows the cycle by cycle mean and standard deviation of SLA with the two orbits. The SLA standard deviations are very close. The gain in variance is plotted on Figure 78. The gain is between -1 and 1 cm2, which is not significant.

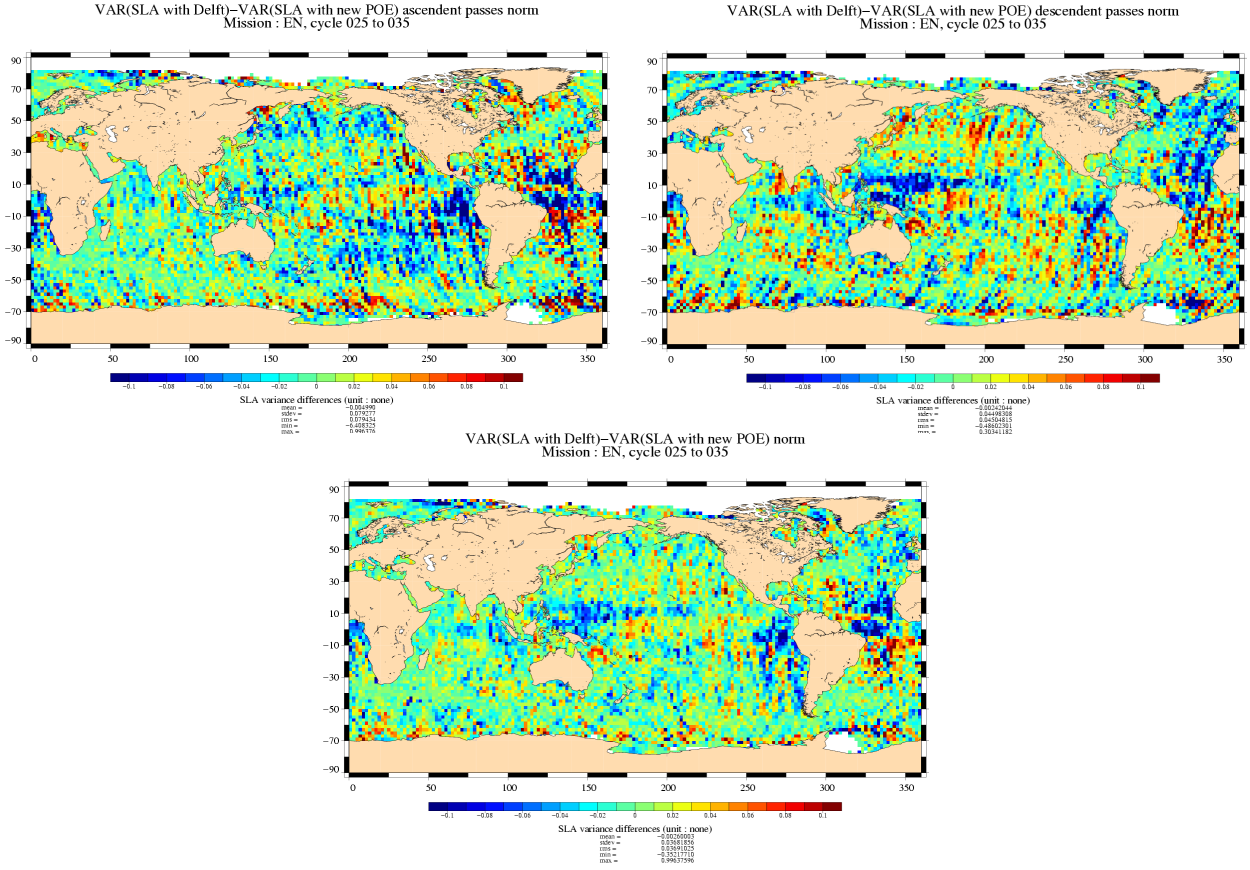

Figure 76: *[Var(SLA with Delft) - Var(SLA with POE July 2005)]/Var(SLA with Delft). Ascending passes (left), descending passes (right) and total (bot).*

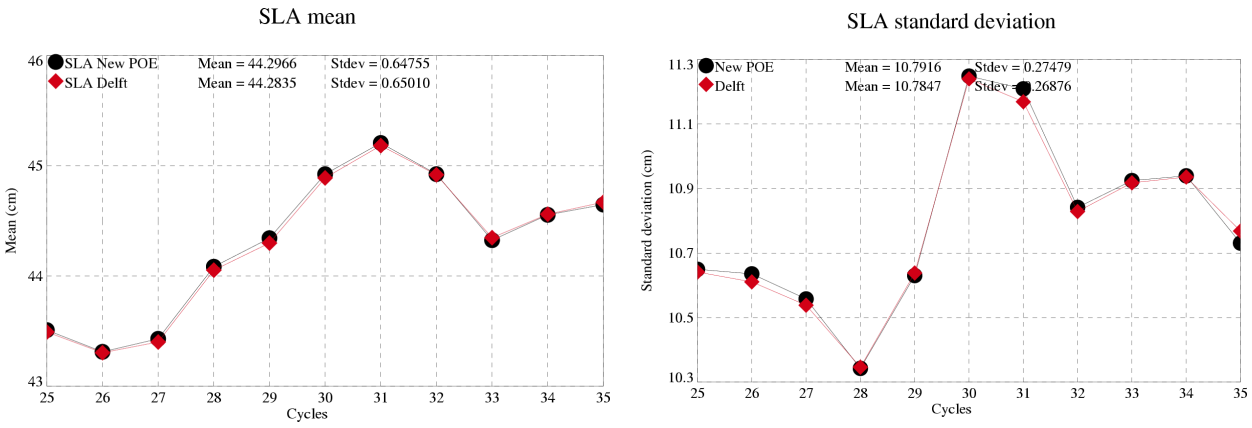

Figure 77: *SLA mean (left) and standard deviation (right) per cycle.*

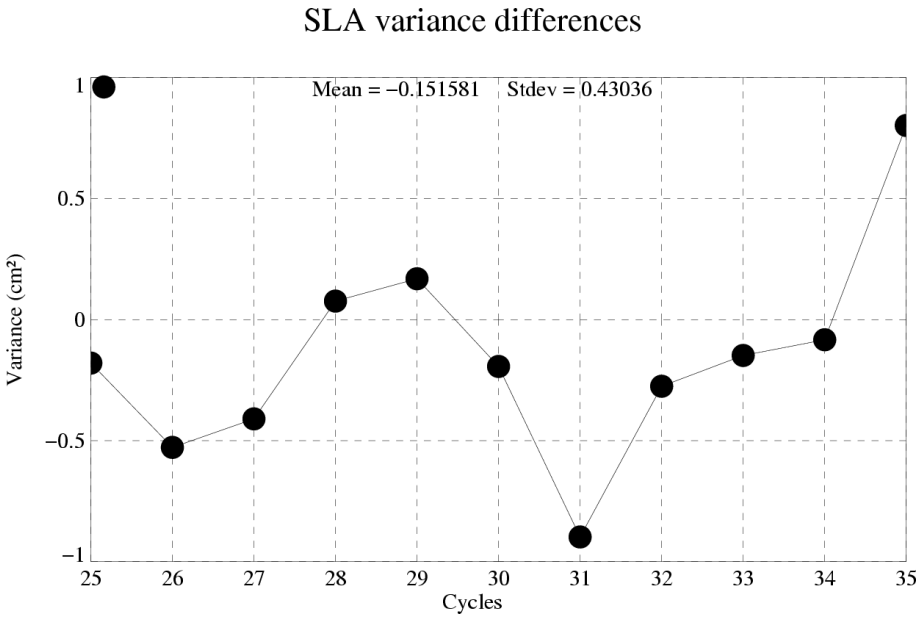

Figure 78: *Var(SLA with Delft) - Var(SLA with POE July 2005).*

8.4.6 Comparison Delft/October POE

8.4.6.1 Orbit differences

Figure 69 shows the mean differences over the period 25-35. On the two figures on the top, the ascending and descending passes have been plotted separately. On the bottom figure all the passes have been taken into account. The differences are quite small, lower than 1 cm. Delft is slightly higher than the POE July 2005 in the Pacific Ocean and slightly lower in the Atlantic and Indian Ocean.

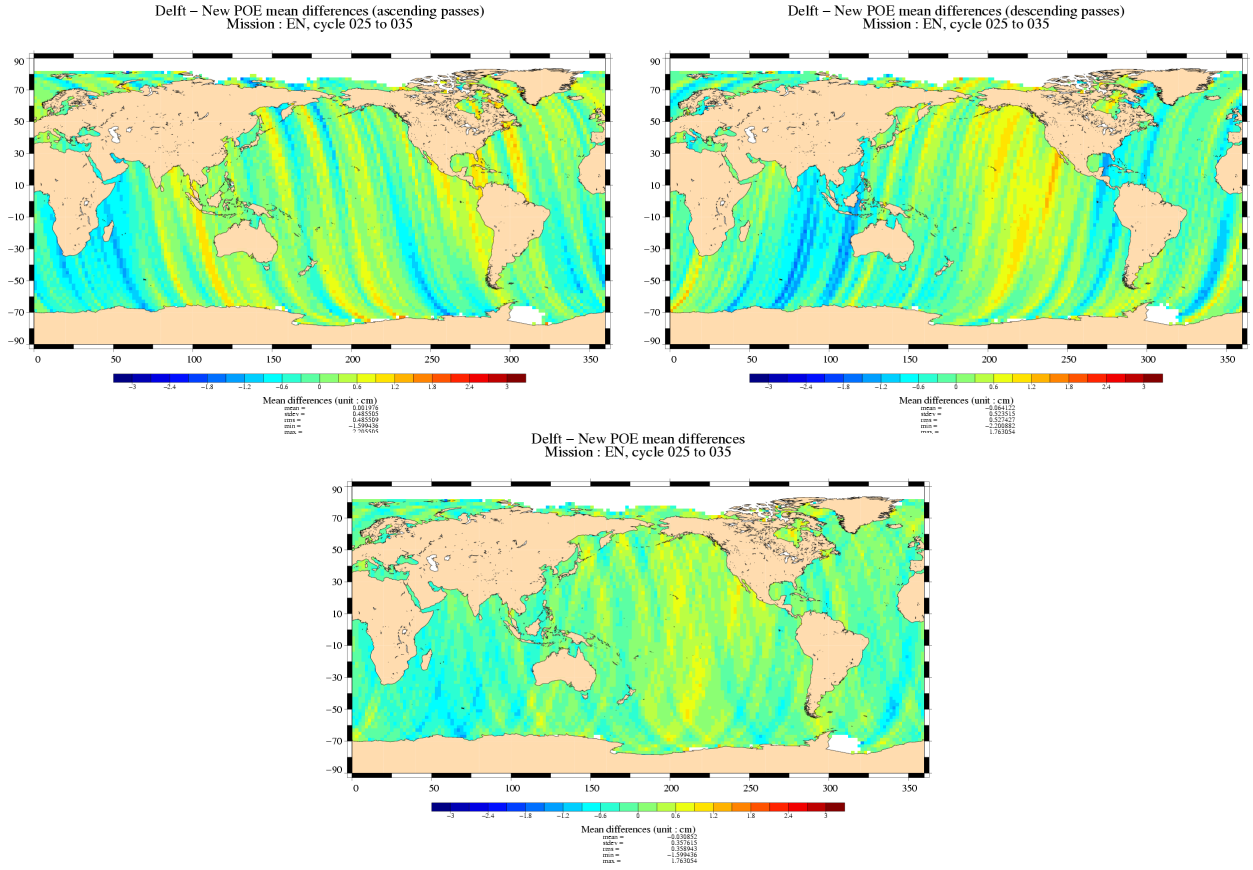

Figure 79: *Delft - POE October 2005 mean differences. Ascending passes (left), descending passes (right) and total (bot).*

Figure 70 shows the variance of the differences. The variance of the difference Delft/October orbit is lower than the difference Delft/July.

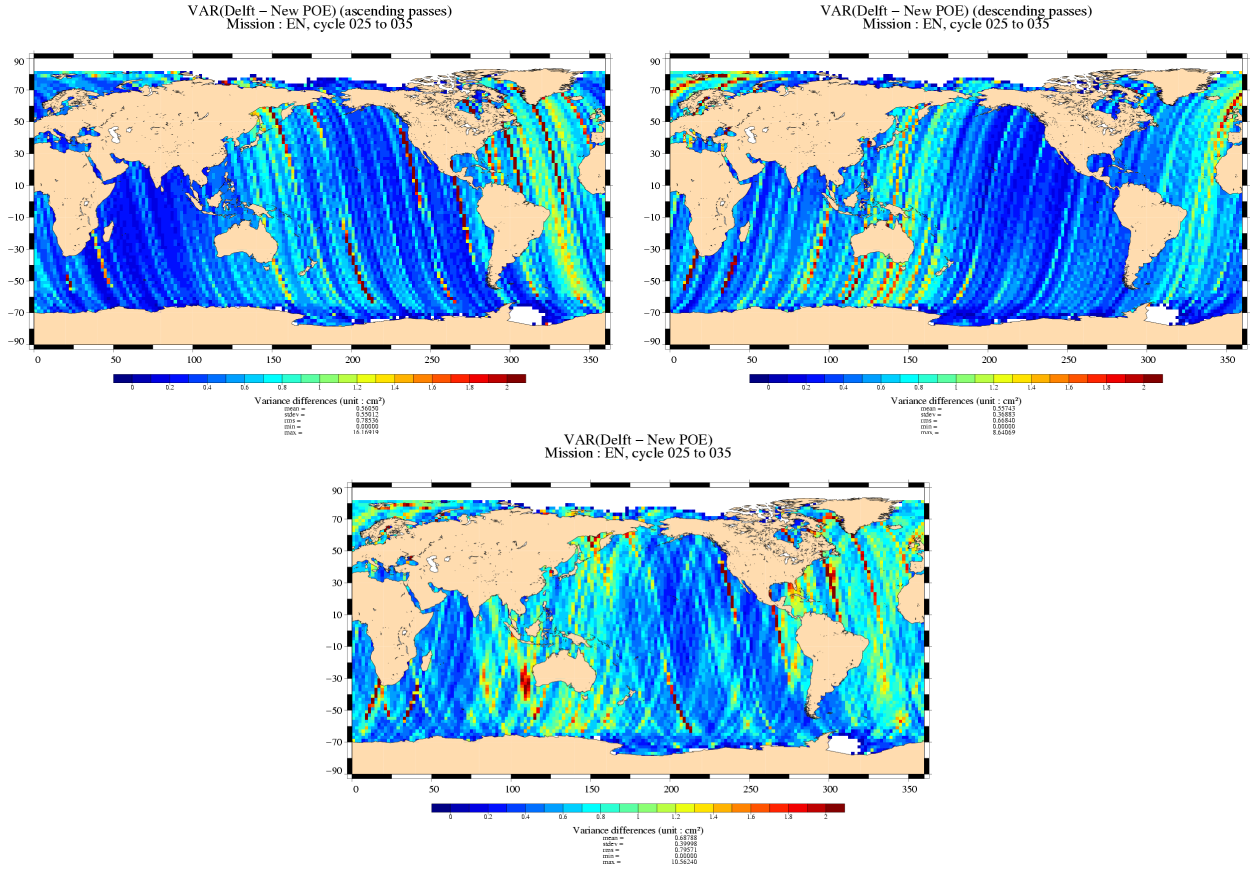

Figure 80: *Var(Delft - POE October 2005). Ascending passes (left), descending passes (right) and total (bot).*

Figure 71 shows the cycle by cycle mean and variance of differences. The global bias between the two orbits is about 0. It is quite stable over the period. The variance is about 0.8 cm2.

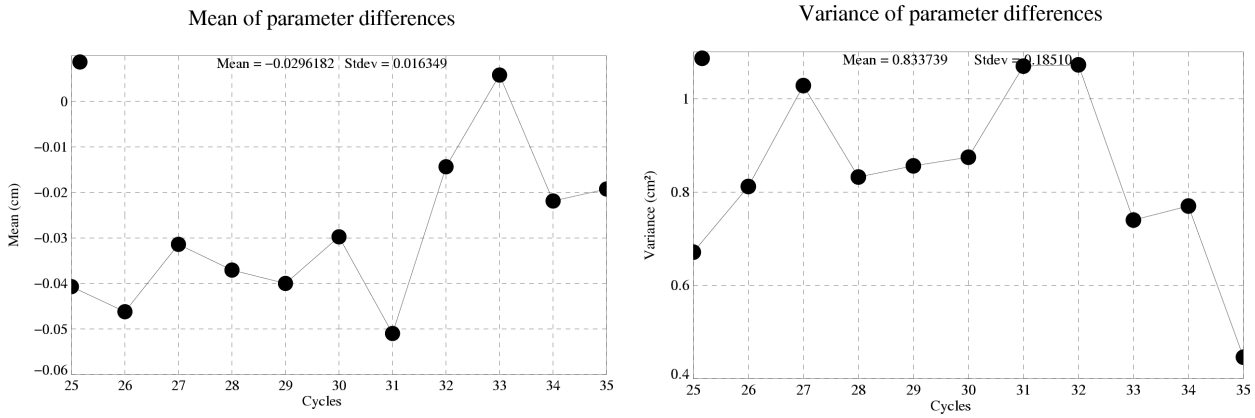

Figure 81: *Statistics per cycle of differences: mean(Delft - POE October 2005) (left) and variance(Delft - POE October 2005) (right).*

8.4.6.2 Performance at crossovers

Figure 72 shows the mean SSH differences at crossovers using the Delft orbit and the October orbit. The geographically correlated errors are lower in the October configuration.

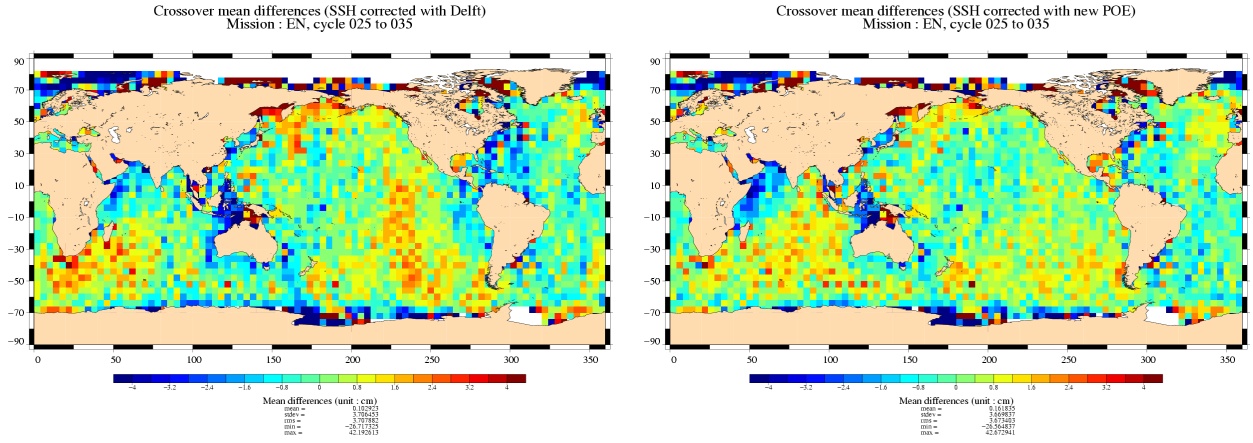

Figure 82: *Crossover mean differences. SSH corrected with Delft (left) and POE October 2005 (right).*

Figure 73 shows the gain in variance of SSH differences at crossovers using the Delft/New orbit. The two orbits seem to have similar performances.

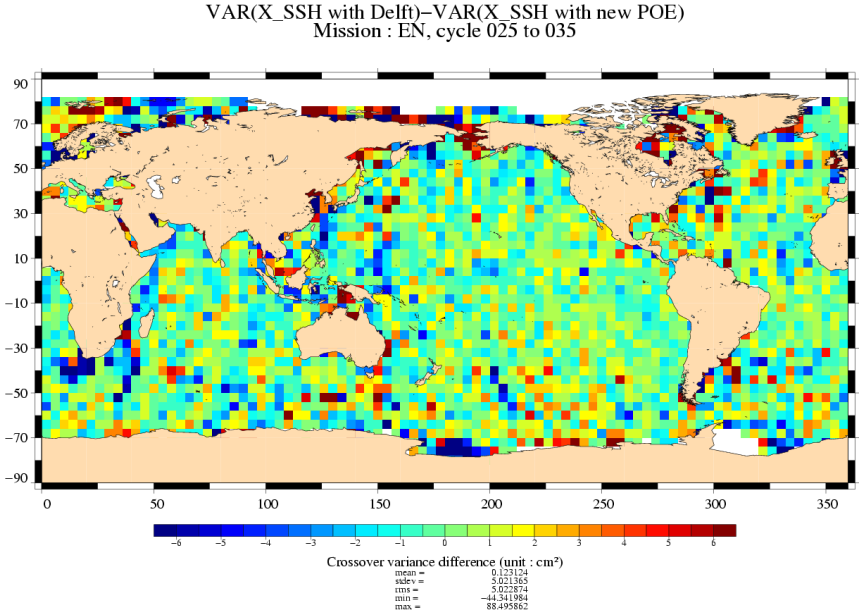

Figure 83: *VAR(X_SSH with Delft) - VAR(X_SSH with POE October 2005).*

Figure 74 shows the cycle by cycle mean and standard deviation of differences. The annual signal is

similar in the two configurations. The standard deviation of SSH difference at crossovers is about the same for the two orbits. The gain in variance is plotted on Figure 75. The gain is between 0 and 1 cm2 that is not significant.

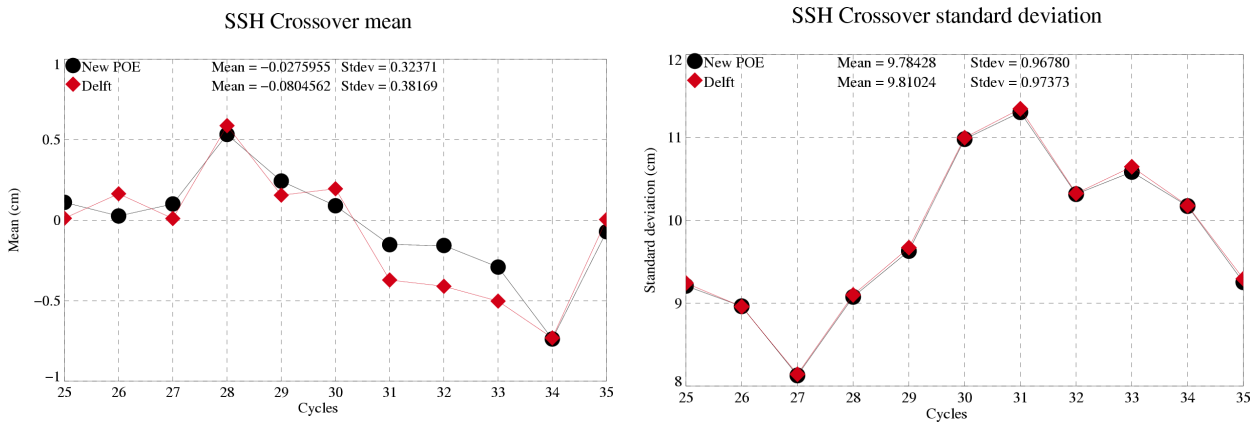

Figure 84: *Statistics per cycle of SSH: crossover mean (left) and crossover standard deviation (right). (Delft - POE October 2005)*

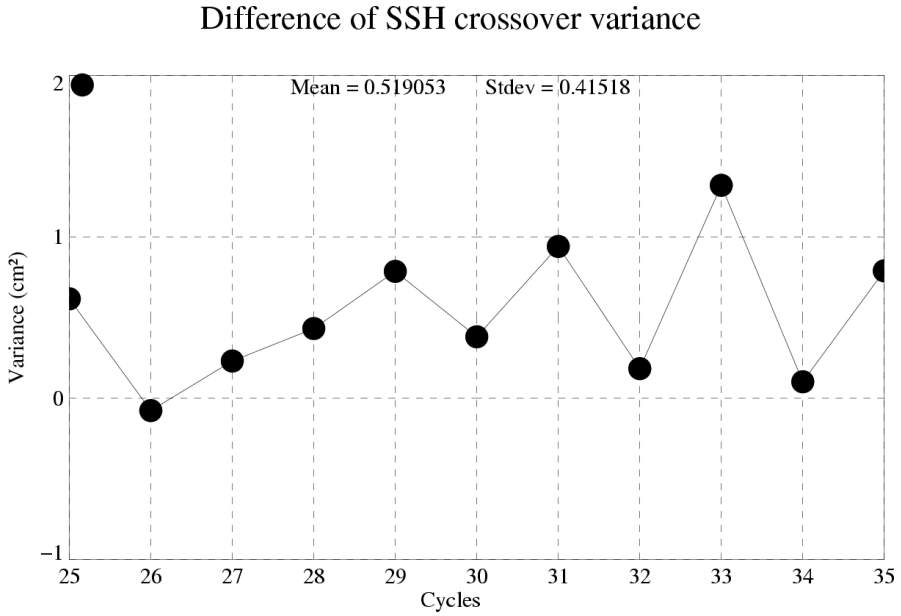

Figure 85: *Var(SSH differences at Xovers with Delft) - Var(SSH differences at Xovers with POE October 2005).*

8.4.6.3 Along track Performance

Figure 76 shows the gain in variance of along track SLA using the Delft/new orbit.

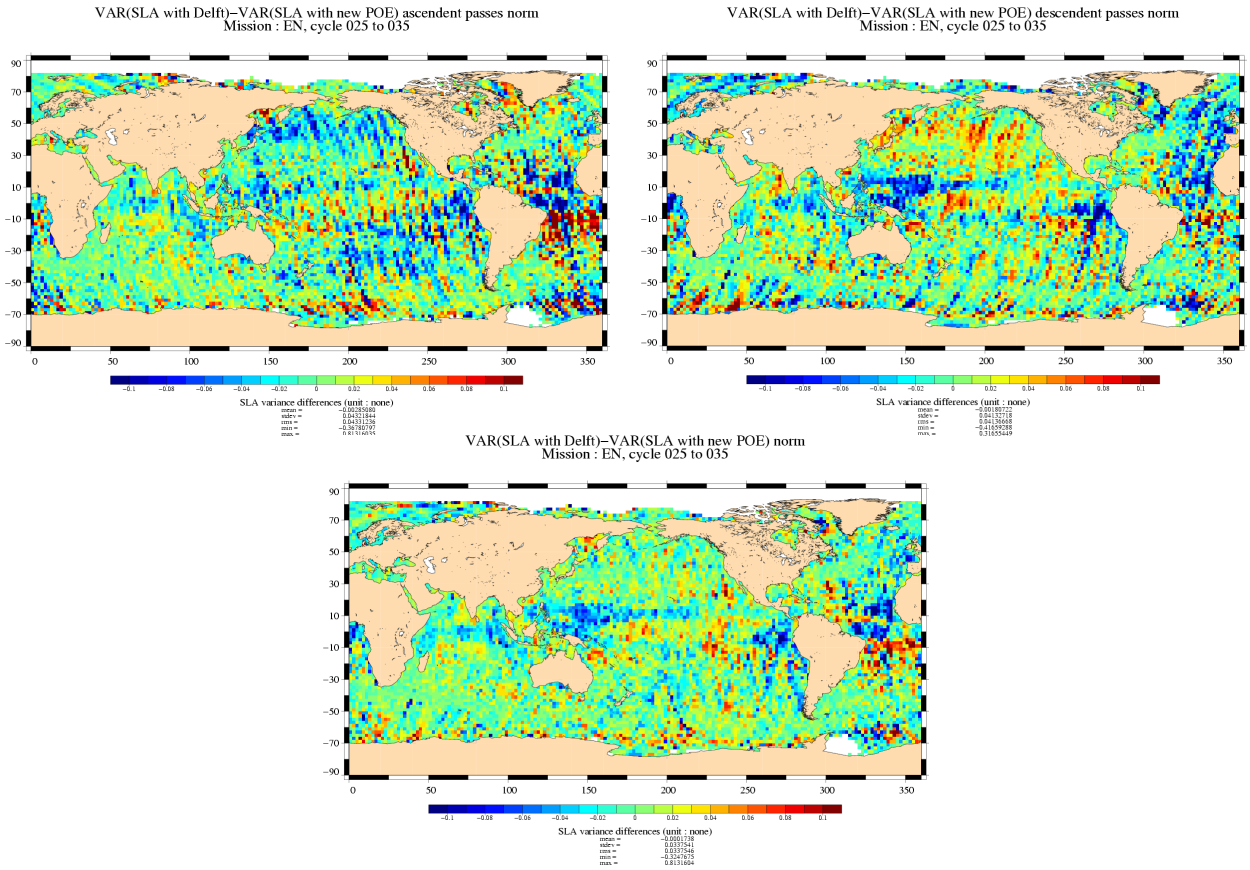

Figure 86: *[Var(SLA with Delft) - Var(SLA with POE October 2005)]/Var(SLA with Delft). Ascending passes (left), descending passes (right) and total (bot).*

Figure 77 shows the cycle by cycle mean and standard deviation of SLA with the two orbits. The SLA standard deviations are very close. The gain in variance is plotted on Figure 78. The gain is between -1 and 1 cm2, which is not significant.

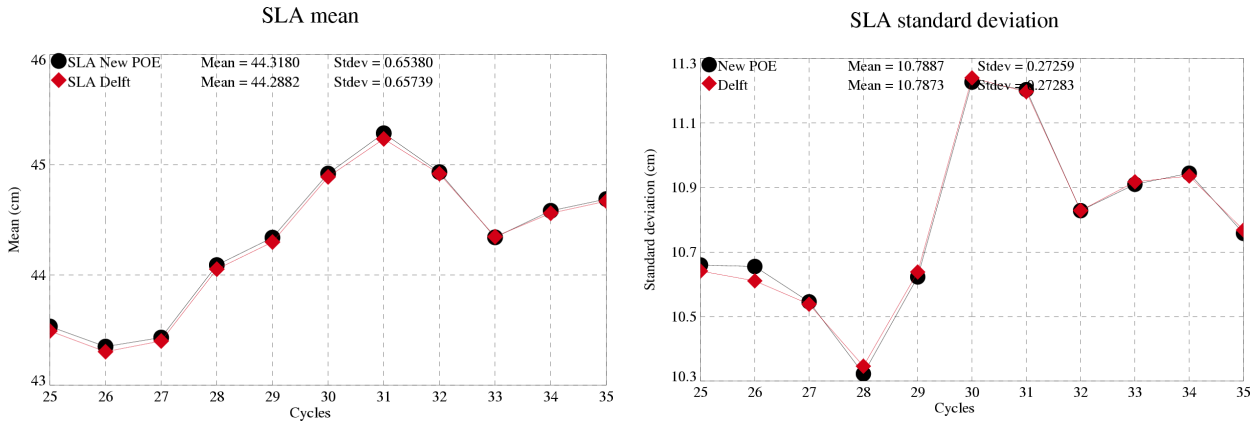

Figure 87: *SLA mean (left) and standard deviation (right) per cycle. (Delft - POE October 2005)*

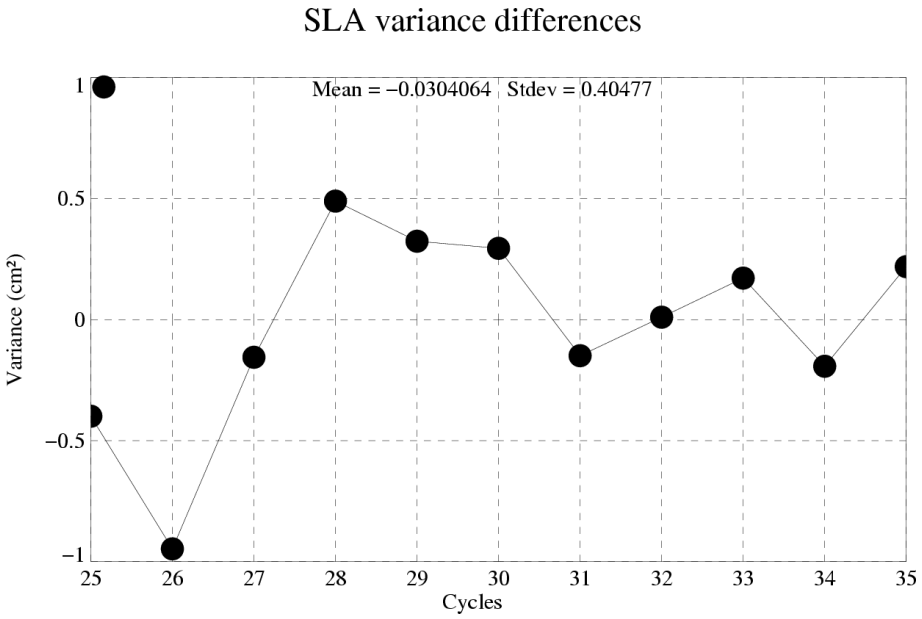

Figure 88: *Var(SLA with Delft) - Var(SLA with POE October 2005).*

8.4.7 Conclusion

Four analyses have been carried out in order to validate the two new CNES POE configurations:
- July versus GDR
- July versus October
- Delft versus July
- Delft versus October

The following tables summarize the main results of these analyses:

-Variance of difference (cm2)

July / GDR	1.5
July / October	0.3
Delft / July	0.9
Delft / October	0.8

-Approximative amplitude of the annual signal (cm)

GDR	1
July	0.8
October	0.6
Delft	0.6

-Gain at crossovers (cm2)

Var(July) - Var(GDR)	-2.1
Var(July) - Var(October)	0.8
Var(Delft) - Var(July)	-0.21
Var(Delft) - Var(October)	0.5

The use of a Grace gravity model reduces systematic geographically correlated errors in the ascending-descending SSH differences. The lowest errors are obtained with the EIGEN-GRACE gravity model. The annual signal observed at crossovers are similar using Delft and October, but higher with the two other con-

figurations. The best performances at crossover are obtained with the October solution. The SLA variability is strongly reduced by more than 10% in the area around South America using the July or October solution. The POE October 2005 and the Delft orbit have similar along track performances.

9 Conclusion

A statistical evaluation of Envisat altimetric measurements over ocean has been presented in this report. With three years of data now available in a homogeneous time series, Envisat altimetric measurements show good general results. A very good availability on every surface and very low editing ratios over ocean are observed. One of the major improvements of the RA-2 with respect to ERS RA is the S-band allowing range corrections due to ionospheric effects. However the so-called S-Band anomaly impacts more than 4 % of the available data on average. This ratio has been improved since cycle 31 and a method is currently under development to reconstruct the impacted S-band waveforms. The ocean-1 altimeter parameters are stable, compared to Jason-1 and ERS-2. The MWR wet troposphere correction has a small trend relative to the ECMWF model. Both high frequency and crossover analysis show that Envisat has performances similar to Jason-1. The time invariant errors, observed on the crossover mean, are mainly due to gravity induced orbit errors and are well corrected by the use of a Grace Gravity model. The time varying errors have to be analysed further to confirm the possible aliasing effect of oceanic tide components. Envisat MSL global trend is consistent to Jason-1 and T/P on the two last years of the period. However, the issue of the unexplained behavior of the first year still remains.

A new configuration is operational since September 2005 and a reprocessing of the whole Envisat altimetric mission is expected to start early 2006. Several improvements in terms of data quality are included in this new version of GDR products, for instance a new orbit configuration, an improved Sea State bias modeling and new geophysical corrections such as the correction of high frequency ocean signals. These new products will further improve the high quality level of the Envisat altimetric mission and will make easier the data fusion for multi-mission altimetry, as it is essential for oceanography and applications.

References

[1] Ablain, M., G. Pontonnier, B. Soussi, P. Thibaut, M.H. de Launay, J. Dorandeu, and P. Vincent. 2004. Jason-1 GDR Quality Assessment Report. Cycle 079. SALP-RP-P2-EX-21072-CLS079, May.

[2] Carrère, L., and F. Lyard, Modeling the barotropic response of the global ocean to atmospheric wind and pressure forcing - comparisons with observations. 2003. Geophys. Res. Lett., 30(6), 1275, doi:10.1029/2002GL016473.

[3] Cazenave, A., et al.,1999: Sea Level Change from Topex/Poseidon altimetry and tide gauges, and vertical crustal motions from DORIS, G. Res. Let., 26, 2077-2080.

[4] Celani C., B. Greco, A. Martini, M. Roca, 2002: Instruments corrections applied on RA-2 Level-1B Product. 2002: Proceeding of the Envisat Calibration Workshop.

[5] Chambers, D., P., J. Ries, T. Urban, and S. Hayes. 2002. Results of global intercomparison between TOPEX and Jason measurements and models. Paper presented at the Jason-1 and TOPEX/Poseidon Science Working Team Meeting, Biarritz (France), 10-12 June.

[6] Dedieu M., L. Eymard, E. Obligis, N. Tran, F. Ferreira, 2005: ENVISAT Microwave Radiometer Assessment Report Cycle 039, Technical Note CLS.DOS/NT/05.147 Available at http://earth.esa.int/pcs/envisat/mwr/reports/

[7] Dorandeu, J. and P.Y. Le Traon, 1999: Effects of Global Atmospheric Pressure Variations on Mean Sea Level Changes from TOPEX/Poseidon. J. Atmos. Technol., 16, 1279-1283.

[8] Dorandeu J., Y. Faugere, F. Mertz, F. Mercier, N. Tran, 2004a: Calibration / Validation Of Envisat GDRs Cross-calibration / ERS-2, Jason-1 Envisat and ERS Symposium, Salzburg, Austria.

[9] Dorandeu, J., M. Ablain, Y. faugere, F. Mertz, B. Soussi, 2004b, Jason-1 global statistical evaluation and performance assessment. Calibration and cross-calibration results Mar. Geod. 27(3-4): 345-372.

[10] Doornbos E., Scharroo R., 2005: Improved ERS and Envisat precise orbit determination, Proc. of the 2004 Envisat and ERS Symposium, Salzburg, Austria.

[11] ECMWF, The evolution of the ECMWF analysis and forecasting system Available at: http://www.ecmwf.int/products/data/operational_system/evolution/

[12] EOO/EOX, October 2005, Information to the Users regarding the Envisat RA2/MWR IPF version 5.02 and CMA 7.1 Available at http://earth.esa.int/pcs/envisat/ra2/articles/

[13] EOP-GOQ and PCF team, 2005: Envisat Cyclic Altimetric Report, Technical Note ENVI-GSOP-EOPG-03-0011 Available at: http://earth.esa.int/pcs/envisat/ra2/reports/pcs_cyclic/

[14] Eymard L., E. Obligis, N. Tran, February 2003, ERS2/MWR drift evaluation and correction, CLS.DOS/NT/03.688

[15] Faugere Y., Mertz F., Dorandeu J., 2003: Envisat GDR quality assessement report (cyclic), Cycle 015. SALP-RP-P2-EX-21072-CLS015, May. Available at http://www.aviso.oceanobs.com/html/donnees/calval/validation_report/en/welcome_uk.html

[16] Faugere Y., Mertz F., Dorandeu J., 2003: Envisat validation and cross calibration activities during the verification phase. Synthesis report. Technical Note CLS.DOS/NT/03.733, ESTEC contract N°16243/02/NL/FF WP6, May 16 2003 Available at http://earth.esa.int/pcs/envisat/ra2/articles/Envisat_Verif_Phase_CLS.pdf

[17] Faugere Y., Mertz F., Dorandeu J., 2004: Envisat RA-2/MWR ocean data validation and cross-calibration activities. Yearly report. Technical Note CLS.DOS/NT/04.289, Contract N° 03/CNES/1340/00-DSO310 Available at http://earth.esa.int/pcs/envisat/ra2/articles/Envisat_Yearly_Report_2004.pdf

[18] Y.Faugere, J.Dorandeu, F.Lefevre, N.Picot and P.Femenias, 2005: Envisat ocean altimetry performance assessment and cross-calibration. Submitted in the special issue of SENSOR 'Satellite Altimetry: New Sensors and New Applications'

[19] Faugere Y., Mertz F., Dorandeu J., 2005: Envisat RA-2/MWR ocean data validation and cross-calibration activities. Yearly report. Technical Note CLS.DOS/NT/04.289, Contract N° 03/CNES/1340/00-DSO310 http://www.jason.oceanobs.com/documents/calval/validation_report/en/annual_report_en_2005.pdf

[20] Labroue, S. and P. Gaspar, 2002: Comparison of non parametric estimates of the TOPEX A, TOPEX B and JASON 1 sea state bias. Paper presented at the Jason 1 and TOPEX/Poseidon SWT meeting, New-Orleans, 21-12 October.

[21] Labroue S. and E. Obligis, January 2003, Neural network retrieval algorithms for the ENVISAT/MWR, Technical note CLS.DOS/NT/03.848

[22] Labroue S., 2003: Non parametric estimation of ENVISAT sea state bias, Technical note CLS.DOS/NT/03.741, ESTEC Contract n°16243/02/NL/FF - WP3 Task 2

[23] Labroue S., 2004: RA-2 ocean and MWR measurement long term monitoring, Final report for WP3, Task 2, SSB estimation for RA-2 altimeter, Technical Note CLS-DOS-NT-04-284

[24] Laxon and M. Roca, 2002: ENVISAT RA-2: S-BAND PERFORMANCE, S., Proceedings of the ENVISAT Calibration Workshop, Noordwijk

[25] Le Traon, P.-Y., J. Stum, J. Dorandeu, P. Gaspar, and P. Vincent, 1994: Global statistical analysis of TOPEX and POSEIDON data. J. Geophys. Res., 99, 24619-24631.

[26] Le Traon, P.-Y., , F. Ogor, 1998: ERS-1/2 orbit improvement using TOPEX/POSEIDON: the 2 cm challenge. J. G. Res., VOL 103, p 8045-8057, April 15, 1998.

[27] Lefèvre, F., and E. Sénant, 2005: ENVISAT relative calibration, Technical Note CLS-DOS-NT-05.074.

[28] Lillibridge J, R. Scharroo and G. Quartly, 2005: rain and ice flagging of Envisat altimeter and MWR data, Proc. of the 2004 Envisat and ERS Symposium, Salzburg, Austria

[29] Luthcke. S. B., N. P. Zelinsky, D. D. Rowlands, F. G. Lemoine, and T. A. Williams. 2003. The 1-Centimeter Orbit: jason-1 Precision Orbit Determination Using GPS, SLR, DORIS, and Altimeter Data. Mar. Geod. 26(3-4): 399-421.

[30] Martini A. and P. Féménias, 2000: The ERS SPTR2000 Altimetric Range Correction: Results and Validation. ERE-TN-ADQ-GSO-6001. 23 November 2000.

[31] Martini A., 2003: Envisat RA-2 Range instrumental correction : USO clock period variation and associated auxiliary file, Technical Note ENVI-GSEG-EOPG-TN-03-0009 Available at http://earth.esa.int/pcs/envisat/ra2/articles/USO_clock_corr_aux_file.pdf http://earth.esa.int/pcs/envisat/ra2/auxdata/

[32] Martini A., P. Femenias, G. Alberti, M.P. Milagro-Perez, 2005: Ra-2 S-band anomaly detection and waveforms reconstruction, Proc. of the 2004 Envisat and ERS Symposium, Salzburg, Austria

[33] Mertz, F., Y. Faugere and J. Dorandeu, 2003: Validation of ERS-2 OPR cycle 083-086. CLS.OC.NT/03.702 issue 083-086.

[34] Mertz F., J. Dorandeu, N. Tran, S. Labroue, 2004, ERS-2 OPR data quality assessment. Long-term monitoring - particular investigations, Report of task 2 of IFREMER Contract n° 04/2.210.714. CLS.DOS/NT/04.277.

[35] Mitchum, G., 1994: Comparison of TOPEX sea surface heights and tide gauge sea levels, J. Geophys. Res., 99, 24541-24554.

[36] Mitchum, G., 1998: Monitoring the stability of satellite altimeters with tide gauges, J. Atm. Oceano. Tech., 15, 721-730.

[37] Obligis E., L. Eymard, N. Tran, S. Labroue, 2005: Three years of Microwave Radiometer aboard Envisat: In-flight Calibration, Processing and validation of the geophysical products, submitted

[38] R D Ray and R M Ponte, 2003: Barometric tides from ECMWF operational analyses, Annales Geophysicae, 21: 1897-1910.

[39] Roca M., A. Martini, 2003: Level 1b Verification updates, Ra2/MWR CCVT meeting, 25-26 March 2003, ESRIN, Rome

[40] Rudolph A., D.Kuijper, L.Ventimiglia, M.A. Garcia Matatoros, P.Bargellini, 2005: Envisat orbit control - philosophy experience and challenge, Proc. of the 2004 Envisat and ERS Symposium, Salzburg, Austria

[41] R. Scharroo and P. N. A. M. Visser, 1998: Precise orbit determination and gravity field improvement for the ERS satellites, J. Geophys. Res., 103, C4, 8113-8127

[42] Scharroo R., A decade of ERS Satellite Orbits and Altimetry, 2002: Phd Thesis, Delft University Press science

[43] Scharroo R., December 12, 2002, Routines for iono corrections, internet communication to the CCVT community

[44] Scharroo R., J. L. Lillibridge, and W. H. F. Smith, Cross-Calibration and Long-term Monitoring of the Microwave Radiometers of ERS, TOPEX, GFO, Jason-1, and Envisat, **Marine Geodesy, 27:279-297**, 2004.

[45] Stum J., F. Ogor, P.Y. Le Traon, J. Dorandeu, P. Gaspar and J.P. Dumont, 1998: "An intercalibration study of TOPEX/POSEIDON, ERS-1 and ERS-2 altimetric missions", Final report of IFREMER contract N_97/2 426 086/C CLS.DOS/NT/98.070.

[46] Tran, N., D. W. Hancock III, G.S. Hayne. 2002: "Assessment of the cycle-per-cycle noise level of the GEOSAT Follow-On, TOPEX and POSEIDON." J. of Atmos. and Oceanic Technol. 19(12): 2095-2117.

[47] Tran N. and E. Obligis, December 2003, Validation of the use of ENVISAT neural algorithm on ERS-2. CLS-DOS-NT-03.901.

[48] Tran N., E. Obligis and L. Eymard, 2006, Envisat MWR 36.5 GHz drift evaluation and correction. CLS-DOS-NT-05.218.

[49] Vincent, P., S. D. Desai, J. Dorandeu, M. Ablain, B. Soussi, P. S. Callahan, and B. J. Haines 2003. Jason-1 Geophysical Performance Evaluation. Mar. Geod. 26(3-4): 167-186.

[50] Witter, D. L., D. B. Chelton, 1991: "A Geosat altimeter wind speed algorithm development", J. of. Geophys. Res. (oceans), 96, 8853-8860, 1991.

[51] Zanife, O. Z., P. Vincent, L. Amarouche, J. P. Dumont, P. Thibaut, and S. Labroue, 2003. Comparison of the Ku-band range noise level and the relative sea-state bias of the Jason-1, TOPEX and Poseidon-1 radar altimeters. Mar. Geod. 26(3-4): 201-238.

10 Appendix 1: Instrument and plateform status

10.1 ACRONYMS

The main acronyms used to described the events are explained below.
CTI tables: Configuration Table Interface. They Contain the setting of the instruments and are uploaded on board after a switch off, a reset
HTR Refuse: Heater Refuse
ICU: Instrument Control Unit, a part of the distributed command and control function implemented on ESA spacecraft. The unit receives, decodes and executes high-level commands for its instrument, and autonomously performs health-checking and parameter monitoring. In the event of anomalies it takes autonomous recovery actions.
MCMD: Macrocommand
OCM: Orbit Controle Mode/maneuvre
P/L SOL: Payload Switch Off Line
SEU: Single Event Upset
SM-SOL by PMC: SM Switch Off Line by Payload Main Computer
SW: Software
TM: Telemetry

10.2 Cycle 010

- RA-2 went to STBY/Refuse (2002/10/09 09 13:34:22 to 2002/10/10 08:56:53)

10.3 Cycle 011

- Ra2 switch-down - Planned SM-SOL by PMC1 (2002/11/18 04:38:00 to 2002/11/19 19:19:21,Pass 382-429)
- DORIS Navigator switch-down - Planned SM-SOL by PMC1 (2002/11/18 04:38:02 to 2002/11/22 12:40:00, Pass 382-505)
- MWR switch-down - Planned SM-SOL by PMC1 (2002/11/18 04:37:59 to 2002/11/20 12:20:06, Pass 382-448)
- Orbit Maintenance Maneuver (2002/11/07 18:15:51 to 2002/11/07 21:06:17,Pass 83-85)
- Orbit Maintenance Maneuver (2002/11/29 03:35:30 to 2002/11/29 06:25:57,Pass 696-698)

10.4 Cycle 012

- RA-2 went to HTR-0 Refuse (2002/12/21 04:31:26 to 2002/12/21 12:52:00, Pass 325-333)
- Orbit Inclination Maneuver (2002/12/18 04:28:18 to 2002/12/18 06:36:46, Pass 238-240)

- Orbit Maintenance Maneuver (2002/12/18 22:17:22 to 2002/12/19 00:17:34, Pass 259-261)

10.5 Cycle 013

- RA-2 went to HTR-0 Refuse (2003-01-16 01:52:36 to 2003-01-17 17:00:35)
- RA-2 went to suspend mode (2003-01-25 23:56:36 to 2003-01-27 19:54:02)
- Orbit Maintenance Maneuver (2003/01/14 00:55:17 to 2003/01/14 03:45:42 TAI)
- Orbit Maintenance Maneuver (2003/02/11 23:04:49 to 2003/02/12 01:04:57 TAI)

10.6 Cycle 014

- SEU's caused a Software Anomaly (2003/03/02 02:46:44 to 2003/03/03 16:46:35).
- Subsystems unavailable - Autonmous P/L switch-off (2003/03/15 04:21:08 to 2003/03/17 19:00:13)
- RA2 in HTR0/Refuse due to HPA primery bus undercurrent (2003/03/17 21:09:32 to 2003/03/18 18:50:40)
- Orbit Maintenance Maneuver (2003/02/21 03:42:57 to 2003/02/21 05:53:24)
- Orbit Maintenance Maneuver (2003/03/03 23:51:14 to 2003/03/04 01:51:22)

10.7 Cycle 015

- Wrong setting of Ra2 parameters (no CTI tables have been up-loaded on-board) from 18 Mar 2003 18:50:40 to 9 Apr 2003 17:12:24, Pass 1 to 452
- RA-2 unavailability (Format Header Error forcing ICU to RS/WT/INI) from 8 Apr 2003 15:08:57.000 to 9 Apr 2003 17:12:24.000, Pass 437 to 452
- RA-2 unavailability (Format Header Error forcing ICU to RS/WT/INI) from 8 Apr 2003 15:08:57.000 to 9 Apr 2003 17:12:24.000, Pass 613 to 624
- RA-2 unavailability: Multiple SEU caused ICU switchdown (2003/04/24 13:20:09 to 2003/04/25 09:15:36,879 to 901)
- Orbit Maintenance Maneuver (2003/04/04 00:40:48 to 2003/04/04 02:40:56 TAI)

10.8 Cycle 016

- RA2 unavailability (known SEU failure) (from 5 May 2003 12:30:17.000 to 6 May 2003 10:01:10.000, Pass 191 to 215)
- RA-2 unavailability (ICU in SUSPEND due to TM FMT Error when a Reduced FMT was requested) (from 11 May 2003 11:06:33.000 to 12 May 2003 10:14:35.726, Pass 361 to 387)
- Orbit Maintenance Maneuver (from 2003/05/14 22:40:13 to 2003/05/15 00:40:19 TAI, Pass 460 to 462)
- RA-2 unavailability (Switch-down for PMC SW upgrade and OCM) from 18 May 2003 06:25:17.000 to 19 May 2003 15:59:28.000, Pass 548 to 602)
- MWR unavailability (Switch-down for PMC SW upgrade and OCM) from 18 May 2003 06:25:24.000 to 19 May 2003 14:45:40.000, Pass 548 to 602)
- DORIS unavailability (Switch-down for PMC SW upgrade and OCM) from 18 May 2003 06:25:25.000 to 19 May 2003 13:21:28.000, Pass 548 to 602)
- Orbit Inclination Maneuver (from 2003/05/20 04:11:53 to 2003/05/20 06:23:31 TAI, Pass 610 to 612)
- RA-2 unavailability (ICU went to RS/WT/INI) from 1 Jun 2003 14:36:40.000 to 2 Jun 2003 09:20:35.000, Pass967 to 987

10.9 Cycle 017

- Orbit Maintenance Maneuver (from 2003/06/07 01:08:16 to 2003/06/07 03:08:23 TAI, Pass 119 to 122)

10.10 Cycle 018

- Orbit Maintenance Maneuver (from 2003/07/11 0:58:45 to 2003/07/11 03:49:08 TAI, Pass 90 to 94)
- RA2 unavailability (RA-2 in STBY/REF due to MCMD timeout) (from 26 Jul 2003 15:28:11 to 26 Jul 2003 17:25:35, Pass 538)
- RA2 unavailability (RA-2 picked up Mission Planning schedule) (from 31 Jul 2003 16:11:02 to 31 Jul 2003 18:06:30, Pass 682)
- Orbit Maintenance Maneuver (from 2003/07/11 0:58:45 to 2003/07/11 03:49:08 TAI), Pass 91 to 94)

10.11 Cycle 019

- Orbit Maintenance Maneuver (from 2003/08/15 1:31:29 to 2003/08/15 03:31:35 TAI, Pass 91 to 93)
- RA-2 went to STBY/Refuse due to Individual Echoes MCMD Timeout (from 2003-08-15 16:40:21 to 2003-08-15 18:35:35, Pass 110)
- RA-2 went to STBY/Refuse due to Individual Echoes MCMD Timeout (from 2003-08-30 15:28:00 to 2003-08-30 20:47:35, Pass 538 to 543)
- PLSOL . Instrument Switch OFF/ON (from 2003-09-04 22:52:52 to 2003-09-06 16:41:09, Pass 689 to 738)

10.12 Cycle 020

- RA-2 in STANDBY / REFUSE MODE (from 2003-09-21 15:36:40 to 2003-09-21 17:33:30, Pass 166 to 167)
- RA-2 is in RS/WT/INT mode (from 2003-09-27 00:28:08 to 2003-09-27 12:52:00, Pass 320 to 333)
- Wrong setting of Ra2 parameters (no CTI tables have been up-loaded on-board) (from 2003-09-27 12:52:00 to 2003-09-30 12:45:00, Pass 334 to 407)
- Orbit Maintenance Maneuver (2003/09/30 00:40:53 to 2003/09/30 02:41:00 TAI, Pass 405 to 407)

10.13 Cycle 021

- Orbit Inclination Maneuver (2003/10/28 04:56:18 to 2003/10/28 07:09:44 TAI, Pass 210 to 212)
- RA-2 is in RS/WT/INT mode. 29 Oct 2003 06 :47 :04 to 29 Oct 2003 12 :58 :35, Pass 242 to 247)
- Orbit Maintenance Maneuver (2003/10/31 01:13:10 to 2003/10/31 03:13:25 TAI, Pass 291 to 293)
- RA-2 is in RS/WT/INT mode. TM format header error (02 Nov 2003 15 :16 :56 to 03 Nov 2003 12 :08 :35, Pass 366 to 389)
- Orbit Maintenance Maneuver (2003/11/18 23:02:30 to 2003/11/19 01:52:55 TAI, Pass 833 to 835)

10.14 Cycle 022

- RA-2 is in RS/WT/INT mode (2003-11-26 13:31:20 to 2003-11-26 19:39:35, Pass 49 to 54)
- RA-2 PLSOL . Instrument Switch OFF/ON (2003-12-03 07:18:43 to 2003-12-05 16:35:05, Pass 241 to 308)
- MWR PLSOL . Instrument Switch OFF/ON (2003-12-03 07:18:43 to 2003-12-04 18:45:41)
- RA-2 is in RS/WT/INT mode. (2003-12-06 15:55:52 to 2003-12-10 19:16:36, Pass 338 to 455)
- Orbit Maintenance Maneuver (2003/12/15 21:02:28 to 2003/12/15 23:02:36, Pass 601 to 603)
- Orbit Maintenance Maneuver (2003/12/26 21:03:30 to 2003/12/26 23:03:34, Pass 916 to 918)

10.15 Cycle 023

Orbit Maintenance Maneuver (2004/01/21 23:54:27 to 2004/01/22 01:54:37))

- Orbit Maintenance Maneuver (2004/01/26 22:26:07 to 2004/01/27 00:26:11))

10.16 Cycle 024

- Orbit Inclination Maneuver (2004/02/04 04:46:39 to 2004/02/04 06:58:05)
- Orbit Maintenance Maneuver (2004/02/05 11:17:21 to 2004/02/05 13:17:23)
- Orbit Maintenance Maneuver (2004/02/24 11:48:39 to 2004/02/24 13:48:45)

10.17 Cycle 025

- Orbit Maintenance Maneuver (2004/04/07 20:05:30 to 2004/04/07 22:05:34)

10.18 Cycle 026

- RA-2 in STANDBY/REF DUE TO MCMD H202 FAILURE (2004-22-04 15:15:36 2004-22-04 17:07:05)
- RA-2 Switch down to RESET/WAIT due to too many SEU's reported. (2004-05-10 02:06:31 2004-05-10 11:27:30)
- Orbit Inclination Maneuver (2004/04/14 04:43:02 2004/04/14 06:55:00)
- Orbit Maintenance Maneuver (2004/05/07 01:08:56 2004/05/07 03:09:04)

10.19 Cycle 027

- RA2 went to suspend owing to repeated type 10 entries in report format (2004/05/31 02:45:27 to 2004/05/31 12:01:50)
- No DORIS data from 2004/06/06 13:00:00 to 2004/06/14 14:52:00. Following an onboard incident, Doris instrument has been switched to the redundant chain. Doris data are unavailable from June, 6th to June, 14th. To allow GDR production, POE with laser only data have been produced during this period.
- RA2 in SUSPEND Mode (2004/06/21 14:47:51 to 2004/06/21 19:24:30, Pass 995 to 999)

10.20 Cycle 028

- RA2 in ICU rs/wt/ini (2004/07/18 13:47:03 to 2004/07/18 19:59:00, Pass 765 to 771)
- Orbit Maintenance Maneuver (2004/06/30 08:08:29 to 2004/06/30 10:08:35, Pass 242 to 244)

10.21 Cycle 029

RA2 in ICU RS/WT/INI. (SDU problem in RAM) (2004/08/10 15:00:39 to 2004/08/11 10:59:30, Pass 423 to 445)

- Orbit Maintenance Maneuver (2004/08/17 02:04:20 to 2004/08/17 04:04:26 , Pass 607 to 609)

10.22 Cycle 030

- RA2 in ICU RS/WT/INI. (SDU problem in RAM) (2004/09/26 13:39:50 to 2004/09/27 16:23:30, Pass 765-795)
- Abnormal behaviour of the RA-2 sensor (2004/09/27 16:23:30 to 2004-09-29 10:21:07, Pass 796-846)
- Collision avoidance Maneuver (2004/09/01 22:52:27 to 2004/09/02 00:52:37, Pass 60-62)
- Collision avoidance Maneuver (2004/09/02 23:44:27 to 2004/09/03 01:44:37, Pass 89-91)
- Orbit Inclination Maneuver (2004/09/21 04:14:37 to 2004/09/21 06:29:19, Pass 610-612)
- Orbit Maintenance Maneuver (2004/09/24 03:53:38 to 2004/09/24 05:53:46, Pass 695-697)

10.23 Cycle 031

- Collision avoidance Maneuver (2004/10/22 03:20:22 to 2004/10/22 07:00:41, Pass 495-498)
- High solar activity (Pass 974-1002)

10.24 Cycle 032

- RA2 in RS/WT/INI. 2004/11/23 13:25:58 to 2004/11/24 14:10:10, Pass 421-449
- RA2 Format header error. 2004/12/01 10:22:30 to 2004/12/01 15:34:29, Pass 647-651
- Orbit Maintenance Maneuver (2004/11/12 01:07:57 to 2004/11/12 03:08:06,Pass 91-93)

10.25 Cycle 033

- RA-2 went to RS/WT/INI due RBI (2004/12/27 02:49:10 to 2004/12/27 13:49:30, 380 to 391)
- Orbit Maintenance Maneuver (2004/12/17 01:03:48 to 2004/12/17 03:03:52, 91 to 93)
- Orbit Maintenance Maneuver (2005/01/05 23:10:28 ro 2005/01/06 01:10:36, 661 to 663)
- Orbit Inclination Maneuver (2005/01/07 04:25:17 to 2005/01/07 06:38:53, 696 to 698)

10.26 Cycle 034

- RA-2 went to RS/WT/INI Mode (2005/01/26 15:50:30 to 2005/01/26 21:07:30, 252 to 257)
- Orbit Maintenance Maneuver (2005/02/18 01:23:24 to 2005/02/18 03:23:28, 893 to 894)

10.27 Cycle 035

- RA-2 went to RS/WT/INI Mode (2005/03/18 04:35:34 to 2005/03/18 12:58:00, 697 to 705)
- Orbit Maintenance Maneuver (2005/03/17 04:51:26 to 2005/03/17 07:06:31, 668 to 669)

10.28 Cycle 036

- RA-2 went to RS/WT/INI mode (2005/04/18 05:01:10 to 2005/04/18 13:22:32, 583 to 591)
- RA-2 went to RS/WT/INI mode (2005/04/18 37:58:10 to 2005/04/24 11:42:30, 742 to 761)

10.29 Cycle 037

- RA-2 went to ICU in RS/WT/INI (RBI ERR 71) (2005/05/14 23:56:37 to 2005/05/15 10:53:45, 348 to 359)
- RA-2 went to ICU in RS/WT/INI (2005/05/21 00:10:45 to 2005/05/21 10:55:35, 520 to 531)

10.30 Cycle 038

- RA-2 went to ICU in RS/WT/INI (2005/07/04 04:41:10 to 2005/07/04 11:19:39, 783 t0 789)

10.31 Cycle 039

- RA-2 went to ICU in RS/WT/INI (2005/07/16 13:32:21 to 2005/07/16 19:58:52,135 to 141)
- RA-2 went to ICU in RS/WT/INI (2005/07/17 14:43:49 to 2005/07/17 19:20:30,165 to 169)
- RA-2 went to ICU in RS/WT/INI (2005/07/29 00:41:41 to 2005/07/29 09:58:30,492 to 501)
- Orbit Maintenance Maneuver (2005/08/09 22:45:44 to 2005/08/10 00:45:50 TAI)

10.32 Cycle 040

- RA-2 went to ICU in RS/WT/INI (2005/08/16 16:41:57 to 2005/08/16 20:22:30,24 to 27)
- RA-2 went to ICU in RS/WT/INI (2005/08/30 16:01:25 to 2005/08/30 19:43:00,424 to 427)
- RA-2 went to ICU in RS/WT/INI (2005/09/12 15:53:09 to 2005/09/12 19:47:00,796 to 799)
- Orbit Maintenance Maneuver (2005/09/07 05:19:53 to 2005/09/07 07:36:31 TAI)

11 Appendix 2: Mean Sea Level (MSL) and Sea Surface Temperature (SST) comparisons

This study has been carried out in order to monitor the MSL seen by all the operational altimeter missions. Long-term MSL change is a variable of considerable interest in the studies of global climate change. Then the objective here is on the one hand to survey the mean sea level trends and on the other hand to assess the consistency between all the MSL. Besides, the Reynolds SST is used to compare the MSL with an external data source. The mean SST is calculated the same way as the MSL.
The following missions have been used : TOPEX/Poseïdon (T/P), Jason-1 (J1), Geosat Follow-On (GFO) and Envisat. The MSL and SST time series have been plotted over global ocean. This allows us to correlate the MSL trends seen by each mission and to compare them with the SST.
In addition to these analysis, the maps of regional MSL change and SST change have been plotted for each mission over the Jason-1 period and the Envisat period. The differences of these maps have been performed; this is a way to display eventual local drifts.

11.1 SSH definition for each mission

The SSH formula is defined for all the satellites as below :

$$SSH = Orbit - Altimeter\ Range - \sum_{i=1}^{n} Correction_i$$

with :

$$\begin{aligned}\sum_{i=1}^{n} Correction_i &= Dry\ troposhere\ correction : new\ S1\ and S2\ atmospheric\ tides\ applied \\ &+ Combined\ atmospheric\ correction :\ MOG2D\ and\ inverse\ barometer \\ &+ Radiometer\ wet\ troposhere\ correction \\ &+ Filtered\ dual\ frequency\ ionospheric\ correction \\ &+ Non\ parametric\ sea\ state\ bias\ correction \\ &+ Geocentric\ ocean\ tide\ height,\ GOT\ 2000 :\ S1\ atmospheric\ tide\ is\ applied \\ &+ Solid\ earth\ tide\ height \\ &+ Geocentric\ pole\ tide\ height\end{aligned}$$

Some additional corrections have been applied :

- For Jason-1 and Envisat the wet troposhere correction has been changed by the ECMWF model in order to remove the effects of abnormal changes or trends observed on the radiometer wet troposhere correction.
- For Envisat, the USO correction (Martini, 2003 [31]) has been applied.

- For T/P, the radiometer wet troposhere correction has been corrected from correction (Scharroo R., 2004 [44])
- For T/P, the relative bias between TOPEX and Poseidon and between TOPEX A and TOPEX B has been taken into account
- For T/P, the drift between the TOPEX and DORIS ionosphere corrections has been corrected for on Poseidon cycles.
- For Geosat Follow-On, the GIM model has been used for the ionospheric correction.

11.2 MSL and SST time series

11.2.1 MSL over global ocean

The MSL has been monitored for each satellite altimeter over global ocean in figure 89 over T/P period and Jason-1 period. The trends are similar for each satellite except for Envisat. The estimation of the Envisat MSL slope seems impacted by a strange behaviour on the first year as explained in Faugere et al. (2005, [18]). However, on the last two years, the Envisat slope is fully consistent with Jason-1 and T/P. The unexplained behavior of the first year of Envisat data is currently under investigation.

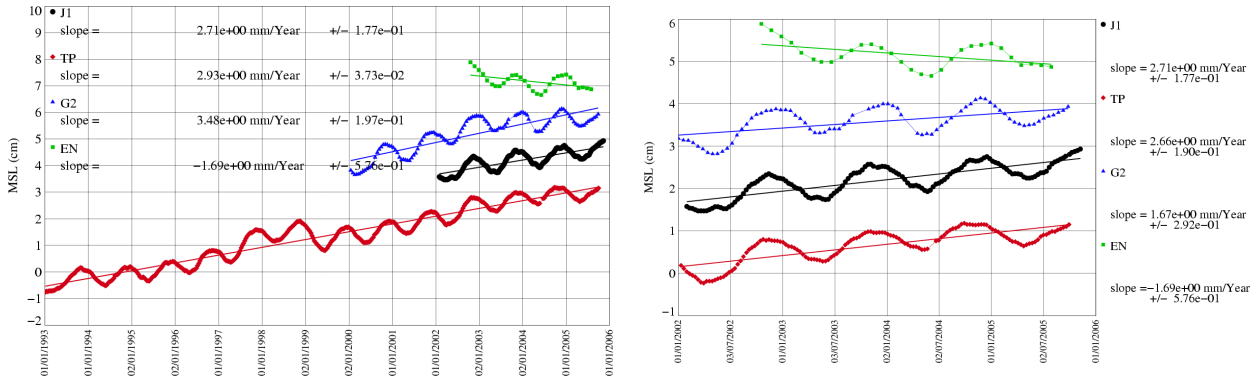

Figure 89: *MSL over global ocean for the T/P period on the left and the Jason-1 period on the right.*

In the following figure 90, MSL have been plotted after removing annual signal, semi-annual signal, and signals lower than 60 days. The T/P, Jason-1 and GFO MSL slopes over the Jason-1 period are still similar, respectively 2.75 mm/year, 2.3 mm/year and 1.8 mm/year with an adjustement formal error arround 0.2 mm/year. Notice that, for GFO, the slope computed over the global period is stronger, 3.2 mm/year. Beside, the orbit quality of Jason-1 early cycles is lower than usual. When those cycles are not taken into account, the Jason-1 slope increases by 0.3 mm/year to reach 2.6 mm/year. The conclusion is that the slope estimation is very sensitive. The formal error adjustement is only a mathematical error, not linked with the physical errors such as the orbit errors for instance.

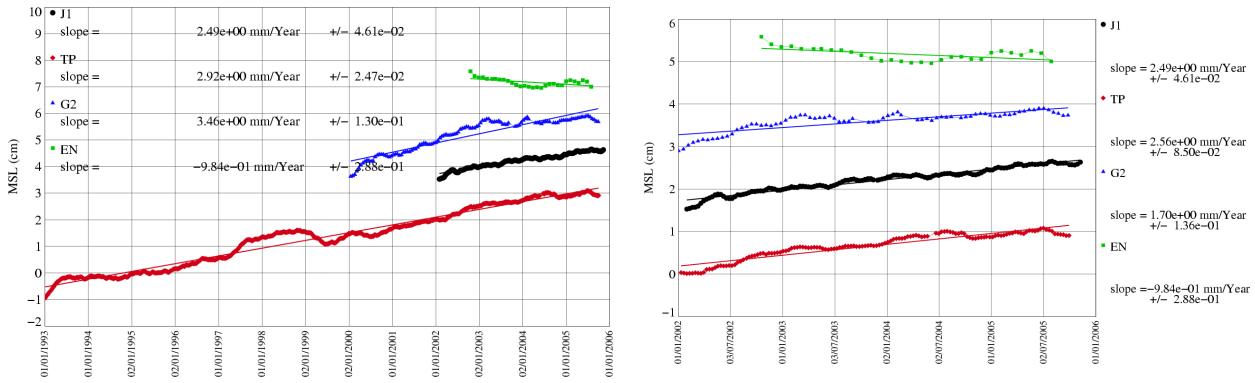

Figure 90: *MSL over global ocean for the T/P period on the left and the Jason-1 period on the right after removing annual, semi-annual and 60-day signals.*

11.2.2 SST over global ocean

In figure 91 on the left, the SST mean is compared to the T/P MSL. In the same figure on the right, annual signal, semi-annual signal, and signals lower than 60 days have been removed. Notice that the SST has been computed exactly over the T/P tracks. The SST increases by about 0.015 degree/year over the T/P period with a formal error close to 0.001 degree/year. The MSL and the SST don't have the same unit ("cm" and "degree"), thus to compare the 2 quantities, the SST scale is adjusted on the MSL scale so that the SST trend and the MSL trend are visually the same. This allows us to highlight that the SST dynamic is stronger than the MSL one. Inter-annual signal or climatic phenomena have a greater impact on the SST than on the MSL. Thus the SST trend estimation over a short period is not significant.

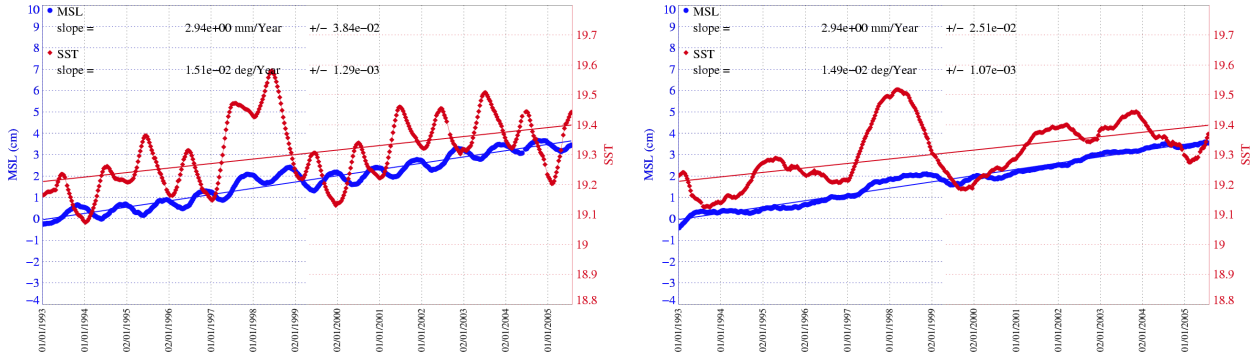

Figure 91: *MSL and SST over global ocean for the T/P period on the left, and after removing annual, semi-annual and 60-day signals on the left.*

11.3 Spatial MSL and SST slopes

11.3.1 Methodology

In order to monitor the MSL, the spatial MSL slopes have been calculated. The SLA grids (2x2 degree bins) have been computed cycle per cycle, and the slope has been computed on each grid point. As for time analysis, 60 day, semi-annual and annual signals have been removed before estimating the slopes. Then, the MSL slopes have been mapped for each mission. These maps are used to compare the MSL slopes between each altimeter mission. This allows us to detect potential local drifts.
Besides, the SST slopes have been computed the same way in order to correlate them with the MSL slopes.

11.3.2 Spatial MSL slopes over Jason-1 period

The MSL slopes have been plotted for Jason-1 (on the right) and T/P (on the left) over Jason-1 period in figure 92. The MSL trends seen by the two satellites are similar. However, differences greater than 4mm/year can be observed on the T/P-Jason-1 map (at the bottom).

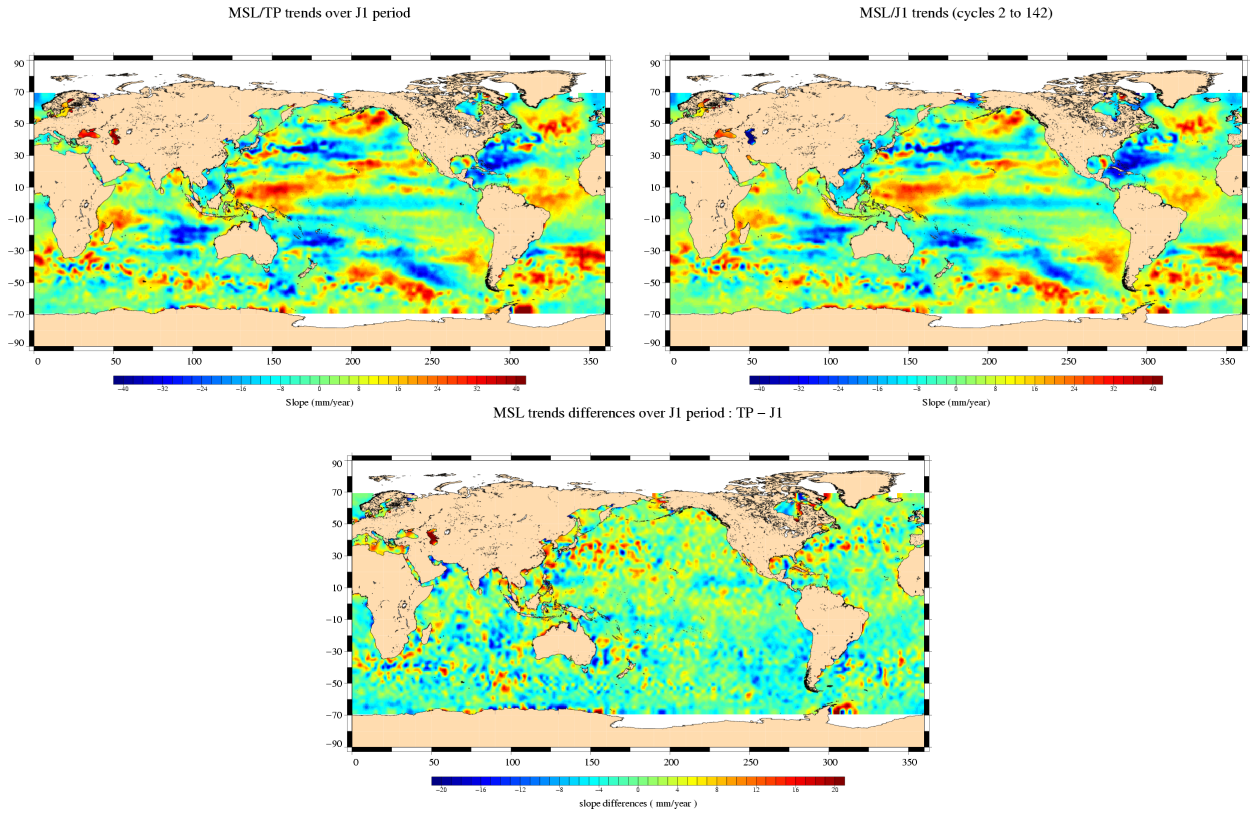

Figure 92: *MSL slopes over Jason-1 period for T/P (left) and Jason-1 (right), MSL slope differences between Jason-1 and T/P (bottom)*

11.3.3 Spatial MSL slopes over Envisat period

The same work has been performed over Envisat period using Envisat data in figure 93. The 3 maps are very similar.
In figure 94, the slope differences between each mission have been plotted. They allow us to observe differences in equatorial areas between Jason-1 and Envisat, and between T/P and Jason-1. Between Envisat and Topex, the difference has not the same geographical pattern. Investigations are on-going to understand the reasons of this observation.

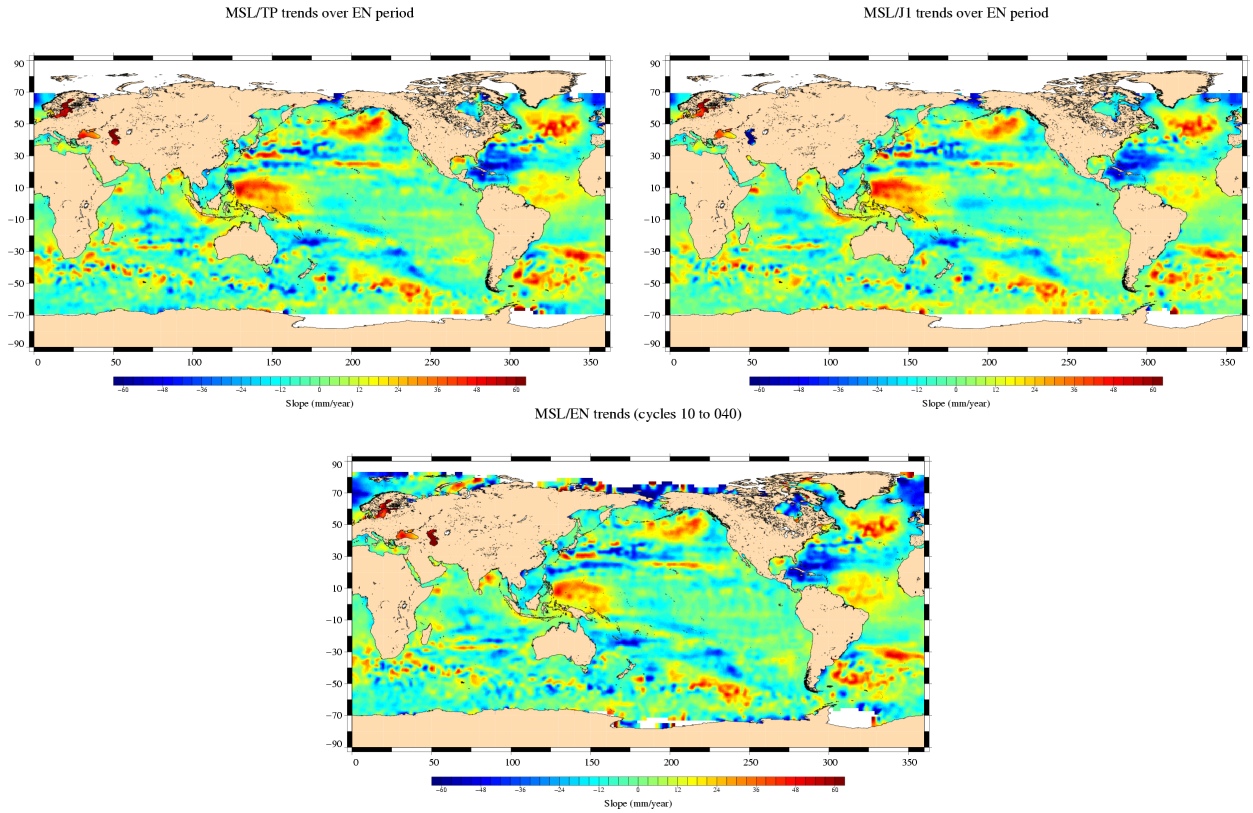

Figure 93: *MSL slopes over Envisat period for T/P (left), Jason-1 (right) and Envisat (bottom)*

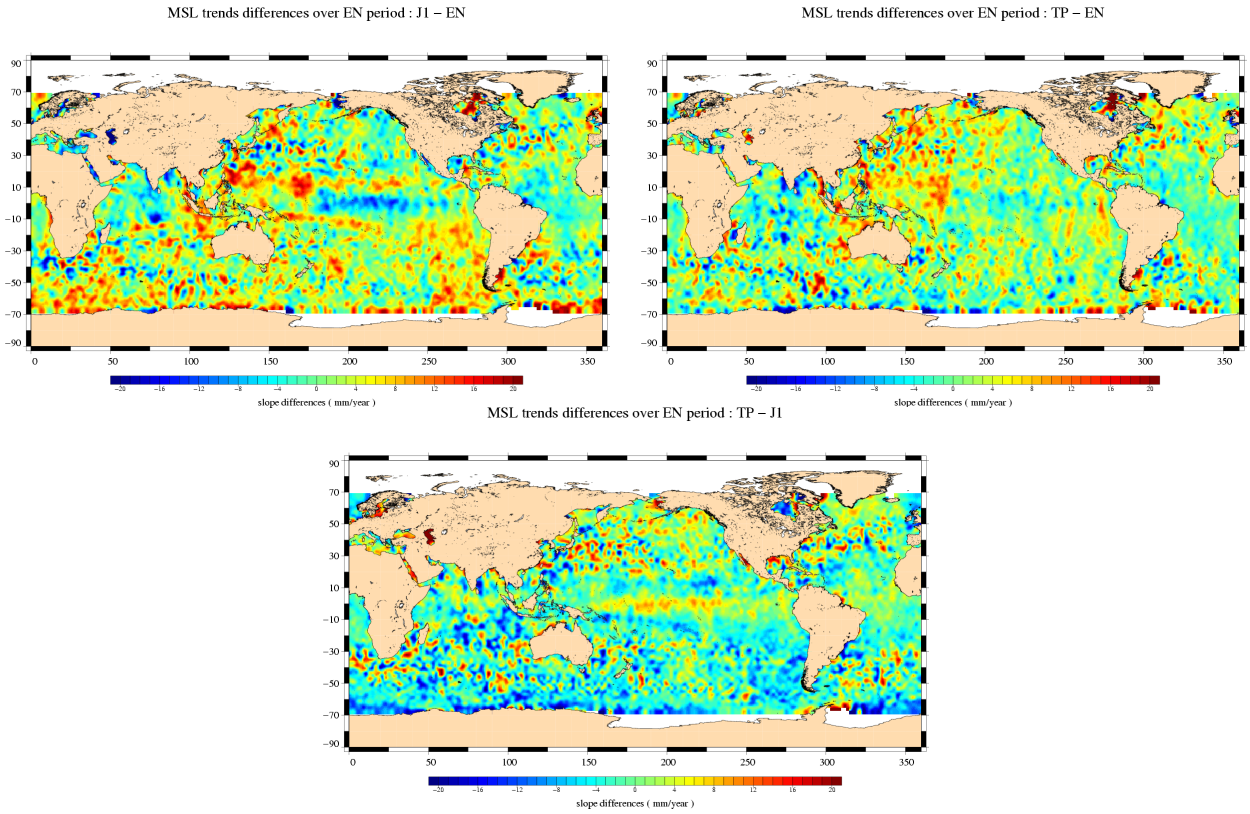

Figure 94: *MSL slopes differences over Envisat period between Jason-1 and Envisat (left), T/P and Envisat (right) and T/P and Jason-1 (bottom)*

11.3.4 Spatial SST and MSL slopes for T/P

The T/P MSL slopes are mapped in figure 95 on the left. In order to correlate the MSL and the SST, the SST slopes have been plotted in the same figure on the right.
13 years of T/P data have been used to estimate the slopes; this allows us to have a good estimation of the local MSL trends. The adjustment errors of the MSL and the SST slopes are mapped in figure 96.

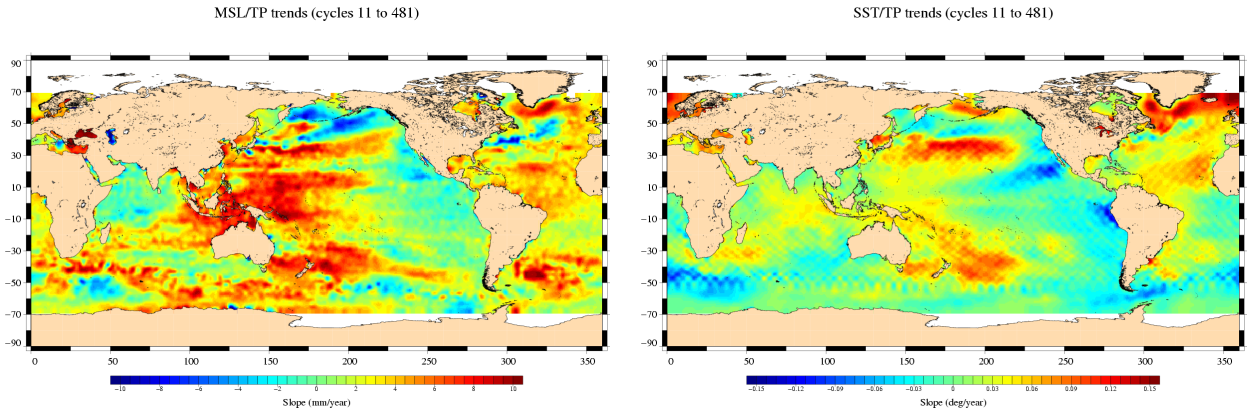

Figure 95: *T/P MSL and SST slopes over 13 years*

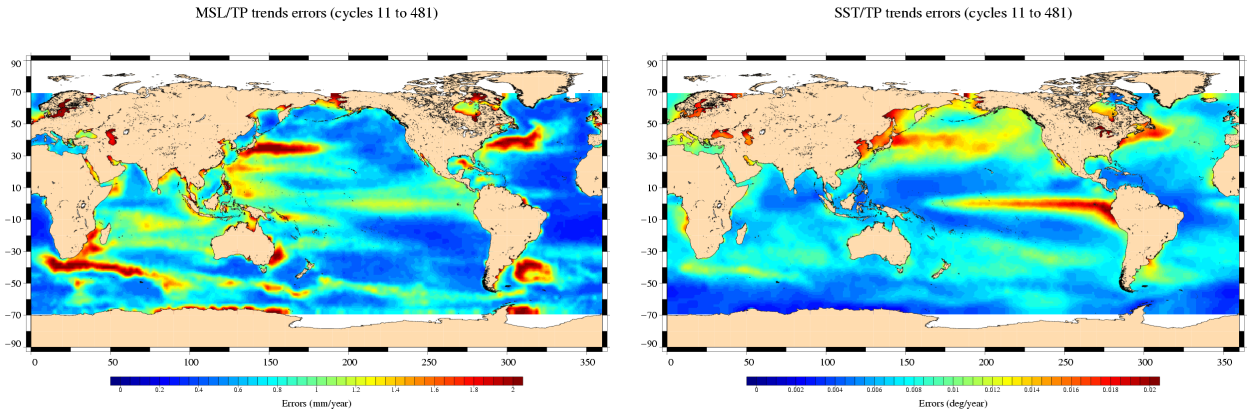

Figure 96: *Adjustment errors of T/P MSL and SST slopes over 13 years*

11.3.5 "El Niño" impact on SST and MSL slope estimations

The MSL and SST regional trends are largely impacted by inter-annual signal or oceanic phenomena such as "El Niño" for instance. The 4 maps in the figure 97 show the trend for the SST and the MSL before and after "El Niño". The first period ranges from 1992 and 1996 included, whereas the second period ranges from 1999 to 2004 included.
MSL and SST trends are stronger for each period separetely than for the global period. In the Pacific ocean, the absolute values are greater than 20 mm/year for the MSL and 0.3 degree/year for the SST. SST and MSL maps show a strong correlation on the two period of time. But for both SST and MSL, the trends on the first period are very different from the trends of the second period. This is particularly true in tropical areas.
Finally, these maps highlight the importance of having long time series to evaluate the regional trends with a good accuracy.

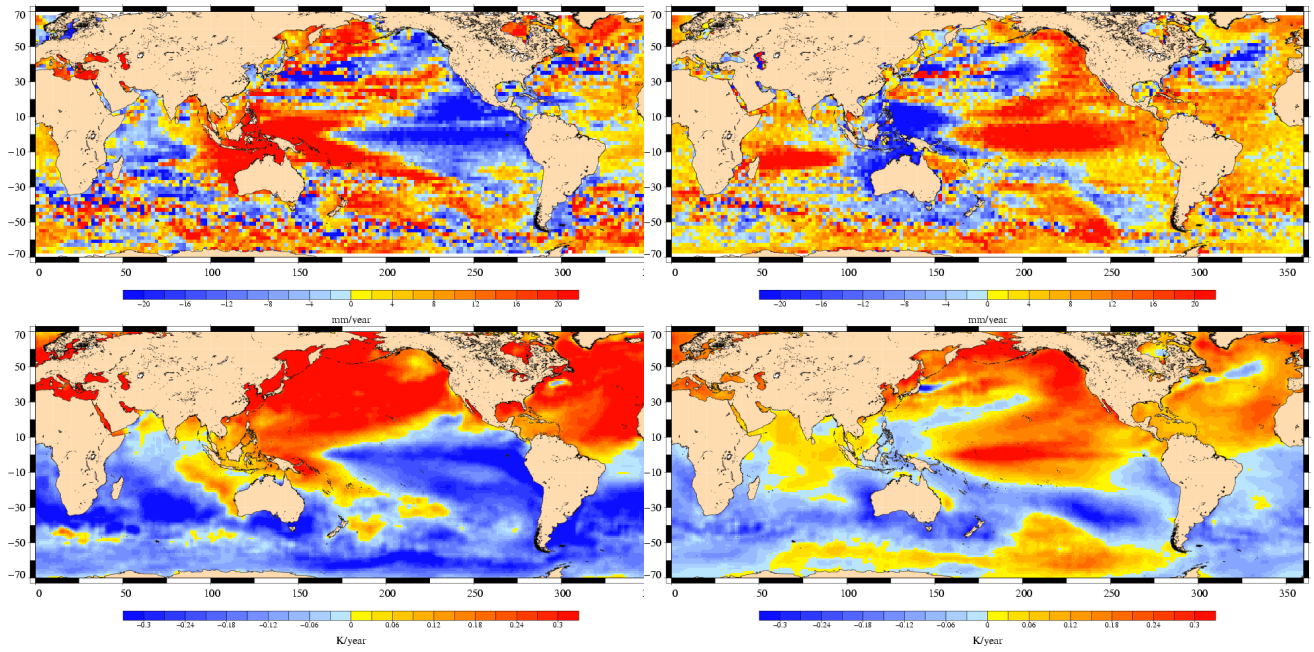

Figure 97: *Adjustment errors of T/P MSL and SST slopes over 13 years before and after "El Niño"*